Mixed Skyhook-Unsprung Negative Skyhook suspension control for the improvement of Ride Comfort of In-Wheel Motor vehicles

Bastiaan Christopher Holten

Technische Universiteit Delft

TU Delft
Delft
University of
Technology

Challenge the future

Mixed Skyhook-Unsprung Negative Skyhook suspension control for the improvement of Ride Comfort of In-Wheel Motor vehicles

by

Bastiaan Christopher Holten

in partial fulfillment of the requirements for the degree of

Master of Science

in Mechanical Engineering

at the Delft University of Technology,

to be defended publicly on Thursday September 5, 2019 at 14:00.

Supervisor:	Dr. ir. B. Shyrokau,	TU Delft, Cognitive Robotics
Thesis committee:	Dr. ing. J. Kober,	TU Delft, Cognitive Robotics
	Dr. ir. B. Shyrokau,	TU Delft, Cognitive Robotics
	Dr. ir. M. Wiertlewski,	TU Delft Cognitive Robotics,

This thesis is confidential and cannot be made public until December 31, 2019.

An electronic version of this thesis is available at `http://repository.tudelft.nl/`.

ABSTRACT

The development of In-Wheel Motor (IWM) vehicles introduces a lot of benefits. Its main drawback however is the increase of unsprung mass. This has a negative effect on the ride comfort, specifically for vibrations in the mid-frequency range of perceivable vibrations. The Unsprung Negative Skyhook (UNS) damper control method offers improvements of ride comfort in the same area. This control method also amplifies the oscillations at the natural frequencies of the vehicle, still causing an overall deterioration of the ride comfort. This research proposes new control methods with the aim of maintaining the benefits of the UNS while eliminating the natural frequency oscillations. The goal is to make the UNS control method applicable to IWM vehicles to achieve an overall increase in ride comfort.

The first proposed control method is based on a Frequency-range selector (FRS). This semi-active control method has been adjusted to be applied in a fully active suspension, using the Skyhook and Unsprung Negative Skyhook control methods as governing models. The second proposed control method uses a Short-Time Fourier Transform (STFT) frequency estimator to determine the instantaneous frequency of the vibration. Depending on the vibration, either one of the governing models is activated to achieve optimal results.

Extensive quarter car simulations have been carried out for a number of state-of-the-art control methods as well as the proposed control methods. These simulations allow for a direct comparison. Next, full vehicle simulations have been carried out for the proposed models and the governing models using IPG CarMaker for realistic vehicle behaviour. To ensure realistic road input files, road profile data from the Gerotek Testing Facility have been used.

During quarter car simulations, both models seem to improve on the UNS model where the FRS control method only achieves slight improvements. The full vehicle results show that the FRS model does not offer an improvement for the complete range of operations, while the STFT does improve on the ride comfort performance.

ACKNOWLEDGEMENTS

This Thesis marks the end of my career as a student at the faculty of Mechanical Engineering at the Delft University of Technology. I have enjoyed the time spent on this research and the years building up to it at the university, even if it has proven to be a bit longer than expected in advance. As this chapter comes to a close, I'd like to use this opportunity to thank those who've helped me during this research project.

First and foremost, I'd like to thank my supervisor Dr. ir. Barys Shyrokau for all the assistance offered during his time as my supervisor not only for this research topic, but also for the previous topic that eventually proved to be too complicated for a Master's Thesis. Thank you for guiding me through both topics and helping me in every part of the process of this Thesis. I am happy to have worked under your supervision for both projects and I definitely hope to get the opportunity to work together in the future.

I also want to thank ir. Tuğrul Irmak for the assistance during both research topics. Most specifically thank you for the useful insights and always being available for questions or discussions on any subject.

A special thanks goes out to ir. Marco Grottoli who acted as my supervisor during my internship prior to the research but was also available to offer assistance on some of the issues which were encountered during this research.

Finally I'd like to thank my family and, to a greater extent, my girlfriend for their support during the research project. I assume they'll be just as relieved as myself after the research comes to a full closure.

Bastiaan Christopher Holten
Delft, August 2019

GLOSSARY

α Frequency-range selector tuning parameter (crossover frequency).

σ_{Fz} Standard deviation of dynamic Tyre load.

α_{gh} Groundhook Linear control tuning parameter.

σ_{gh} Groundhook damping parameter for Hybrid control.

α_{hyb} Semi-active Hybrid control tuning parameter.

ω_i Crossover frequency. Where $i = 1, 2, 3$.

ω_s Sprung mass resonance frequency.

α_{sh} Skyhook Linear control tuning parameter.

σ_{sh} Skyhook damping parameter for Hybrid control.

ω_u Unsprung mass resonance frequency.

F_c Control force.

F_{gnd} Groundhook control force.

F_{hyb} Hybrid control force.

F_{sky} Skyhook control force.

F_z Tyre load, dynamic tyre force.

F_{z0} Static Tyre normal load.

T Total duration of the measurement signal.

c_a Active suspension damping ratio.

c_{hyb} Hybrid control active damping component.

c_s Suspension passive damping ratio.

c_t Tyre damping ratio.

e_c Control effort.

f_{sample} Sampling frequency for windowing.

g Gravitational constant $9.81\,\mathrm{m\,s^{-1}}$.

k_s Suspension spring stiffness.

k_t Tyre spring stiffness.

m_s Sprung mass.

m_u Unsprung mass.

z_x Vertical displacement of body x. Where $x = s, u, r$ for sprung mass, unsprung mass, or road.

Acronyms

ADD Acceleration Driven Damper.

D.o.F. Degree of Freedom.

E.o.M. equations of motion.

FRS Frequency-range selector.

GH Groundhook.

HC half car.

ICE Internal Combustion Engine.
IWM In-Wheel Motor.

KPI Key Performance Indicators.

LQR Linear Quadratic Regulator.

QC quarter car.

RMS Root Mean Square.

SH Skyhook.
STFT Short-Time Fourier Transform.

UNS Unsprung Negative Skyhook.

VDV Vibration Dose Value.

WBV Whole Body Vibrations.

CONTENTS

List of Figures **3**

List of Tables **5**

1 Introduction **7**
- 1.1 Project background . . . 7
- 1.2 Problem definition . . . 9
- 1.3 Research contributions . . . 10
- 1.4 Report outline. . . . 10

2 Vehicle modelling & evaluation **11**
- 2.1 Quarter car vehicle model. . . . 11
- 2.2 Quarter car vehicle dynamics . . . 11
- 2.3 Quarter car design objectives . . . 12
  - 2.3.1 Design objective: Ride comfort . . . 13
  - 2.3.2 Design objective: road holding capacity . . . 13
  - 2.3.3 Design trade-off . . . 14
- 2.4 Frequency response evaluation . . . 14
  - 2.4.1 Frequency response . . . 14
  - 2.4.2 Ride comfort evaluation . . . 14
  - 2.4.3 Road holding capacity evaluation . . . 16
  - 2.4.4 Reference model evaluation . . . 17
- 2.5 Road bump test . . . 17
- 2.6 Full vehicle model . . . 19
- 2.7 Full vehicle simulation road input . . . 19
  - 2.7.1 Road profile - Parallel Corrugations . . . 20
  - 2.7.2 Road profile - Angled Corrugations . . . 20
  - 2.7.3 Road profile - Potholes. . . . 21
  - 2.7.4 Road profile - Fatigue . . . 21
  - 2.7.5 Road profile roughness . . . 22
- 2.8 Full vehicle evaluation . . . 23
  - 2.8.1 Ride comfort. . . . 23
  - 2.8.2 Road holding capacity . . . 25
  - 2.8.3 Control effort . . . 25
- 2.9 Vehicle model selection. . . . 27

3 State of the art suspension modelling and control **29**
- 3.1 In-Wheel Motor design . . . 29
- 3.2 Suspension control . . . 31
  - 3.2.1 Suspension control classification . . . 31
- 3.3 Semi-active suspension control . . . 33
  - 3.3.1 Skyhook control . . . 33
  - 3.3.2 Groundhook control . . . 37
  - 3.3.3 Hybrid control . . . 39
- 3.4 Fully-active suspension control . . . 41
  - 3.4.1 Active Skyhook control. . . . 41
  - 3.4.2 Active Groundhook control . . . 42
  - 3.4.3 Active Hybrid control . . . 43
  - 3.4.4 Linear Quadratic Regulator - Optimal control . . . 43
  - 3.4.5 Unsprung Negative Skyhook damper control . . . 45
  - 3.4.6 Active model performance evaluation . . . 45

3.5 Summary . . . 45

4 Mixed Unsprung Negative Skyhook control 49
- 4.1 Governing models . . . 49
  - 4.1.1 Unsprung Negative Skyhook model . . . 49
  - 4.1.2 Determining the optimal model . . . 50
- 4.2 Frequency switching . . . 51
  - 4.2.1 Frequency-range selector . . . 51
  - 4.2.2 Short-Time Fourier Transform (STFT) . . . 53
- 4.3 Summary . . . 56
  - 4.3.1 Frequency-range selector control . . . 56
  - 4.3.2 Short-Time Fourier Transform control . . . 56

5 Quarter Car Simulation Results 57
- 5.1 Performance metrics . . . 57
- 5.2 Road input . . . 57
- 5.3 Simulation results . . . 58
  - 5.3.1 Frequency-range selector . . . 58
  - 5.3.2 STFT frequency estimator . . . 60
- 5.4 Time domain analysis . . . 62
- 5.5 Single-wheel road input . . . 62
- 5.6 Simulation results . . . 63
  - 5.6.1 Road bump . . . 63
  - 5.6.2 Random road . . . 65
- 5.7 Discussion . . . 68

6 Full Vehicle Simulation Results 71
- 6.1 Full vehicle simulation results . . . 71
  - 6.1.1 Simulation results - Parallel Corrugations . . . 71
  - 6.1.2 Simulation results - Angled Corrugations . . . 74
  - 6.1.3 Simulation results - Potholes . . . 76
  - 6.1.4 Simulation results - Fatigue . . . 78
- 6.2 Discussion . . . 80

7 Conclusion 81
- 7.1 Conclusions . . . 82
- 7.2 Recommendations . . . 82

A Appendix: Suspension type properties 83

Bibliography 85

LIST OF FIGURES

1.1 In-Wheel Motor design as presented by Mitsubishi 8

2.1 Basic quarter car model[1] 12
2.2 Effect of IWM design on vehicle dynamics. Frequency response of A) Sprung mass acceleration, B) Sprung mass displacement C) Unsprung mass acceleration D) Tyre deflection 15
2.3 Normalized performance evaluation of the IWM models versus the conventional model. For highlighted IWM models: Nominal ($c_s = 1200$) - High damping model ($c_s = 2000$) - Low damping model ($c_s = 800$) 17
2.4 Road profile for the road bump test 18
2.5 Sprung (top) and unsprung (bottom) mass motion for the Nominal model during the road bump test 18
2.6 Image of the IPG vehicle model used for the simulations.. 19
2.7 Height map of the road with parallel corrugations used for full vehicle simulation. 20
2.8 Height map of the road with angled corrugations used for full vehicle simulation. 20
2.9 Height map of the ’Potholes’ road used for full vehicle simulation. 21
2.10 Height map of the ’Fatigue’ road used for full vehicle simulation. 21
2.11 Each of the road profiles at the Gerotek testing facility being mapped for digital use.[2] 22
2.12 Vertical acceleration frequency weighting filter 24
2.13 Motion sickness acceleration frequency weighting filter 25

3.1 Michelin Active Wheel: An In-Wheel Motor design concept by Michelin 30
3.2 Overview of different suspension system categories in terms of activity/passivity[3] 32
3.3 Skyhook control system[1]. 33
3.4 Semi-Active Skyhook suspension control methods. Frequency response of A) Sprung mass acceleration B) Sprung mass displacement C) Unsprung mass acceleration D) Tyre deflection . . . 35
3.5 Performance evaluation of the semi-active Skyhook methods versus the reference models: Nominal ($c_s = 1200$) - Low damping ($c_s = 800$) - High damping ($c_s = 2000$) 36
3.6 Groundhook control system[1] 37
3.7 Semi-Active Groundhook suspension control methods. Frequency response of A) Sprung mass acceleration B) Sprung mass displacement C) Unsprung mass acceleration D) Tyre deflection . 38
3.8 Performance evaluation of semi-active Groundhook control methods versus the reference models: Nominal ($c_s = 1200$) - Low damping ($c_s = 800$) - High damping ($c_s = 2000$) 39
3.9 Hybrid control system[1] 40
3.10 Semi-Active Hybrid suspension control methods. Frequency response o A) Sprung mass acceleration B) Sprung mass displacement C) Unsprung mass acceleration D) Tyre deflection 41
3.11 Normalized performance of the semi-active Hybrid model for different values of tuning parameter α versus the reference models Nominal ($c_s = 1200$) - Low damping ($c_s = 800$) - High damping ($c_s = 2000$): 42
3.12 LQR suspension control. Frequency response of A) Sprung mass acceleration B) Unsprung mass acceleration C) Suspension deflection D) Tyre deflection 44
3.13 Active system frequency responses of A) Sprung mass acceleration B) Sprung mass displacement C) Unsprung mass acceleration D) Tyre deflection 46
3.14 Normalized performance of each of the fully active control methods with reference models: Nominal ($c_s = 1200$) - Low damping ($c_s = 800$) - High damping ($c_s = 2000$) 46

4.1 Comparison of the frequency responses of the sprung mass for the active Skyhook and Unsprung Negative Skyhook models 51
4.2 Working principle of the frequency range selector. Left: a visualisation of the inequality equation. Right: the positivity of the inequality function as a function of vibration frequencies.[4] . . 52

4.3 Example of a Hamming window with a window size of $n = 150$ 54
4.4 Examples of an STFT spectrum of a windowed signal. Left: Response of a chirp single. Right: Response of a random road signal. 55

5.1 General example of a chirp signal for a low end frequency of 0.1 Hz and an upper frequency of 5 Hz 58
5.2 Frequency response results of the FRS model. The figure show the responses of the following signals: (A) Sprung mass acceleration (B) Sprung mass displacement (C) Unsprung mass acceleration (D) Tyre deflection 59
5.3 Normalised performance of the FRS Mixed Model compared to its governing models and the passive system. Note that the Passive model of figure 5.2 is displayed here as the nominal model. 60
5.4 Frequency response results of the STFT model. The figure show the responses of the following signals: (A) Sprung mass acceleration (B) Sprung mass displacement (C) Unsprung mass acceleration (D) Tyre deflection 61
5.5 Normalised performance of the STFT Mixed Model compared to its governing models and the passive system. 61
5.6 Road input signal for the road bump test 62
5.7 Fragments of the randomly generated road. The left graph shows a 10 second snip of the full signal. The right graph shows a detailed look at the road profile over 1 second 63
5.8 Sprung body displacement for single-wheel road bump using the FRS control method 64
5.9 Sprung body displacement for single-wheel road bump using the STFT control method 64
5.10 Estimated frequency of the STFT model for the single-wheel road bump 65
5.11 Single-wheel road bump results relative to the nominal results (dashed). 66
5.12 Fragment of the sprung body displacement of the FRS model during the random road simulation 66
5.13 Fragment of the sprung body displacement of the STFT model during the random road simulation 66
5.14 Comparison of model performance for the single-wheel random road simulation. Normalised to the performance of the nominal model (dashed). 68

6.1 Ride comfort and road holding results compared to the passive nominal model for the Parallel Corrugated road simulation, $v = 10\,\mathrm{km\,h^{-1}}$ 72
6.2 Ride comfort and road holding results compared to the passive nominal model for the Parallel Corrugated road simulation, $v = 60\,\mathrm{km\,h^{-1}}$. 73
6.3 Ride comfort and road holding results compared to the passive nominal model for the Angled Corrugated road simulation, $v = 10\,\mathrm{km\,h^{-1}}$. 74
6.4 Ride comfort and road holding results compared to the passive nominal model for the Angled Corrugated road simulation, $v = 60\,\mathrm{km\,h^{-1}}$. 75
6.5 Ride comfort and road holding results compared to the passive nominal model for the Pothole road simulation, $v = 10\,\mathrm{km\,h^{-1}}$. 76
6.6 Ride comfort and road holding results compared to the passive nominal model for the Pothole road simulation, $v = 60\,\mathrm{km\,h^{-1}}$. 77
6.7 Ride comfort and road holding results compared to the passive nominal model for the Fatigue road simulation, $v = 10\,\mathrm{km\,h^{-1}}$. 78
6.8 Ride comfort and road holding results compared to the passive nominal model for the Fatigue road simulation, $v = 60\,\mathrm{km\,h^{-1}}$. 79

A.1 Full detailed overview of different suspension system types and their properties[4] 83

LIST OF TABLES

2.1 Physical quarter car model properties for conventional vehicle design . . . 12
2.2 IPG CarMaker™ Simulation vehicle parameters . . . 19
2.3 Roughness coefficient and index per road profile.[2] . . . 22

3.1 Vehicle properties: Conventional vehicle vs. IWM vehicle . . . 29
3.2 Complete list of physical properties of the controlled IWM vehicle models . . . 31

5.1 Single-wheel road bump numerical results . . . 65
5.2 Single-wheel random road numerical results . . . 67

6.1 Full vehicle simulation results for the Parallel Corrugated road, $v = 10\,\mathrm{km\,h^{-1}}$ . . . 71
6.2 Full vehicle simulation results for the Parallel Corrugated road, $v = 60\,\mathrm{km\,h^{-1}}$ . . . 73
6.3 Full vehicle simulation results for the Angled Corrugated road, $v = 10\,\mathrm{km\,h^{-1}}$ . . . 74
6.4 Full vehicle simulation results for the Angled Corrugated Road, $v = 60\,\mathrm{km\,h^{-1}}$ . . . 75
6.5 Full vehicle simulation results for the Pothole road, $v = 10\,\mathrm{km\,h^{-1}}$ . . . 76
6.6 Full vehicle simulation results for the Pothole road, $v = 60\,\mathrm{km\,h^{-1}}$ . . . 77
6.7 Full vehicle simulation results for the Fatigue road, $v = 10\,\mathrm{km\,h^{-1}}$ . . . 78
6.8 Full vehicle simulation results for the Fatigue road, $v = 60\,\mathrm{km\,h^{-1}}$ . . . 79

1

INTRODUCTION

1.1. PROJECT BACKGROUND

People are always in pursuit of improving on the way they do things. Transportation is no exception to this phenomenon. Since the horse-drawn carriage, the biggest revolution in transportation has been the introduction of motorised vehicles. Nowadays, these motorised vehicles are so widely used, it is almost impossible to imagine a world without them. This has not, however, stopped people from searching for ways to keep improving their means of transportation.

Transportation by car is currently one of the most used methods of travel around the world. A recent estimation states that, as of 2016, more than 1.3 billion motorised vehicles have been registered. An amount of nearly 1 billion is attributed to passenger vehicles or more specifically, cars. In comparison, in the European Union in 2017, the combined total of distance travelled by passenger vehicles is almost double the amount of the combined total of distance travelled by individuals by railroad vehicles[1]. This means that if each passenger vehicle would have just a single passenger, this would mean that people have travelled almost twice the distance by car that has been travelled by rail. In reality, cars can transport multiple passengers at once. That means that the distance travelled by passenger vehicles should be multiplied by the average number of passengers in a passenger vehicle in order to obtain the combined total of distance travelled by individuals through motorised vehicles. This shows that cars make up a dominating part of personal transport.

It is therefore not surprising that, ever since their introduction, people have been researching ways to improve on these motorised vehicles. With advancing research, technologies usually find their way into territories that they weren't originally designed for, offering new approaches and improvements to existing problems. With the coming of motorised vehicles, suspension systems were also introduced in order to improve the comfort aspect of the vehicles.

Research into the optimization of the comfort of a vehicle has been present ever since the introduction of suspension systems. At first, mostly passive systems were used. The performance of these systems has been researched dating back at least to the 1970's[5], where both the comfort as the road holding capacity of the passive suspension is investigated. This relatively early research already shows the dilemma that is faced when designing a suspension system. Optimal road holding capacity is achieved for much suspensions with much higher damping than optimal comfort. This is the classical design dilemma that is always encountered in vehicle suspension design.

Due to technological advancements, new suspension systems were introduced, incorporating an active element into the suspension system[6]. It is shown that the active suspension system can be used in tandem with a passive system. This combined design shows that this can improve the behaviour of a passive system, but not as much as a system comprised solely of active systems. It does show that activity in suspension systems offer improvements, if used properly.

Apart from the suspension systems, one of the fields of research within automotive engineering is the de-

---

[1] As published by the International Transport Forum at: https://www.itf-oecd.org/key-transport-statistics-2018-2017-data

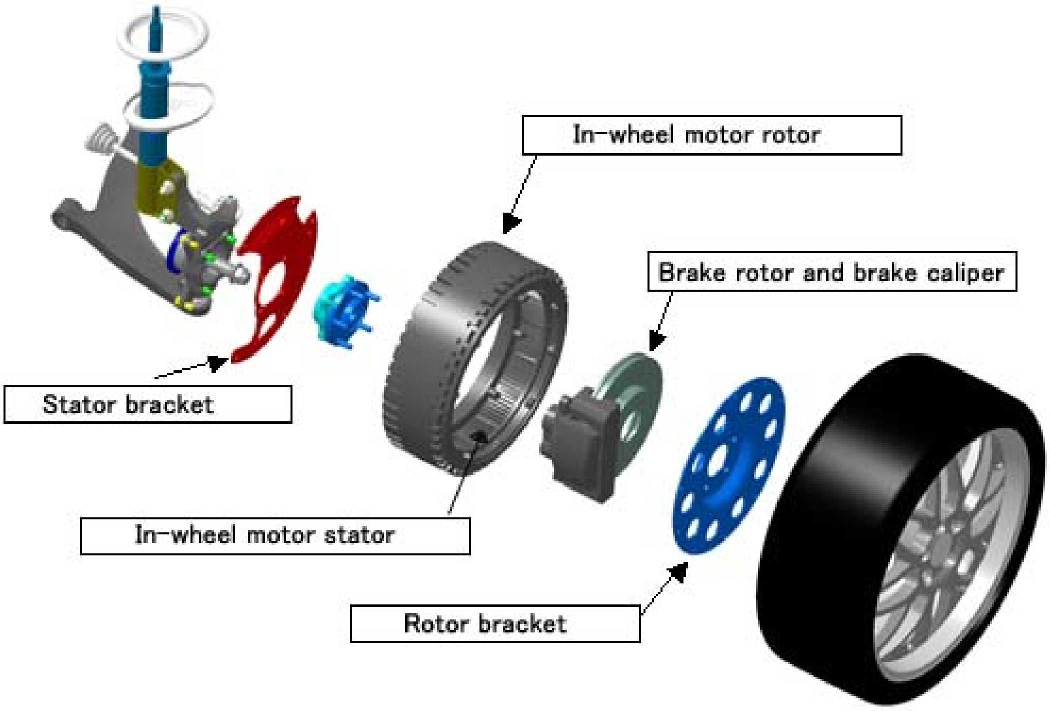

Figure 1.1: *In-Wheel Motor design as presented by Mitsubishi*[2]

velopment of electric vehicles. For many years manufacturers have tried to develop vehicles using electric propulsion rather than the traditional Internal Combustion Engine (ICE)[7]. It is only recently relatively recently that manufacturers actually successfully designed and produced these electric vehicles. The success of these electric vehicles offer the opportunity to implement other techniques or improve on existing ones.

One of these techniques is the design of In-Wheel Motor (IWM) vehicles. For conventional ICE vehicles, various vehicle packages have been investigated where the placement of the engine as well as the configuration of driven wheels all influence the behaviour of the vehicle dynamics. However, the introduction of electric motors open up the way to a configuration that is not available to the conventional ICE vehicles. The IWM design offers both dynamic improvements and spatial design freedom[8]. In this type of design, each of the wheels is equipped with its own electric power unit. This dramatically reduces the distance between the power unit itself and the driven wheel, eliminating the need for a multitude of mechanical links that a conventional ICE requires. As each link introduces efficiency losses into a system, reducing the amount of mechanical links will improve on the overall efficiency of the vehicle. In conventional vehicles, the power of the ICE is transported to the driven wheels by means of the drive shaft, or, more generally speaking, the drive transmission. Using IWM design, eliminates the need for the transmission. Next to improving the efficiency, this also opens op a lot of spatial room in the vehicle which can be used either for other components, or more room for the passengers of the vehicle.

Apart from improving the efficiency and spatial features of the vehicle, IWM design also adds a lot of controllability to the vehicle. One technique that benefits from this type of design is a technique called torque vectoring[9]. This technique shows that the ability to control the yaw rotations, or the rotations in a plane parallel to the road, increases the overall control of the vehicle, improving not only on efficiency but also safety. In conventional design, torque vectoring is achieved by controlling the brakes of a vehicle. This way, the total applied torque on a wheel can be controlled. Combining this technique with IWM design, however, offers major further improvements. Since an electric motor can operate in both motor and generator modes, it is possible to apply both positive and negative torques to the individual wheels. As the brakes can only offer negative torques, the operation range of the torque vectoring technique will drastically increase.

---

[2] Mitsubishi press release to be found at: https://www.mitsubishi-motors.com/en/corporate/pressrelease/corporate/detail1321.html

Unfortunately, IWM does not solely offer benefits when compared to conventional design. For simplicity, any car can be described by two linked body masses, the sprung and unsprung mass. The sprung mass represents the total weight of the vehicle body and anything rigidly attached to it. The unsprung mass is comprised of the suspension system, which includes the wheel hubs and wheels of the vehicle and is connected to the sprung mass by the suspension springs and dampers. In conventional design, the ICE can be assumed to be rigidly attached to the sprung mass. The mass of the ICE itself is therefore included in the sprung mass. In IWM design, the electric motors are directly installed onto the vehicle's wheel hubs. The weight is therefore transferred from the sprung mass and onto the unsprung mass.

The sprung and unsprung masses both influence the dynamical behaviour of the vehicle. The influence of the unsprung mass on the overall vehicle dynamics has already been researched. This research shows that increasing the unsprung mass of a vehicle leads to less a lower ride quality, or a decrease in the ride comfort of the vehicle[10]. The influence on both the road holding capacity and the ride comfort is detailed. It can be seen that the ride comfort can be slightly improved by reducing the sprung mass. It is noted that it is only possible to achieve small improvements if the road holding capacity is to remain approximately equal. This research therefore shows once again the traditional design trade-off as well as the negative effect of an increased unsprung mass.

The introduction of IWM design is therefore a promising technology with a potential to increase both the vehicle's efficiency and its controllability. On the other hand, IWM design results in higher unsprung masses, which negatively affects the ride comfort of the vehicle. Obviously, a way should be found to counteract the negative effects of IWM design so the technology can be more easily applied.

A recent study has attempted to design a new control method in order to improve the ride comfort in this mid-frequency range[11]. This research resulted in a new semi-active control method. This method is originally based on the Skyhook control method, which has been extensively researched over the years[12]. The new model introduces an additional force proportional to the stroke velocity of the suspension itself. If this proportionality is chosen to be of an equal value as the Skyhook damping coefficient, the effective damping force is defined in the positive direction of the unsprung mass. Instinctively it would seem that this would excite the body even more and increase the body vibrations, effectively decreasing the vehicle ride comfort. It is shown that this indeed the case for the resonance frequencies of the system. At other frequencies, however, the newly proposed model attenuates vibrations better than the reference Skyhook model. Since this model effectively uses the negative unsprung mass velocity to determine the Skyhook force, it is aptly named Unsprung Negative Skyhook (UNS) damper control.

1.2. PROBLEM DEFINITION

IWM design is shown to introduce a deterioration of vehicle ride comfort for a certain frequency range. The UNS control method offers improvements in ride comfort for this same frequency range. It is therefore suited to counteract the undesired dynamical behaviour of the increase in unsprung mass. The UNS however also introduces powerful oscillations at the natural frequencies of the suspension system. This research aims to find a control method to attenuate or even eliminate these undesired oscillations. This goal can be formulated as follows:

> *Design a control method that attenuates the oscillations of the Unsprung Negative Skyhook (UNS) damper control method, with the aim of improving the overall ride comfort of an In-Wheel Motor vehicle.*

The following three global goals can be extracted from this definition:

- The natural frequency oscillations of the UNS should be attenuated.
- The mid-frequency range ride comfort improvement of the UNS should be maintained.
- The control method should achieve a real-time computational process in order to be properly implemented in a vehicle.

1.3. RESEARCH CONTRIBUTIONS

In order to achieve the goal of this research, new control methods are designed. In general suspension control applications, both active and semi-active, different control methods all follow a similar approach. The control force is usually determined by an imaginary damper[12]. These methods all assume a constant damping ratio for this damper. In this research, new active control methods are developed where the damping ratio is not constant, but can be adjusted according to the nature of the frequency of the disturbance vibration. Two separate approaches are developed. One uses a Frequency-range selector (FRS) to alter the damping ratio. This method is similar to the semi-active Skyhook-Acceleration Driven Damper (ADD) control method[4] but is instead combined with fully active suspension control methods. Another method employs a Short-Time Fourier Transform (STFT) to estimate the instantaneous frequency. According to this frequency, the damping ratio of the imaginary damper is adjusted.

Furthermore, the control methods are tested in full vehicle simulation using IPG CarMaker™[13]. This software is widely used in the industry for obtaining realistic vehicle simulations. For these simulations, the following assumptions are in place:

- Each wheel hub is controlled individually following the control laws.
- The system is considered to be causal. No information or estimation of future states is required.

The road profiles have been established at the Gerotek Testing Facility, South Africa[14]. This testing facility is used by car manufacturers around the globe in order to test their vehicles for a wide range of realistic road profiles.

Simulations are carried out for the newly designed models as well as for the state-of-the-art control methods to create a clear and direct comparison

1.4. REPORT OUTLINE

This report is laid out as follows: Chapter 2 lays out the basic background for the project. In this chapter the general vehicle dynamics of the different vehicle models that are used for this research are discussed. Chapter 3 will supply an overview of currently available and generally used control methods which can later be used to compare to the proposed control method. Next, in Chapter 4 the new model will be proposed. The details of the working principle will be shown. According to the theoretical proposal, expectations will be made concerning the results of the proposed model. Chapters 5 and 6 will display and elaborate on the results of the simulations carried out with the proposed model. These chapters discuss the results of the simulations for the quarter car and full vehicle models respectively. Finally, chapter 7 will discuss the results shown in the previous chapter after which it is possible to draw final conclusions on this research, as well as allowing to suggest subjects for further research.

2

VEHICLE MODELLING & EVALUATION

This chapter will elaborate on the background of the research project. It will provide details on the vehicle models and the evaluation methods used. Two different types of vehicle models are used in this research:

- quarter car (QC) model
- full vehicle model

The first part of this chapter elaborates on the quarter car model and the full vehicle models. For both of these model types, their respective road input is discussed. The last part of the chapter supplies an overview of evaluation methods for the simulations.

2.1. QUARTER CAR VEHICLE MODEL

The QC model represents a single wheel and suspension system. In this model $1/4^{\text{th}}$ of the vehicle weight is used so for the sprung mass m_s to have the model properly represent a quarter of the total vehicle.

Figure 2.1 shows a representation of a QC model. The model is divided into two different sections, namely the sprung mass m_s and the unsprung mass m_u. The sprung mass is defined as the vehicle body mass. In the case of a quarter care vehicle it will be represented by $1/4^{\text{th}}$ of the total vehicle mass. The other mass, the unsprung mass, consists of the vehicle suspension and the wheel hub.

The sprung and unsprung mass are connected by the suspension system. This suspension system is modelled as a spring with stiffness k_s and a damper with damping coefficient c_s.

Finally, the unsprung mass is connected to the ground by the wheel. The wheel itself is modelled as a spring with stiffness k_t and damping coefficient c_t.

The damping ratio of the tyre is generally many orders of magnitude smaller than the spring stiffness. The force generated by the damping coefficient, and in turn the damping coefficient itself, is therefore considered to be negligible in this type of system.

2.2. QUARTER CAR VEHICLE DYNAMICS

The system shown in Figure 2.1 is a regular quarter car model for use in vehicle dynamic modelling. This model will be used as the vehicle model of choice for this research. It is then important to understand how the vehicle model behaves dynamically. The description of the dynamic behaviour of the vehicle model is governed by the systems' equations of motion (E.o.M.). The system of Figure 2.1 can therefore be described in the following way [1] :

---

[1] N.B. Remember that c_t is assumed to be negligible i.e. $c_t = 0$

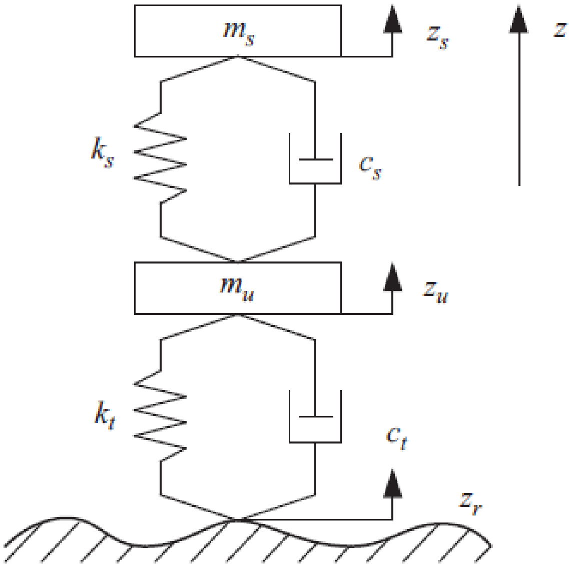

Figure 2.1: *Basic quarter car model[1]*

Table 2.1: *Physical quarter car model properties for conventional vehicle design*

	Value
m_s	500 kg
m_u	80 kg
k_s	30 000 N m^{-1}
c_s	1200 N s m^{-1}
k_t	300 000 N m^{-1}
c_t	0 N s m^{-1}

$$m_s\ddot{z}_s = c_s(\dot{z}_u-\dot{z}_s)+k_s(z_u-z_s) \tag{2.1}$$

$$m_u\ddot{z}_u = -c_s(\dot{z}_u-\dot{z}_s)-k_s(z_u-z_s)+k_t(z_r-z_u) \tag{2.2}$$

These equations clearly show the purpose of the QC model as motion in the vertical z-direction is the only type of motion that is included. It is important to note that we assume the system to operate in the linear range of its components. The stiffness values k_s and k_t and the damping ratio c_s are therefore assumed to be constant values in the passive model. These constant values and other vehicle properties are shown in table 2.1. This table contains the values that will be used for the conventional design vehicle. This vehicle model represents the vehicle that is using the conventional ICE design. Also note that the tyre damping ration c_t is undefined, as its influence on the vehicle is neglected.

2.3. QUARTER CAR DESIGN OBJECTIVES

In order to be able to compare different control methods, it is necessary to both determine metrics on how to accurately measure performance and establish a reference model with which the different control methods will be compared. For the reference model, the passive IWM model, henceforth named the Nominal Model, will be used as has been defined in tables 2.1 and 3.1. The Nominal IWM model will be the reference model with which any and all other models in this research will be compared.

In vehicle suspension design, there are generally two different design objectives; ride comfort and road holding capacity, each with their own Key Performance Indicators (KPI). Since we have made a choice for the model of the vehicle, it is now possible to determine these KPI's. These parameters should give us insight on the performance of the vehicle for each of the design objectives.

Apart from determining the design objectives, it is also very important to determine the operating range within the system will be analysed. For the QC model, the system is disturbed by the vertical displacement of the road surface. This disturbance can be modelled as a vibration. It is therefore important that the range of operating frequencies are relevant for our design goals. For ride comfort, it is necessary to know what kind of vibrations humans perceive as uncomfortable.

The susceptibility of humans to vibrations has been readily researched[15]. This research shows the absorption rate of vertical whole body vibrations for humans. It can be seen that the human body attenuates well for high frequencies. It has been shown that the perception of vibrations by humans decreases greatly at frequencies over 31.5 Hz[16]. At the lower end of the spectrum, humans have been found to be sensitive to low frequency vibrations as low as 1 Hz[17]. Vibrations with smaller frequencies tend to go unnoticed by human passengers. The frequency range of interest can therefore be set from 1 Hz up to 30 Hz for this research.

2.3.1. DESIGN OBJECTIVE: RIDE COMFORT

An important aspect for the drivers of vehicles is the ride comfort of a vehicle[18]. Manufacturers constantly seek new ways to improve on the ride comfort of their vehicles. It is therefore important to establish a method to objectively measure the ride comfort performance of the vehicle. In general, the main sources of discomfort are unwanted motions and vibrations. However, not all vibrations and motions are directly perceived by the driver of a vehicle. The driver will only perceive the motion and vibrations of the vehicle's body, its sprung mass. To analyse the perceived comfort of a vehicle, the main characteristic to examine is the sprung mass vibrations. For this research, the comfort will be addressed by investigating the sprung mass accelerations, which is a primary indicator of vibrations. These accelerations will give us insight on how the sprung mass behaves under different road inputs and will enable us to compare different control methods in terms of ride comfort. As vibrations are the cause of discomfort, smaller vibrations of the sprung mass indicate better ride comfort. The aim of improving the vehicle ride can therefore be determined as the minimization of the body accelerations[19].

$$\min(\ddot{z}_s) \tag{2.3}$$

Keep in mind that, as stated previously, not all vibrations are found to attribute to the ride comfort of the vehicle. Therefore, only vibrations between 1 Hz and 20 Hz are considered for the analysis of ride comfort.

2.3.2. DESIGN OBJECTIVE: ROAD HOLDING CAPACITY

The second important aspect of vehicle performance is the road holding capacity. This aspect is an indicator of the vehicle's driving performance. The road holding capacity is a way to describe the amount of grip that a vehicle achieves. When the vehicle has more grip, it is better able to transfer power from the engine into motion which increases the cornering capabilities of the vehicle. This research focuses on commercial applications for suspension control methods. As such, the road holding capacity is generally considered less important than the ride comfort, but important nonetheless. In order to determine the desired behaviour in terms of measurable properties, it is necessary to understand the basis which defines the road holding capacity. Essentially, the road holding capacity can be directly related to the grip of a vehicle. Grip is a non-linear property that depends on many different factors like the steering angle, road surface friction, and the normal force of the vehicle on the road. In the QC model, steering is not included. The influence of different road surfaces is also considered to be constant for the simulations. The road holding capacity can then be assumed to depend on the normal forces of the vehicle on the road surface. This normal force consists of a static load and a fluctuating tyre contact force.

$$F_z = (m_s + m_u) \cdot g - k_t(z_u - z_r) \tag{2.4}$$

Where the first term denotes the total mass of the vehicle which is multiplied by the gravitational constant g to acquire the vehicle's static load. The tyre forces are defined by the product of the tyre stiffness k_t and the difference between the unsprung mass motion and the road motion, or the tyre deflection, $z_u - z_r$. In this definition, the vehicle mass and the gravitational constant describe the static load of the vehicle. This value will typically not change during operation of the vehicle. The tyre forces, however, introduce oscillations in the normal force of the vehicle. Even though these oscillations can increase the amount of grip for up to half of the oscillation period, the other half of the period will introduce a reduction in normal force.It is therefore generally considered to be unwanted behaviour. Improving on the road holding of a vehicle is therefore defined as minimizing these normal force oscillations, which are dependent on the tyre deflection[19].

$$\min(z_u - z_r) \tag{2.5}$$

2.3.3. DESIGN TRADE-OFF

In general, comfort and performance are opposing design objectives. Improving the ride comfort generally results in a decline of the road holding capacity. It is therefore desirable to find a new approach that improves ride comfort without compromising the road holding capacity. The following section will detail on how the performance of a given model is calculated corresponding to the design objectives.

2.4. FREQUENCY RESPONSE EVALUATION

In the previous sections, the design objectives have been determined and elaborated on. It is now possible to determine the metrics with which to analyse the different systems. As previously established, the aim of the comfort design objective is to minimize the sprung mass accelerations $\ddot{z}_s$ whereas the aim of the road holding design objective is to minimize the tyre deflections $(z_u - z_r)$. These two system signals can then be used to determine the overall performance of the vehicle in each specific design objective. These signals will be normalized by comparing the results to those of a reference system which has been defined previously, and will be detailed more precisely in a later section of this chapter.

2.4.1. FREQUENCY RESPONSE

For this research, we are interested in the dynamical behaviour of the vehicle within a certain range of frequencies. In order to analyse the complete dynamic behaviour in this range, the frequency response of the system is examined. This frequency response is acquired in the following way. First, for each system, the ground is excited by the input signal:

$$z_r = A\sin(\omega t) \tag{2.6}$$

Where the signal frequency ω spans a range from 1 Hz up to 30 Hz. The amplitude A is limited to small deflections up to 0.05 m in order to ensure linear behaviour of the passive spring and damper components. For the displayed simulation results in the rest of this research, an amplitude of 0.01 m is used.

The resulting responses from the time domain are then transferred to the frequency domain by calculating their Fourier Transform functions. This decomposes the time domain signal into its frequency components. These frequency responses can be examined to analyse the frequency dependent behaviour of each model.

Figure 2.2 shows the frequency response results of the conventional model and the IWM model as defined by the properties of tables 2.1 and 3.1. The differences in dynamic behaviour can clearly be seen. The change of resonance frequencies, as determined by equations (3.2) and (3.3), are seen to have a significant impact on the model behaviour for different frequency ranges.

First of all, the low frequency behaviour remains relatively unchanged up to the first resonance frequency, as the sprung mass resonance frequency only slightly increases for the IWM model.

The vibrations between the two resonance frequencies seem to increase due to the relatively large shift of the unsprung resonance frequency. This shift has the dual effect of increasing vibrations for frequencies lower than the unsprung resonance frequency, but reducing vibrations for higher frequencies. This shows that the main region of interest is the mid frequency range if we are to improve the vehicle's dynamic behaviour compared to that of the conventional model.

2.4.2. RIDE COMFORT EVALUATION

Observing the frequency responses and road bump test responses will give us an understanding of how the vehicle behaves. It does not yet, however, provide us with a way to determine a metric for the vehicle performance. Using only the frequency responses and road bump test responses, it will not be possible to objectively determine whether one system is actually "better" than another.

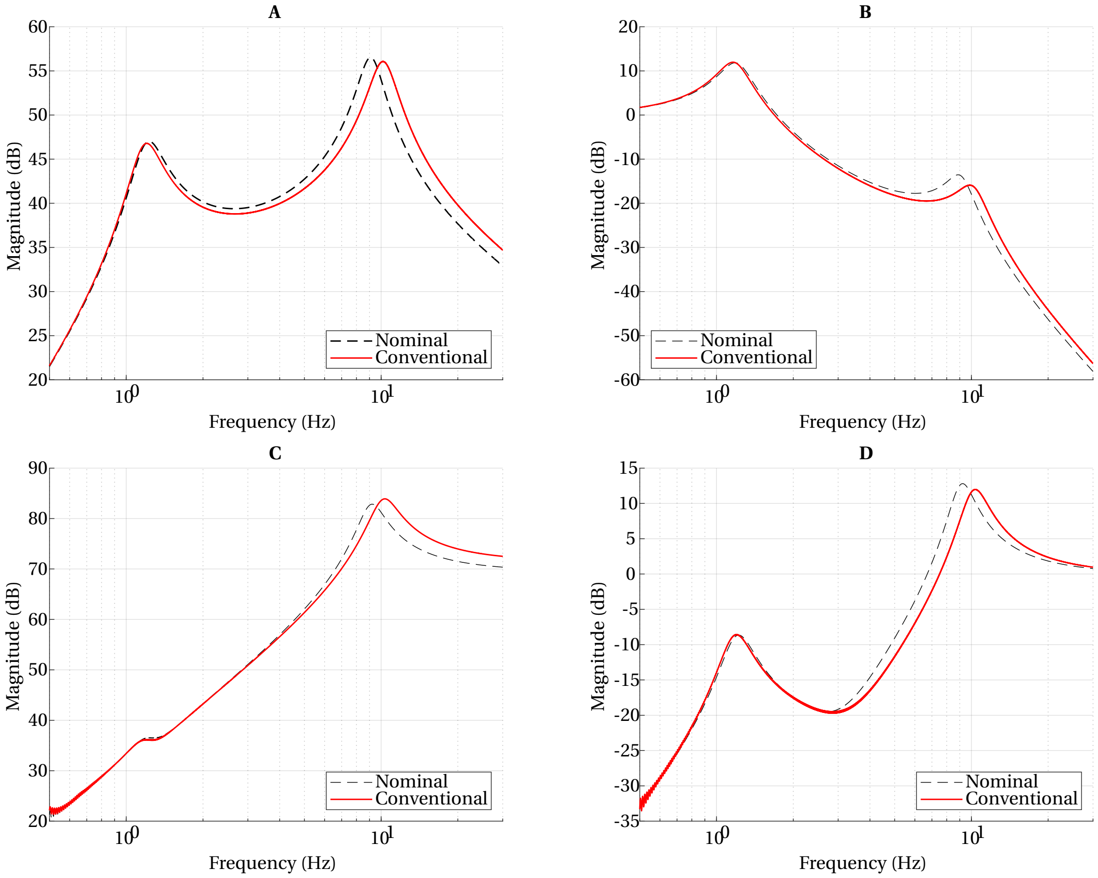

Figure 2.2: *Effect of IWM design on vehicle dynamics. Frequency response of A) Sprung mass acceleration, B) Sprung mass displacement C) Unsprung mass acceleration D) Tyre deflection*

The overall comfort performance of a vehicle can be defined by integration of the comfort related Power Spectral Density function over the frequency range of interest. This Power Spectral Density is calculated by using the frequency responses from the simulation. If $F(f)$ is the frequency dependent Fourier transform of a signal, the Fourier transforms of an output signal of interest and the input signal can be used to determine the Power Spectral Density function $X(f)$ of the output response.

$$X(f) = \frac{F_{\text{out}}^2(f)}{F_{\text{in}}^2(f)} \tag{2.7}$$

This Power Spectral Density function is then integrated over the frequency range of interest to determine the absolute evaluation metric.

$$\int_{\underline{f}}^{\overline{f}} |X(f)|^2 \mathrm{d}f \tag{2.8}$$

The integration boundaries $\underline{f}$ and $\overline{f}$ are the lower and upper boundaries respectively of the frequency range over which the integration is calculated.

This integration will first be performed on a reference model, also referred to as the nominal model. This nominal model will set the values for the relative performance of other systems. The relative, or normalised, performance of every model is then defined as:

$$J = \frac{\int_{\underline{f}}^{\overline{f}} |X(f)|^2 \mathrm{d}f}{\int_{\underline{f}}^{\overline{f}} |X^{\text{ref}}(f)|^2 \mathrm{d}f} \tag{2.9}$$

As defined previously, the comfort of a vehicle is mainly defined by the vibrations of the sprung mass. The evaluation of the comfort criterion can therefore be defined as:

$$J_{\text{c}} = \frac{\int_{\underline{f}}^{\overline{f}} |z_s(f)|^2 \mathrm{d}f}{\int_{\underline{f}}^{\overline{f}} |z_s^{\text{nom}}(f)|^2 \mathrm{d}f} \tag{2.10}$$

As defined previously, the comfort oriented design objective is the minimization of the sprung mass vibrations, see equation (2.3). This means that values between 0 and 1 for the normalised performance index indicate an increase in ride comfort. Values exceeding 1 indicate a decrease in ride comfort compared to the nominal model.

2.4.3. ROAD HOLDING CAPACITY EVALUATION

The comfort performance of each vehicle model will be defined similarly to the evaluation of the ride comfort. Using the general approach to the model evaluation as defined in equation (2.9) and combining this with the road-holding oriented design objective as defined in equation (2.4), the evaluation of the road-holding performance index can be determined:

$$J_{\text{rh}} = \frac{\int_{\underline{f}}^{\overline{f}} |(z_u - z_r)(f)|^2 \mathrm{d}f}{\int_{\underline{f}}^{\overline{f}} |(z_u - z_r)^{\text{nom}}(f)|^2 \mathrm{d}f} \tag{2.11}$$

As with the definition of the comfort evaluation metric, an increase of road-holding is indicated by the reduction of the tyre deflection. Values between 0 and 1 are therefore an improvement of the system, while values exceeding 1 indicate worse road-holding performance.

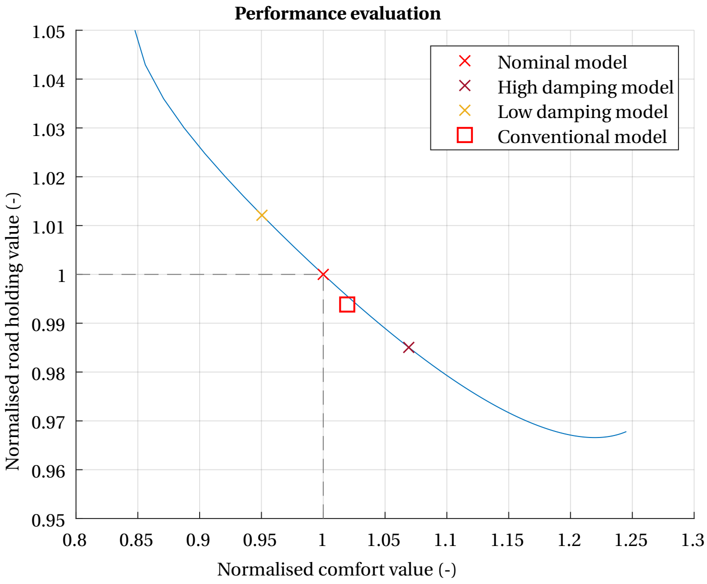

Figure 2.3: *Normalized performance evaluation of the IWM models versus the conventional model. For highlighted IWM models: Nominal ($c_s = 1200$) - High damping model ($c_s = 2000$) - Low damping model ($c_s = 800$)*

2.4.4. REFERENCE MODEL EVALUATION

With the evaluation methods determined, it is possible to determine how the IWM vehicle model compares to the Base vehicle model. Remember that the passive IWM model will be used as the nominal model for the other suspension control methods. Keeping in mind the definition of the design objective parameters, equations (2.10) and (2.11), the passive IWM model will obviously be located at the nominal location of the graph $(1,1)$.

Figure 2.3 then shows the normalized performance of the passive IWM model and the conventionally designed Base model. The continuous line on the graph shows the attainable normalized performance of the IWM model for a range different suspension damping values. These values range from $100\,\mathrm{N\,s\,m^{-1}}$ up to $10\,000\,\mathrm{N\,s\,m^{-1}}$. These values are extreme in order to show the complete range of the passive model's capabilities.

Since the design objective is to minimize the vibrations and tyre deflections, a system is more desirable when it is located closer to the graph's origin.

It can easily be seen that the performance of the Base model[2] is closer to the origin than the nominal model in terms of comfort. This shows that the IWM model indeed performs worse in terms of ride comfort than the Base model due to the shifting of the vehicle mass. In order to improve on the IWM performance, several control methods can be used to cleverly apply additional damping.

2.5. ROAD BUMP TEST

The frequency response is the main method to evaluate the behaviour of a system. In reality, a road profile as defined by equation (2.6) will not occur often, if ever at all. For that reason, another method of performance evaluation will be employed. In order to get a better understanding of how each system behaves under more realistic inputs, the road bump test is used.

Figure 2.4 shows the road profile, or vertical road displacement, that is used for the road bump test. This simulates a regular road bump of a height of 0.06 m. The time domain signals will allow us to better understand the improvements of each system. Figure 2.5 shows the results of the IWM passive model for a road bump test. It shows the motion of the system while being excited by the signal as displayed in figure 2.4.

The road bump test results show that the displacement of the unsprung mass is primarily excited by the road

---

[2] The performance of the Base model has been defined using the same damping value as the Nominal model.

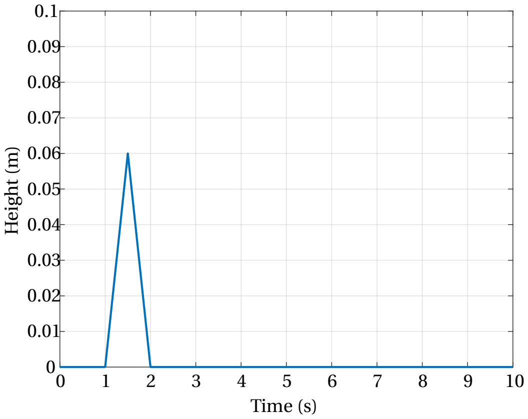

Figure 2.4: *Road profile for the road bump test*

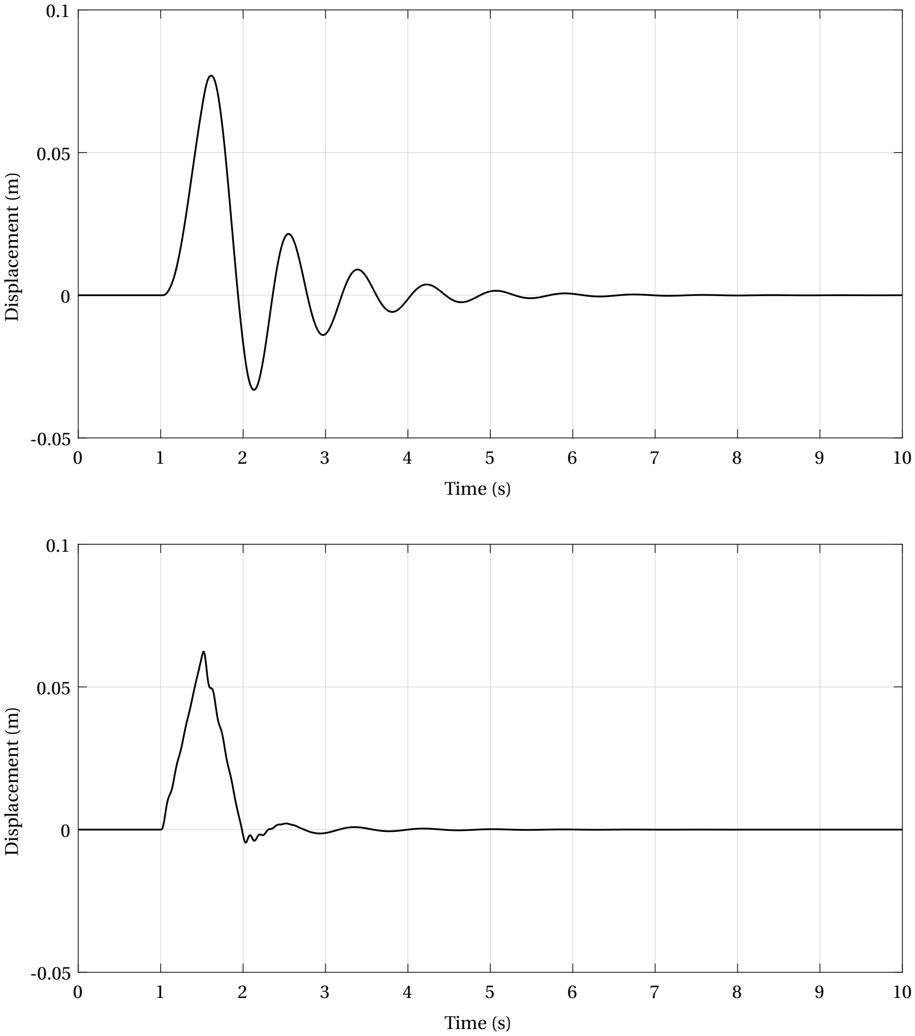

Figure 2.5: *Sprung (top) and unsprung (bottom) mass motion for the Nominal model during the road bump test*

displacement itself. The high tyre stiffness almost directly transfers the road displacement to the unsprung mass. It also causes small, persisting, oscillations. As the tyre damping coefficient is assumed to be negligible, the only damping in the system occurs by the damper between the sprung and unsprung masses. These responses will be used as a reference to compare with other systems.

2.6. FULL VEHICLE MODEL

For the full vehicle simulation, IPG CarMaker™[13] will be used to carry out the simulations. IPG CarMaker is especially developed for testing passenger cars and light-duty vehicles. It uses a detailed vehicle model, as well as a multibody system for the suspension at each wheel. It uses the TNO Delft Tyre, also known as the Magic Formula Swift tyre model for the tyre forces[20] to generate realistic tyre forces. Figure 2.6 shows the model of the vehicle used for the simulations.

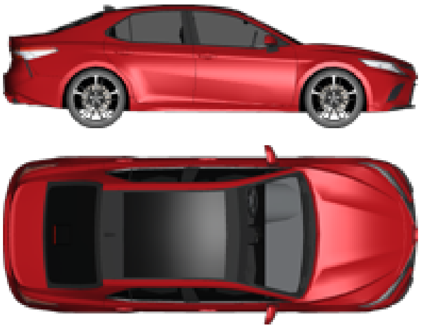

Figure 2.6: *Image of the IPG vehicle model used for the simulations..*

The vehicle model parameters that were used for these simulations can be found in table 2.2

Table 2.2: *IPG CarMaker™ Simulation vehicle parameters*

	Property value
Total vehicle weight	1619.96 kg
Wheelbase	2.800 m
CoG distance to front axle	1.075 m
CoG distance to rear axle	1.725 m
Front spring stiffness	$25\,000\,\mathrm{N\,m^{-1}}$
Rear spring stiffness	$30\,000\,\mathrm{N\,m^{-1}}$
Front damping ratio	$2500\,\mathrm{N\,s\,m^{-1}}$
Rear damping ratio	$3000\,\mathrm{N\,s\,m^{-1}}$

2.7. FULL VEHICLE SIMULATION ROAD INPUT

In order to analyse more realistic situations, four different road types have been analysed, all of which will be detailed in this section.

Each of the road models are obtained by mapping different segments of the Gerotek Testing facility[14], which is used by manufacturers worldwide. These segments have been carefully designed and mapped for use in realistic simulations[2].

2.7.1. ROAD PROFILE - PARALLEL CORRUGATIONS

The first road used for simulations is a road with parallel corrugations over the length of the test track. Figure 2.7 shows the height map of the digital road profile. These corrugations have a height of 25 mm and are equally spaced in the longitudinal direction.

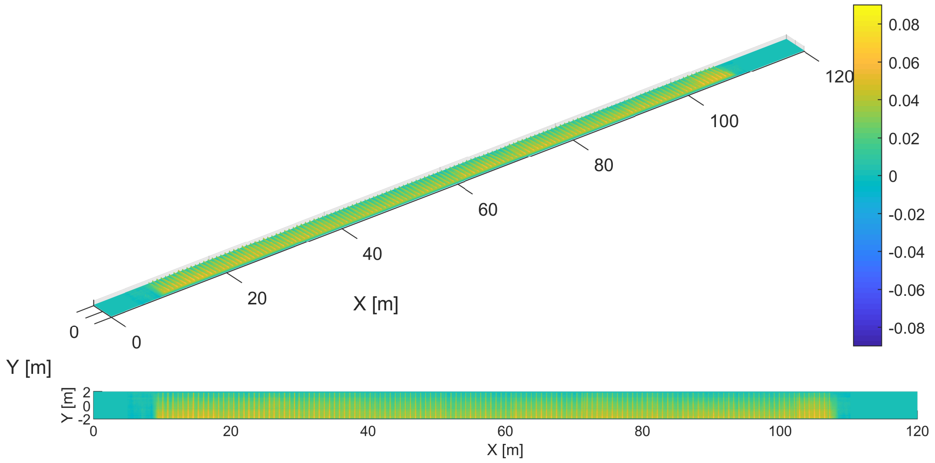

Figure 2.7: *Height map of the road with parallel corrugations used for full vehicle simulation.*

2.7.2. ROAD PROFILE - ANGLED CORRUGATIONS

The second road resembles the corrugations of the first road. For this segment, the corrugations are not completely perpendicular to the longitudinal driving direction, but angled by a varying angle over the length of the road in order to increase the amount of roll induced by the road displacements. Figure 2.8 shows the height map of the angled corrugated road.

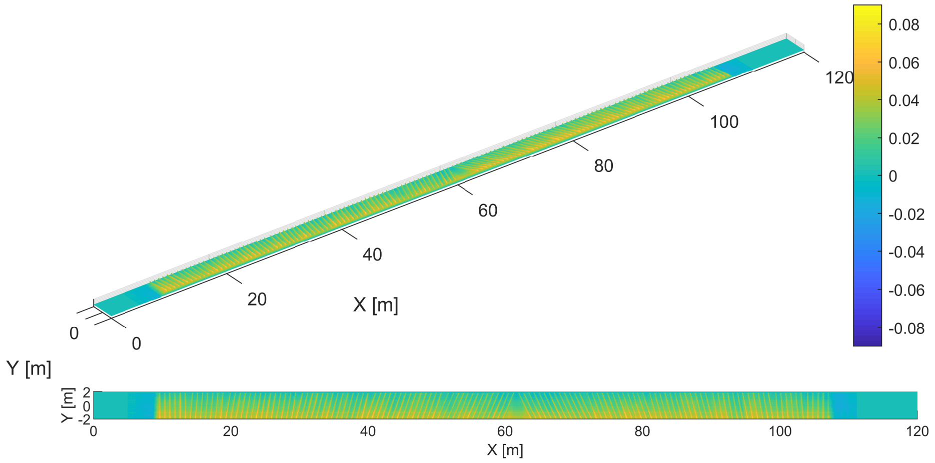

Figure 2.8: *Height map of the road with angled corrugations used for full vehicle simulation.*

2.7.3. ROAD PROFILE - POTHOLES

The third road profile contains potholes. This road has been designed to test the capabilities of heavy duty vehicles by having them cross potholes with a depth of 80 mm. The height map of the pothole road segment can be found in figure 2.9.

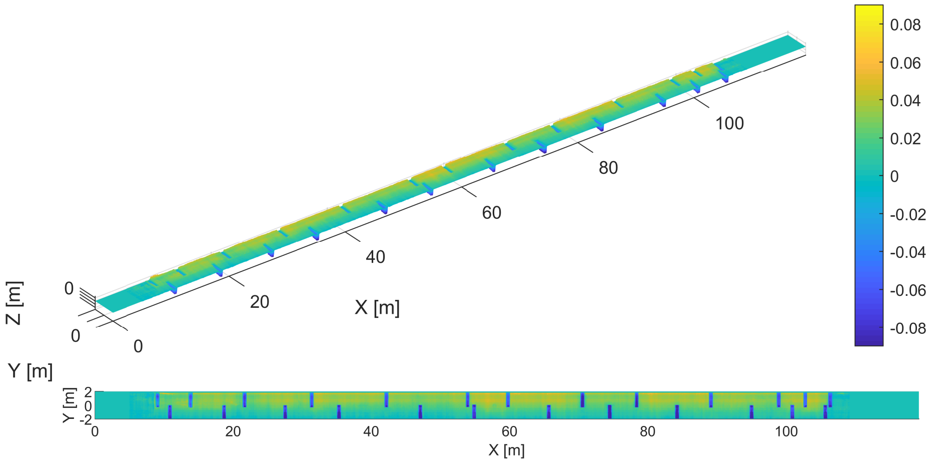

Figure 2.9: *Height map of the 'Potholes' road used for full vehicle simulation.*

2.7.4. ROAD PROFILE - FATIGUE

The final road profile that will be used for the simulation is the 'Fatigue' road. This road segment has been designed to accelerate the fatigue life of the suspension by performing repeatable and comparative suspension tests under simulated conditions. The resulting road has a relatively high RMS value for the road roughness. Though it might seem in figure 2.10 that the road is relatively smooth, the continuous roughness of the road results in extreme vibrations in the vehicle.

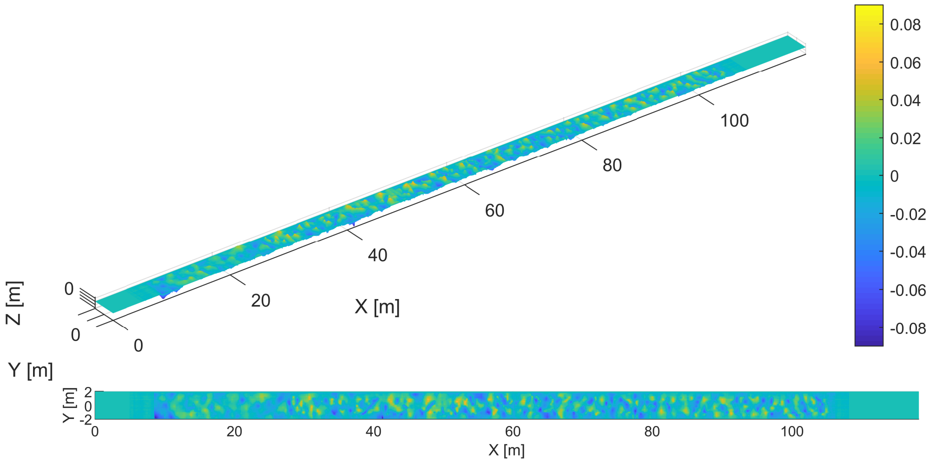

Figure 2.10: *Height map of the 'Fatigue' road used for full vehicle simulation.*

Figure 2.11 shows the actual road segments at the Gerotek testing facility. On the pictures a mapping device can be seen which was used to create the digital height maps of each of the road profiles.

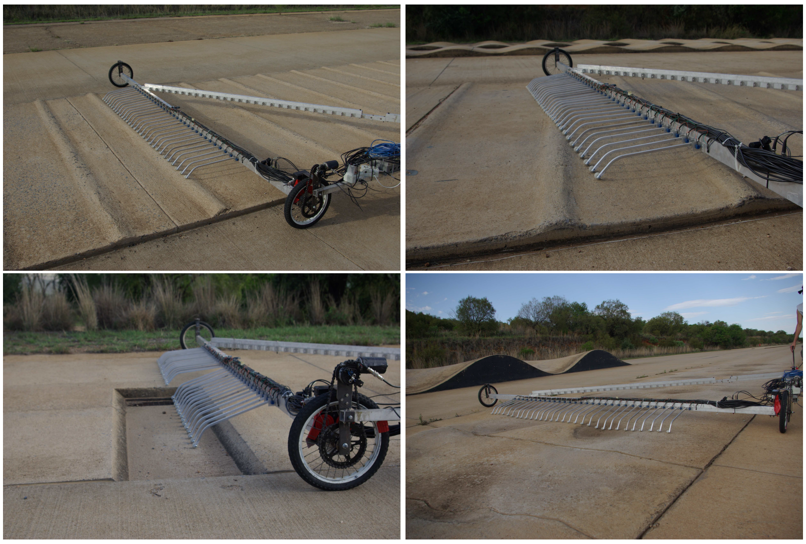

Figure 2.11: *Each of the road profiles at the Gerotek testing facility being mapped for digital use.*[2]

2.7.5. ROAD PROFILE ROUGHNESS

Each of these road profiles has been analysed in terms of its roughness coefficient and index by using an inverse power law equation[2]:

$$S_z = A\phi^n \tag{2.12}$$

Where A is the road roughness coefficient, n the road index and ϕ is determined as the spatial frequency of the road profile. The road roughness coefficient is an indication of the magnitude of the individual road profile disturbances. This describes the severity of the individual disturbance events. The road index n is tied to the spatial frequency of the disturbances ϕ.

The index is therefore an indication of the severity of the disturbance events when they are spaced according to spatial frequency ϕ. The index is therefore an indication of the severity of the overall ride rather than an individual event.

These two parameters, A and n, can be used to identify the characteristics of the road profiles. Table 2.3 shows the roughness coefficient and index values for the road profiles as obtained from the Gerotek testing facility.

Table 2.3: *Roughness coefficient and index per road profile.*[2]

	Roughness coefficient $A\left(\frac{m^2}{cycles \cdot m^{-1}}\right)$	Index n
Parallel Corrugations	$2.2 \cdot 10^{-6}$	1.6
Angled Corrugations	$7.67 \cdot 10^{-6}$	1.9
Potholes	$5.30 \cdot 10^{-5}$	2.2
Fatigue	$3.42 \cdot 10^{-5}$	2.9

It shows that the Potholes road contains the highest road roughness coefficient while the Fatigue road displays the highest index number. This can be explained by examining the inverse power law of equation (2.12). This shows that the Potholes can be considered of a higher roughness due to its extremely large displacements in the road profile. The Fatigue road, on the other hand, is less rough but the spacing of the displacements imply that the repeated motions have a greater influence on the overall power spectrum.

2.8. FULL VEHICLE EVALUATION

As it is unrealistic to encounter a road profile that resembles a chirp signal, the performance of the proposed models will be analysed in the time domain for more realistic road profiles as well. For these simulations, one cannot assume there will be sufficient frequency information to generate a proper frequency response. The previously introduced performance metrics, which are based on frequency responses, are therefore not adequate to analyse these time domain analyses. This section will therefore introduce other performance metrics to assess the performance in more realistic environments. Note that these performance metrics and evaluation methods are primarily used for the full vehicle simulation, but will also be used in evaluation of the QC simulation where a frequency response analysis is not feasible.

2.8.1. RIDE COMFORT

The main objective of the proposed models is to improve on the overall comfort of IWM vehicles. This section introduces several metrics by which to measure the comfort of the proposed models. The comfort is directly related to the vibrations of the driver's body, known as Whole Body Vibrations (WBV). In these simulations, the driver body itself will not be simulated. The first contact point that is included in the simulation, is the vehicle body, or sprung mass. At this point, the sprung mass accelerations will be used as a starting point to determine the model comfort performance.

VERTICAL ACCELERATION COMFORT

WBV contribute differently to the perceived comfort depending on several factors [21]. The main parameters to determine the effect of a vibration are magnitude, frequency, and direction. Obviously, magnitude is generally directly included in the calculation of comfort. As the signal values are generally integrated over a select time period, a large magnitude vibration results in a large contribution to the overall value. In this type of calculation, vibration frequency and direction are generally not readily included. As these simulations focus only on vertical accelerations, it is important to determine just exactly how this impacts the perception of comfort for the proposed models.

For these different directions and frequencies, weighting filters have been determined to accurately correspond to measurement data[22]. For vertical accelerations, a weighting filter has been designed with the following characteristics:

$$W_v(s) = \frac{87.72s^4 + 1138s^3 + 11336s^2 + 5453s + 5509}{s^5 + 92.6854s^4 + 2549.83s^3 + 25969s^2 + 81057s + 79783} \tag{2.13}$$

The frequency response of this filter is shown in figure 2.12. It can be seen that the human body is most perceptive for vibrations around 7 Hz when attributing vibrations to comfort. Coincidentally, the area where the human body is more perceptive to vibrations, is the same area that the UNS improves on.

Since the simulations are all based on Simulink™ modelling, the obtained signals can be frequency weighted by applying a transfer function using the definition in equation (2.13).

MOTION SICKNESS

Motion sickness is often not investigated during the comfort analysis of systems. It is, however, not easily assumed to be negligible. If a system results in motion sickness for the driver, after all, the system cannot be considered to be comfortable. Another weighting filter has therefore been designed to assess the performance of a vehicle in terms of motion sickness as well[22]. This filter is defined by the following characteristics:

$$W_{ms}(s) = \frac{0.1457s^4 + 0.2331s^3 + 13.75s^2 + 1.705s + 0.3596}{s^5 + 7.757s^4 + 28.37s^2 + 18.52s + 7.230} \tag{2.14}$$

These characteristics result in a filter of which the magnitude response can be viewed in figure 2.13. It is immediately apparent that motion sickness is caused by vibrations of a completely different frequency range than discomforts. Vibrations below and up to 1 Hz are shown to be the main contributors to motion sickness. Any frequencies above 1 Hz almost completely insignificant. This shows that a studies focussed purely on frequencies higher than 1 hertz will not inherently reduce motion sickness when improving comfort. It is therefore important to also incorporate analyses for motion sickness in order to obtain a more complete image of the model performance.

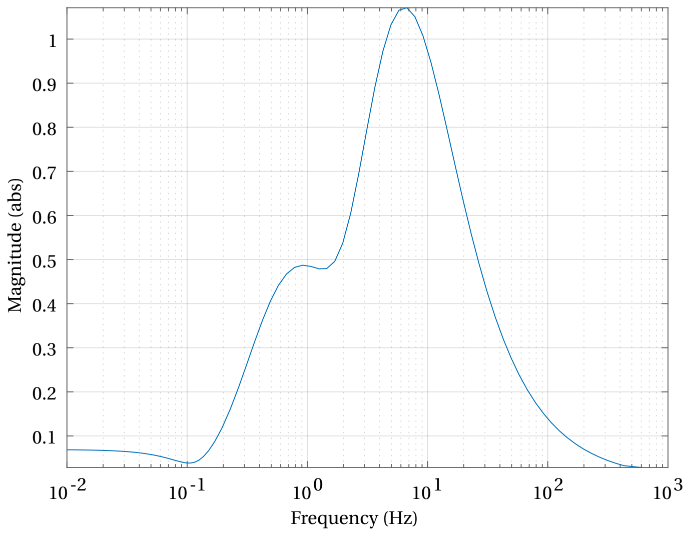

Figure 2.12: *Vertical acceleration frequency weighting filter*

Like the vertical acceleration frequency weighting, the motion sickness weighting is applied by a transfer function corresponding to that of equation (2.14).

VIBRATION DOSE VALUE

Using the previously introduce weighting filters will result in acceleration signals that are each adjusted for different purposes. These weighted signals can then be used to compare different systems for identical input signals. A direct comparison will then be able to identify the superior model in terms of either vertical acceleration comfort or motion sickness.

When the results of one measurement are compared to those of another measurement using different input signals however, an easy comparison cannot be made. An attempt was therefore made to represent the model performance for a signal type as a single value.

A common method to achieve this is through the use of Root Mean Square (RMS) values. This method is efficient for steady state processes as it calculated an average value over time. Vehicle vibrations cannot be assumed to be steady state. Aside from that, averaging values are not accurate for another reason. A short, very uncomfortable ride may, for instance, be more comfortable than a slightly uncomfortable ride of a much longer durations. The average values would claim the opposite to be true. A method that incorporates a solution for these issues is the Vibration Dose Value (VDV)[21]:

$$\mathrm{VDV} = \left[\int_{t=0}^{t=T} a_w^4(t)\,\mathrm{d}t \right]^{\frac{1}{4}} \tag{2.15}$$

Where $a_w(t)$ is the frequency weighted acceleration signal. Opposed to the RMS, the VDV isn't divided by the measurement duration T. This results in a non-averaging method and allows a comparison between two completely different situations.

The weighting filters for vertical vibrations as well as motion sickness will be used to determine the corresponding accelerations signals[23]. The VDV will then be applied to both frequency weighted signals in order to obtain values for the comfort due to vertical accelerations and motion sickness.

PEAK ACCELERATION

Not only the overall comfort of the models are important to define their characteristics, the ability to attenuate high magnitude vibrations is also characteristic to each model. Aside from the values obtained by the VDV, the peak acceleration is also obtained. It has been shown that the peak acceleration of Whole Body Vibrations

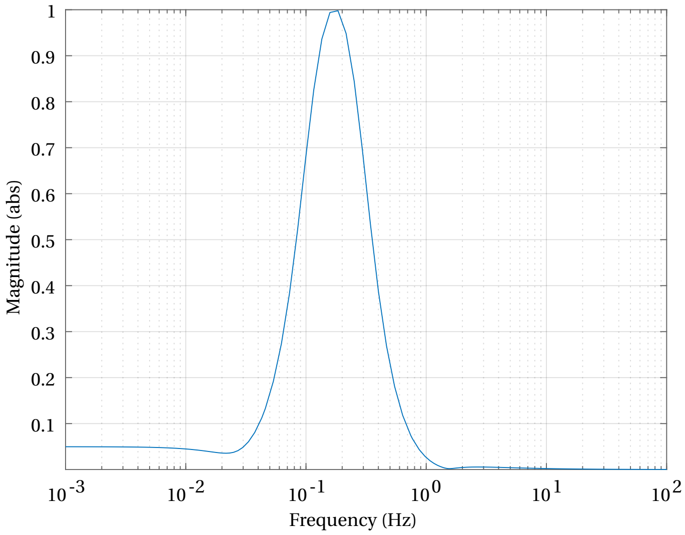

Figure 2.13: *Motion sickness acceleration frequency weighting filter*

is used to asses specific parts of the body[24]. In this simulation, the human body will not be simulated. Instead the peak acceleration of the vehicle body is determined as this will provide insights of the vibrations that are directly passed on to the passenger's body.

2.8.2. ROAD HOLDING CAPACITY

According to the classic design trade-off, road-holding capacity is compensated when ride comfort is improved. The newly proposed models are an attempt to improve on the overall performance of the UNS model. It is therefore necessary to determine the performance in terms of road-holding capacity as well.

Road-holding generally suffers from large variations in the tyre load. Road-holding oriented control methods are therefore aimed at reducing tyre vibrations in order to reduce load variations as well. This means that the tyre load variation is a good measure for road-holding performance.

$$\sigma_{Fz} = \sqrt{\frac{1}{T}\int_{t=0}^{t=T} \frac{(F_z(t) - F_{z0})^2}{F_{z0}^2}\mathrm{d}t} \tag{2.16}$$

Where F_z is the tyre load, either measured or calculated by the tyre deflection. F_{z0} is the stationary tyre load. Equation (2.16) then defines the standard deviation of the normalised tyre load. A deviation closer to 0 is then more beneficial for the road-holding capacity.

2.8.3. CONTROL EFFORT

Finally, not only the effective performance of the new control method is analysed, but also the amount of energy that is required. The control effort is a means to identify which system requires the least energy to operate. This is beneficial for all systems, but especially so for electric systems, where the energy is otherwise available to the driving motor. A good way to measure the control effort is by examining the absolute maximum control output. Since the controller output for this system is a force, the control effort is determined by the maximum exerted force for the measurement.

$$e_c = \max\left(\left|F_c(t)\right|\right) \tag{2.17}$$

Note that, opposed to the other performance metrics, the control effort metric cannot be normalised for the nominal model. Since the nominal reference model is passive, it contains no control force and can therefore not be used to directly compare the results. The control effort performance will thus be judged by their absolute values.

2.9. VEHICLE MODEL SELECTION

This research focuses mainly on vertical motion of the vehicle, also known as heave. The full vehicle model also introduces additional motion, such as rotations around one or more axes. For the purpose of comparing different control methods with respect to vehicle ride it is not necessary to retrieve information about these rotations. The vibrations caused by the vertical motion of the vehicle contribute the most to the perception of vehicle ride comfort[25]. The aim of the new model is to reduce vertical motion of the vehicle by influencing the suspension characteristics. Even though rotational motion will contribute to the actual comfort of the vehicle, the control method will not incorporate any information of the vehicle's rotations nor will it depend on this information. It will therefore suffice to employ the quarter car model for the purpose of analysing the effect of different control methods.

The quarter car model will be used develop a new control method and to analyse the effects of the new control method on the vehicle dynamics. When the control method has been developed, it will also be applied to a full vehicle model for more rigorous simulations. This will of the opportunity to see how the interpreted results of the QC model translate to the full vehicle dynamics and will offer a more realistic set of results.

3

STATE OF THE ART SUSPENSION MODELLING AND CONTROL

The dynamics of different suspension types have already been thoroughly researched[26]. In this section, state-of-the-art suspension control methods will be detailed, explained, and compared. This will not only offer an overview of the state-of-the-art control methods, but also an opportunity to compare proposed control methods with the current established control methods.

3.1. IN-WHEEL MOTOR DESIGN

Recent developments have made way for new technologies to be adapted more properly. The development in the field of electrically propelled vehicles has paved the way for the rise of In-Wheel Motor (IWM) design[27]. In traditional design, a single large power train is used to supply the power for vehicle propulsion. This power is then transported to the vehicle's wheels by the drivetrain. In IWM design, the main power train is replaced by multiple smaller power trains. Each of these power trains consists of a smaller electric motor that is located at one of the wheels of the vehicle. This relocation of the power train reduces the mechanical distance between the motor and the wheels, i.e. there are less mechanical parts and connections required to transfer the power from the motor to the wheel. As every mechanical transmission has a non-perfect efficiency, reducing the amount of mechanical transmissions will increase the overall efficiency of the power train.

The IWM design, however, also brings along some issues. The different, smaller, engines are now attached to the wheel hubs of the vehicle, rather than the vehicle chassis. This causes a change in the dynamic behaviour of the vehicle. For simplicity, the QC model divides the vehicle into two separate masses, as shown in figure 2.1. These two masses are called the sprung and unsprung mass. The sprung mass is the mass of the vehicle chassis and body. The unsprung mass encompasses the wheels as well as the suspension system. Since IWM design places the electric motors directly at the wheel hubs, this adds to the unsprung mass. As the conventional ICE is no longer present, the sprung mass is decreased at the same time.

In order to compare the conventional design vehicle with the In-Wheel Motor design, a passive IWM model has been used to show the differences in dynamical behaviour. The conventional model is defined as a quarter car model of a conventional ICE vehicle, as defined previously by the properties of table 2.1. The IWM vehicle is then defined by increasing the unsprung mass of the conventional model by 25%. The sprung mass is then reduced by an equal amount in order to keep the sum of both masses equal in both cases. Table 3.1 shows the properties of the IWM vehicle model.

Table 3.1: *Vehicle properties: Conventional vehicle vs. IWM vehicle*

Property	Conventional model	IWM model
m_s	500 kg	480 kg
m_u	80 kg	100 kg

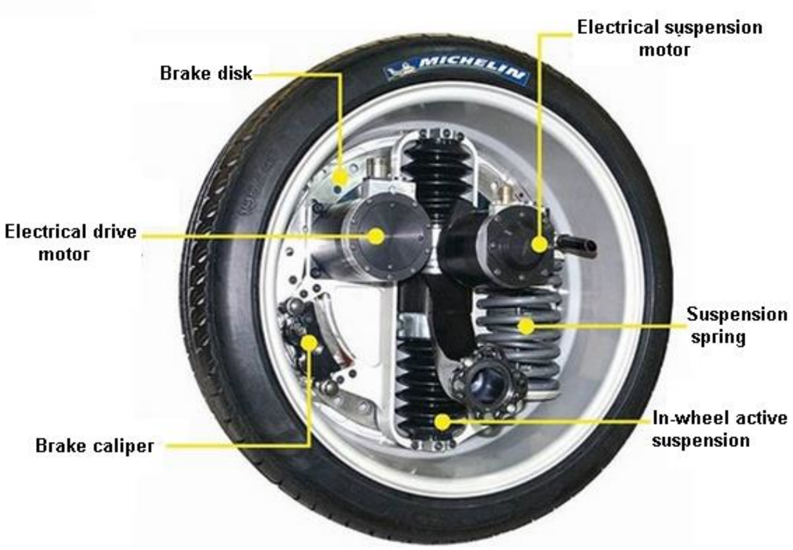

Figure 3.1: *Michelin Active Wheel: An In-Wheel Motor design concept by Michelin*

This change in vehicle properties will have an influence on the dynamic behaviour of the vehicle. One of the simplest ways to investigate a change of behaviour is by examining the natural, or resonance frequencies of the vehicle. These resonance frequencies are a quick and easy way to acquire a primary indication of the change in vehicle dynamics. In general, the resonance frequencies of a 2 D.o.F. QC model are defined as:

$$\omega_s = \sqrt{\frac{1}{m_s}\frac{k_s k_t}{k_s + k_t}} \qquad \omega_u = \sqrt{\frac{k_s + k_t}{m_u}} \tag{3.1}$$

The IWM model is created by increasing the unsprung mass of the conventional model by 25%. As this increase in mass represents the electric motors that are added to the wheel hub, the absence of the ICE should also be taken into account. For simplicity, the four electrical motors are assumed to have a total mass equal to the ICE. In order to simulate the ICE being replaced by electric motors, the sprung mass is reduced by an amount equal to the amount of mass that is added to the unsprung mass.

As the sprung mass is generally much greater than the unsprung mass, the ratio of the sprung masses of the conventional and IWM vehicles are much smaller than the ratio of the unsprung masses. In other words, increasing the unsprung mass by 25% and reducing the sprung mass by an equal amount of mass, will generally imply a reduction much less than 25% of the sprung mass. The effect of this transfer will therefore have a greater effect on the resonance frequency of the unsprung mass ω_u than on that of the sprung mass ω_s. The resonance frequencies for the conventional model are calculated at:

$$\omega_s^{\text{conv}} \approx 1.18\,\text{Hz} \qquad \omega_u^{\text{conv}} \approx 10.22\,\text{Hz} \tag{3.2}$$

After transferring the mass from sprung mass to the unsprung mass, the resonance frequencies of the IWM model become:

$$\omega_s^{\text{IWM}} \approx 1.20\,\text{Hz} \qquad \omega_u^{\text{IWM}} \approx 9.14\,\text{Hz} \tag{3.3}$$

As the unsprung mass undergoes the larger relative transformation, the unsprung resonance frequency will therefore also change the most. This change in resonance frequencies will have an impact on the overall behaviour of the IWM model. As the sprung mass m_s is slightly decreased, the sprung mass resonance frequency

Table 3.2: *Complete list of physical properties of the controlled IWM vehicle models*

Property	Value
m_s	480 kg
m_u	100 kg
k_s	30 000 $\mathrm{N\,m^{-1}}$
c_s	1200 $\mathrm{N\,s\,m^{-1}}$
c_{as}	800 $\mathrm{N\,s\,m^{-1}}$
k_t	300 000 $\mathrm{N\,m^{-1}}$
c_t	0 $\mathrm{N\,s\,m^{-1}}$

ω_s will slightly increase. Vice versa, since the unsprung mass m_u is increased, the resonance frequency ω_u will obviously decrease.

To find out how the behaviour differs exactly due to these shifts of the natural frequencies, we will need to establish criteria on how to evaluate different systems first. It will then be possible to find out exactly what happens when the unsprung mass is increased. This will also enable us to determine the overall performance of the models in question.

3.2. SUSPENSION CONTROL

In an attempt to improve on the comfort of vehicles, control methods have been developed to control the suspension dynamics of the vehicle. In order to influence the dynamic behaviour, a control force has to be exerted on the system. Ideally this control force is exerted only on the body that we wish to affect. In practice it is not possible to introduce such a force. This would mean that a vehicle body should connect to a point in space which does not move with respect to the vehicle's centre of gravity. It is impossible to create such a point. Instead, the behaviour of the control methods can be approached by an actuator that is connected to the sprung- and the unsprung masses. These actuators can generally be divided into two different types. These types will be discussed in the following section. Table 3.2 gives a complete overview of the vehicle parameters that will be used for the controlled IWM vehicle models. Note the inclusion of the active suspension damping ratio c_{as} in this list. This damping ratio will be the amount of damping that the controlled systems can add to the existing passive damping ratio. Whenever a damping ratio for a semi-active or active system is defined in the rest of this research, it will use this active system damping ratio.

3.2.1. SUSPENSION CONTROL CLASSIFICATION

There are different ways to approach the control of a suspension system. These different approaches be divided into several different categories of which this research will include two:

- Active damping
- Semi-active damping

The difference between these classifications is the operating principle on which the damper is based. Fully active dampers are actuators that can exert a force on the system as desired. These dampers can therefore be used to introduce additional forces very accurately according to the user's desires. This force is calculated by the internal model. The benefit of this type of suspension is that the control force can be accurately generated. This type of suspension does however require incredible amounts of power in order to generate the required force on the vehicle bodies.

Semi-active dampers are based on a very different approach. Instead of introducing a force directly by means of an actuator, semi-active suspensions alter the damping characteristics of the suspension. This way, the behaviour of the system can still be altered according to the user's desires, albeit less extensively when compared to fully active systems. The benefit of this type of system is that the energy consumption is incredibly low when compared to fully-active suspensions. The drawback is that the forces generated by these systems are generally a much less accurate approach of the desired forces.

These different working principles result in different requirements for each system. A simple comparison [4] shows how different types of have different characteristics.

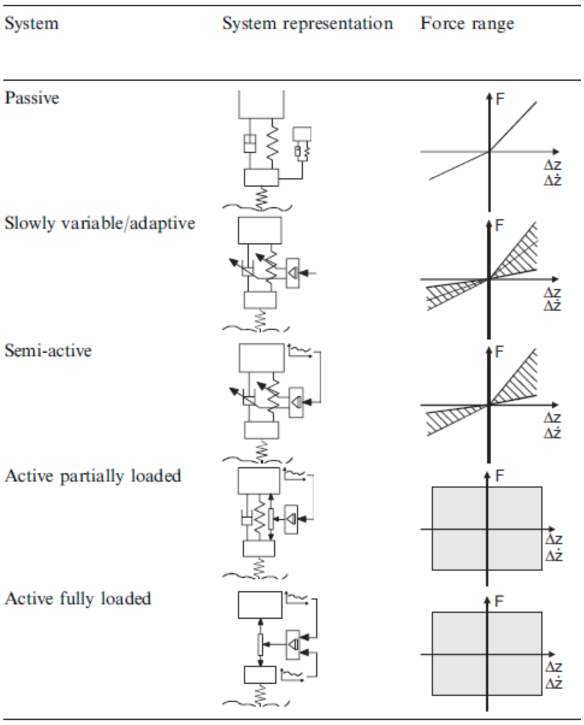

Figure 3.2: *Overview of different suspension system categories in terms of activity/passivity[3]*

Figure 3.2 shows an overview of different suspension types[1]. For this research the focus will be on the semi-active and the partially loaded active system. Their main difference in operating range can be found at the force range of each suspension type[28]. The semi-active system is bound to the passivity constraint, which means it cannot actively introduce energy into the system, therefore the forces are bound to reside in the first and third quadrant of the force vs. suspension velocity graph. The controllability of semi-active systems can be found in the slope of this force curve, which represents the damping coefficient, which can be influenced. Simple systems are often able to switch between two different coefficients whereas more complex systems are able to alter the slope within a certain range.

The active systems can generate forces in all four quadrants, indicating that this type of system is able to actively introduce energy into the system. This adds a lot of flexibility to the system.

Another notable difference is found at the power consumption. It is obvious that there is a large difference between the systems in this area. In order to create a force, an equal amount of energy is needed in another form. The actuator of the active system can then convert this energy into the desired force. In order for the suspension to have an influence on the behaviour the amount of energy required is incredibly high.

The energy required for a semi-active suspension is on the other hand very low. These systems only use additional energy to alter the damping characteristic of the variable damper. The resulting damping force can be adjusted so that is simulates the effect of an additional force. Of course it will not be possible to achieve the same results with a semi-active suspension as with a fully active one.

The benefits of reduced energy consumption by semi-active suspensions, however, do outweigh the drawbacks of reduced effectiveness when compared to fully active systems. On top of that, semi-active suspensions are also much less expensive to design and fabricate. These combined benefits are the main reasons manufacturers prefer semi-active systems over fully active systems. In the next part of this chapter, both types of suspension will be discussed.

---

[1] A full overview of different suspension system characteristics can be found at figure A.1

3.3. SEMI-ACTIVE SUSPENSION CONTROL

In this section, different approaches to Semi-Active suspension control are discussed[29]. These control methods are aimed at improving the vehicle ride or performance by altering the suspension characteristics. The most notable control methods are the Skyhook and Groundhook control methods. These methods, a Hybrid method combining the two, and their Semi-Active applications are discussed in the following sections.

3.3.1. SKYHOOK CONTROL

In order to reduce the vibrations on the sprung mass of a vehicle, the Skyhook model was designed. This model introduces an imaginary damper to the system, connected to both the sprung mass and a fixed point in vertical space. This damper, as shown in Figure 3.3, introduces a force negatively proportional to the sprung body velocity. This force is intended to reduce vibrations by reducing the sprung mass accelerations. As these vibrations are the main causes of discomfort, it is desired to reduce these vibrations as much as possible. This newly introduced Skyhook model can be described as an additional force imposed on the sprung mass. The new E.o.M. are then defined for the following case, also known as the Ideal Skyhook model:

$$m_s\ddot{z}_s = c_s(\dot{z}_u-\dot{z}_s)+k_s(z_u-z_s)-F_{\text{sky}} \tag{3.4}$$
$$m_u\ddot{z}_u = -c_s(\dot{z}_u-\dot{z}_s)-k_s(z_u-z_s)+k_t(z_r-z_u) \tag{3.5}$$
$$F_{\text{sky}} = \dot{z}_s c_{\text{sky}} \tag{3.6}$$

In reality, it is obviously not possible to have a damper connected to a fixed point in space as it is intended for the Skyhook model. Instead, several control methods have been introduced as a way to approach the ideal Skyhook suspension behaviour. These models add damping to the passive suspension damping c_s in order to emulate the imaginary force that would be generated by the Skyhook damper c_{sky}.

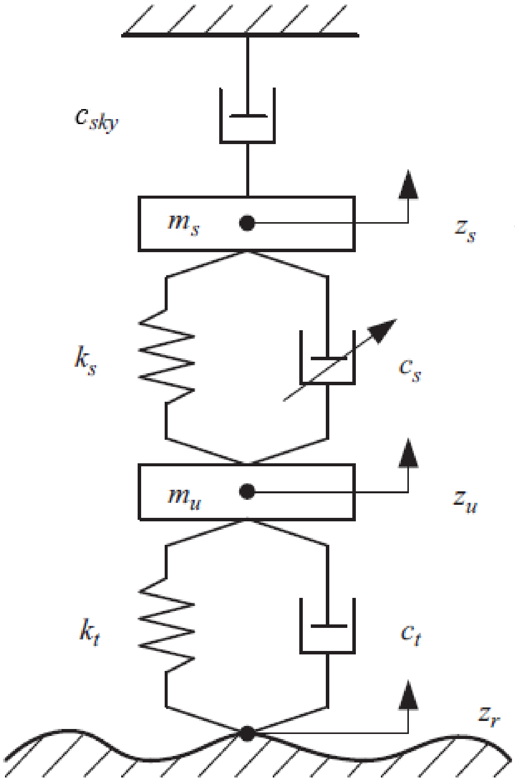

Figure 3.3: *Skyhook control system[1].*

SKYHOOK SEMI-ACTIVE CONTROL METHODS

In an attempt to simulate the behaviour of the Skyhook model as seen in Figure 3.3, different semi-active control methods have been designed. These control methods are an attempt to create the ideal Skyhook behaviour. The control laws are based on the different available damper types. This variable damper is shown in Figure 3.3 as c_s. In a simple Skyhook system, this variable damping is the only controllable variable. Different control methods can be achieved by using data from different system parameters. The rest of this section will elaborate on some of the most commonly used control methods used in suspension systems with a Skyhook control approach.

2-state control As mentioned before, the control method is partly based on the type of variable damper in the system. We have seen earlier that manufacturers have the option to use either fully active or semi-active suspension systems. The less expensive semi-active dampers are obviously preferred by manufacturers. One of the simplest approaches to a semi-active damper is a switching damper that can be switched to either its maximum or minimum damper ratio. The 2-state control approach uses this property and switches the damper ratio based on the velocities of both the sprung and unsprung mass. The 2-states control approach can be described as follows:

$$c_s = \begin{cases} c_{\max}, & \text{if } \dot{z}_s(\dot{z}_s - \dot{z}_u) > 0 \\ c_{\min}, & \text{otherwise} \end{cases} \tag{3.7}$$

This type of control uses only 2 different system parameters as a reference, namely the sprung mass and unsprung mass velocities. The second term of the condition in equation (3.7) describes the velocity of the suspension. Basically, this indicates that the damping ratio is switched to its maximum ratio when the sprung mass velocity is in the same direction as the suspension velocity. The suspension velocity is considered to be positive when expanding.

The benefit of this system is that its control output is extremely simply designed. Since the method only outputs the minimal or maximal damping ratio, the controller itself can be relatively simple. This has a benefit of being fast and responsive. It does not, however, approach the behaviour of an ideal Skyhook optimally. Other control laws attempt to improve on the 2-state control in different ways to improve the performance.

Linear control One way to improve on the previously explained 2-state control, is to increase the amount of control. The linear control does this by adjusting the damping ratio of the variable damper. This way the system closer resembles the behaviour of the ideal Skyhook as the resulting force is now not only dependent on the suspension velocity, but it is also controlled by the varying damping ratio. The linear control law is described as follows:

$$c_s = \begin{cases} sat\left(\frac{\alpha_{\text{sh}} c_{\max}(\dot{z}_s - \dot{z}_u) + (1-\alpha_{\text{sh}}) c_{\max} \dot{z}_s}{\dot{z}_s - \dot{z}_u}\right), & \text{if } \dot{z}_s(\dot{z}_s - \dot{z}_u) > 0 \\ c_{\min}, & \text{otherwise} \end{cases} \tag{3.8}$$

The parameter α_{sh} in equation (3.8) is the tuning parameter for the linear system. When tuning to $\alpha_{\text{sh}} = 1$ the system behaves identically to the 2-state control of equation (3.7). This parameter can be used to tune the system behaviour.

It should be noted that even though this system does not require any additional sensors, it does require a more sophisticated actuator. The measured units for this control can still be retrieved by the same sensors required by the 2-state system. The output of the control law is however not as easy as the 2-states control. The linear output covers damping ratios that are to be achieved on a continuous range. This increases the complexity of the total controller. Since the damping ratio of variable dampers are largely nonlinear, it is more computationally heavy to determine the desired control output that results in the desired damping ratio and, in turn, the desired damping force. Apart from that it is important to have an exact knowledge of the damping ratio in order to be able to control the damping ratio accurately. This trade-off in complexity should be considered when comparing the increased effectiveness of the linear model.

Acceleration Driven Damper (ADD) control Another way to improve on the simple 2-state control is to alter the control law conditions. In ADD control the system refers to the acceleration of the sprung mass instead of the sprung mass velocity but still employs the 2-State control outcomes[30]. The ADD control method can then be described as:

$$c_s = \begin{cases} c_{\max}, & \text{if } \ddot{z}_s(\dot{z}_s - \dot{z}_u) > 0 \\ c_{\min}, & \text{otherwise} \end{cases} \tag{3.9}$$

This form of control can be achieved with exactly the same sensors and actuation knowledge as the regular 2-state control. Usually the signal of an accelerometer is used to determine the velocity by integration. In this case, the direct signal of the accelerometer can be used for the switching law. This alteration is therefore incredibly easy to implement for the Skyhook systems while it promises a significant improvement in comfort.

SKYHOOK CONTROL METHOD COMPARISON

The previously described Semi-Active control approaches of Skyhook control are compared in this section. The most important indicators for performance are the accelerations of the sprung and unsprung masses, and the deflections of the suspension and tyre.

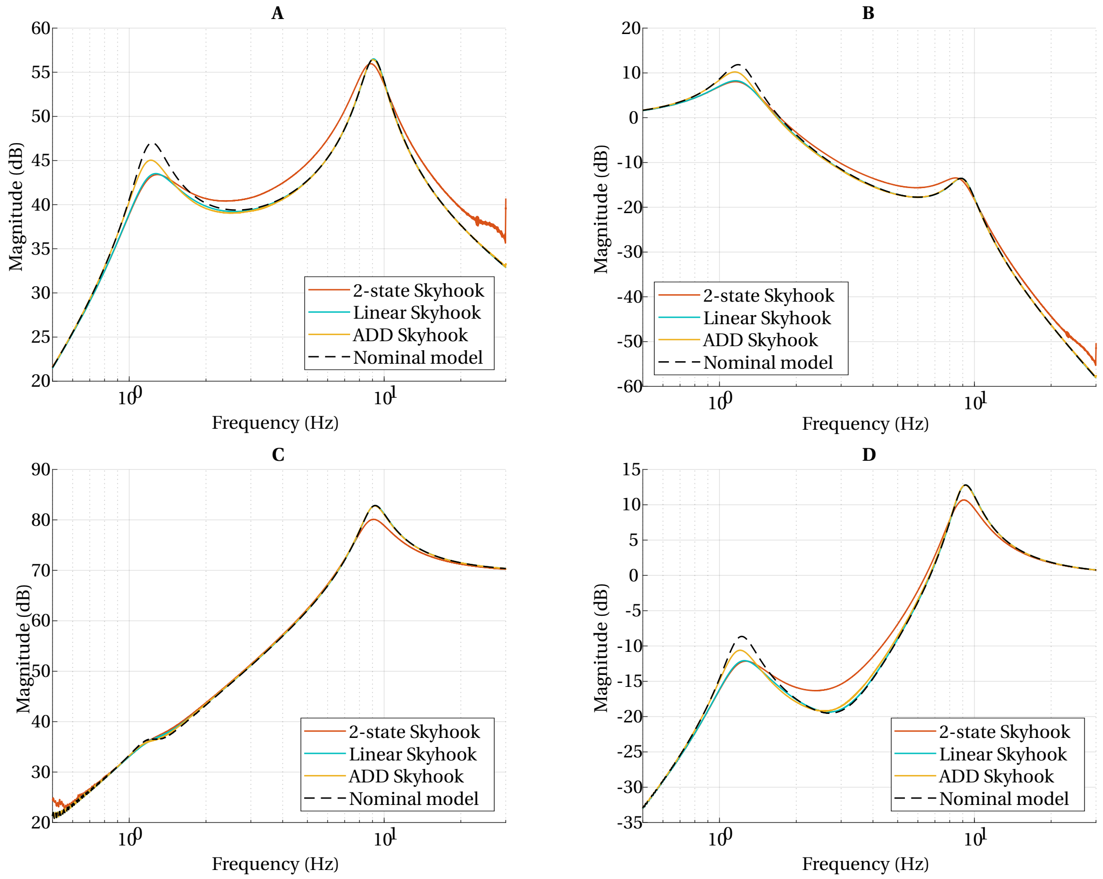

Figure 3.4: *Semi-Active Skyhook suspension control methods. Frequency response of A) Sprung mass acceleration B) Sprung mass displacement C) Unsprung mass acceleration D) Tyre deflection*

Frequency responses Vibrations of the car are the primary source of discomfort for drivers and passengers. Frequencies up to 25 Hz are attributed by the driver to the comfort of the vehicle. Vibrations of higher frequencies are attributed to road irregularities and are mostly dampened by the dynamic properties of the vehicle. The focus of the suspension results are therefore aimed at frequencies between 0 Hz and 25 Hz.

The first graph of Figure 3.4 shows the acceleration of the sprung mass. The large areas of the 2-State and ADD control result from the switching behaviour of the control method. Despite this negative switching behaviour, the overall improvement of the Skyhook can be seen when compared to the passive behaviour of the IWM QC model. It can be seen that all models show an improvement in the mid-frequency range (between the

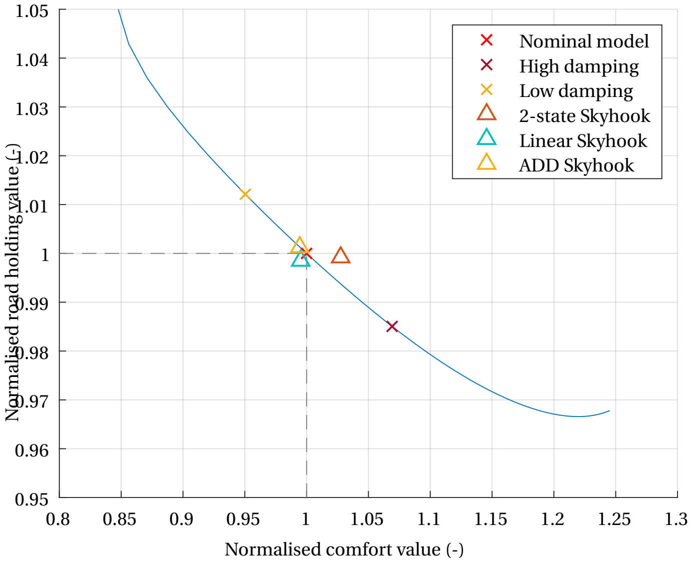

Figure 3.5: *Performance evaluation of the semi-active Skyhook methods versus the reference models: Nominal* ($c_s = 1200$) *- Low damping* ($c_s = 800$) *- High damping* ($c_s = 2000$)

resonance frequencies of the masses) and the high-frequency range (beyond the unsprung mass resonance frequency).

It can be seen that Linear approach and the ADD approach achieve approximately equal results in the mid- and high-frequency range. The main difference can be found at the sprung mass resonance frequency, where the Linear control method outperforms the ADD method. As stated previously, however, the Linear approach does require a more complex suspension system. It is therefore necessary to address the increased cost for the complexity when comparing the overall performance of these systems. Since the ADD approach equals the comfort levels of the Linear method but requires only a relatively simple suspension system, this system may be considered to be superior to the other Skyhook methods.

The other important KPI is the Road-Holding capacity of the system. It can be seen in the last graph of Figure 3.4 that the tyre deflections are also reduced. This means that the performance of the vehicle is also increased when considering the Road-Holding capacity of the Skyhook vehicle.

Performance evaluation The relative performance of the Skyhook approaches is also determined using the metrics as defined in equations (2.10) and (2.11). Figure 3.5 shows the relative performance of the different Skyhook systems when compared to the passive IWM model. The relative performance shows that the Skyhook models offer an increase in comfort performance while subtracting from the road holding performance. The graph also shows that the simplest control method, 2-state control, has difficulty on improving the model. At first glance it seems that the 2-state model doesn't improve on the vehicle performance of the nominal model. Keep in mind that this 2-state model switches its damping values between the nominal model and the model with damping ratio $c_s = 2000$. When comparing the 2-state model with the high damping passive model, the comfort is obviously increased very much.

It also seems that both the Linear control and ADD control methods offer the same improvement in terms of comfort. The linear model, however, also offer a slight improvement on the road holding performance whereas the ADD method offers a slightly worse road holding performance. This difference is however very small, and the increased mechanical complexity that is required for the Linear approach should be taken into account as well. Combining the performance of the ADD control approach with its relative simplicity, makes this arguably the best Skyhook control approach.

3.3.2. GROUNDHOOK CONTROL

The Groundhook control method is designed similarly to the Skyhook control method. However, for Groundhook control the imaginary damper is supposed to be connected to the unsprung mass as opposed to the sprung mass for the Skyhook control method. A schematic overview can be seen in Figure 3.6. This immediately has implications for the results of this control method. This type of control is more focused at reducing the motion of the unsprung mass. This will in turn reduce the tyre deflections, making the Groundhook a performance oriented control method. The ideal Groundhook model can be described as:

$$m_s\ddot{z}_s = c_s(\dot{z}_u - \dot{z}_s) + k_s(z_u - z_s) \tag{3.10}$$

$$m_u\ddot{z}_u = -c_s(\dot{z}_u - \dot{z}_s) - k_s(z_u - z_s) + k_t(z_r - z_u) - F_{\text{sky}} \tag{3.11}$$

$$F_{\text{gnd}} = \dot{z}_u c_{\text{gnd}} \tag{3.12}$$

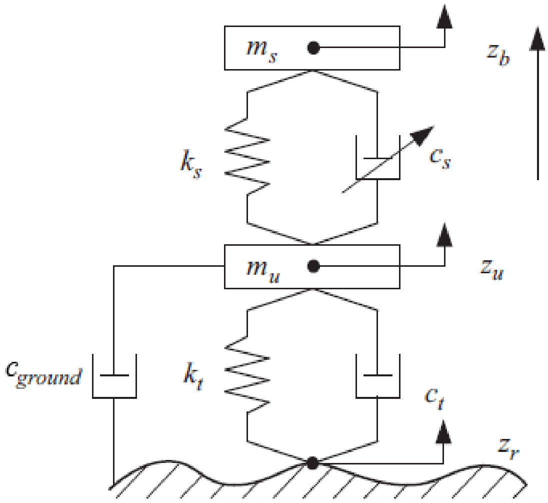

Figure 3.6: *Groundhook control system[1]*

The different control laws used with a Groundhook control method are similar to those as detailed for the Skyhook control method.

2-state control This control method is very similar to the 2-state control as it was proposed for the Skyhook suspension model. Of course, this control method is aimed at the unsprung mass instead of the sprung mass. The difference between the Skyhook 2-state control method of equation (3.7) and the Groundhook control of equation (3.13) is that the switching law now includes the unsprung mass velocity and the negative suspension velocity.

$$c_s = \begin{cases} c_{\max}, & \text{if } \dot{z}_u(\dot{z}_u - \dot{z}_s) > 0 \\ c_{\min}, & \text{otherwise} \end{cases} \tag{3.13}$$

The Skyhook 2-state control caused the suspension damping ratio to be maximal when the velocity of the sprung mass has the same direction as the suspension velocity. As the Groundhook model uses the unsprung mass and the negative suspension velocity, the damping ratio is switched to its maximum value when the directions of the unsprung mass and the suspension are opposing.

linear control As for the Skyhook control method, the Groundhook control method also includes a linear approach. As can be seen in equation (3.14), this approach follows the same concept as the linear control for Skyhook suspensions.

$$c_s = \begin{cases} sat\left(\frac{\alpha_{\mathrm{gh}} c_{\mathrm{max}}(\dot{z}_s-\dot{z}_u)+(1-\alpha_{\mathrm{gh}})c_{\mathrm{max}}\dot{z}_u}{\dot{z}_s-\dot{z}_u}\right), & \text{if } \dot{z}_u(\dot{z}_u-\dot{z}_s)>0 \\ c_{\mathrm{min}}, & \text{otherwise} \end{cases} \tag{3.14}$$

As seen before with the regular 2-state control approach, the differences between the Skyhook linear control (3.8) and the Groundhook linear control above is determined by the measured unit. This being the unsprung mass in this case as opposed to the sprung mass being used as a reference for the Skyhook models.

ADD control Finally, the ADD control approach has also been applied to the Groundhook system. It is no surprise that this control method follows the same trend as the previous models that are adapted to the Groundhook system.

$$c_s = \begin{cases} c_{\mathrm{max}}, & \text{if } \ddot{z}_u(\dot{z}_u-\dot{z}_s)>0 \\ c_{\mathrm{min}}, & \text{otherwise} \end{cases} \tag{3.15}$$

The control methods mentioned above are identical to those proposed for the Skyhook method. The next section will present the results of each of these methods when they are applied to the QC model. As with the Skyhook results, the control methods are assumed to be ideal without any actuator dynamics involved.

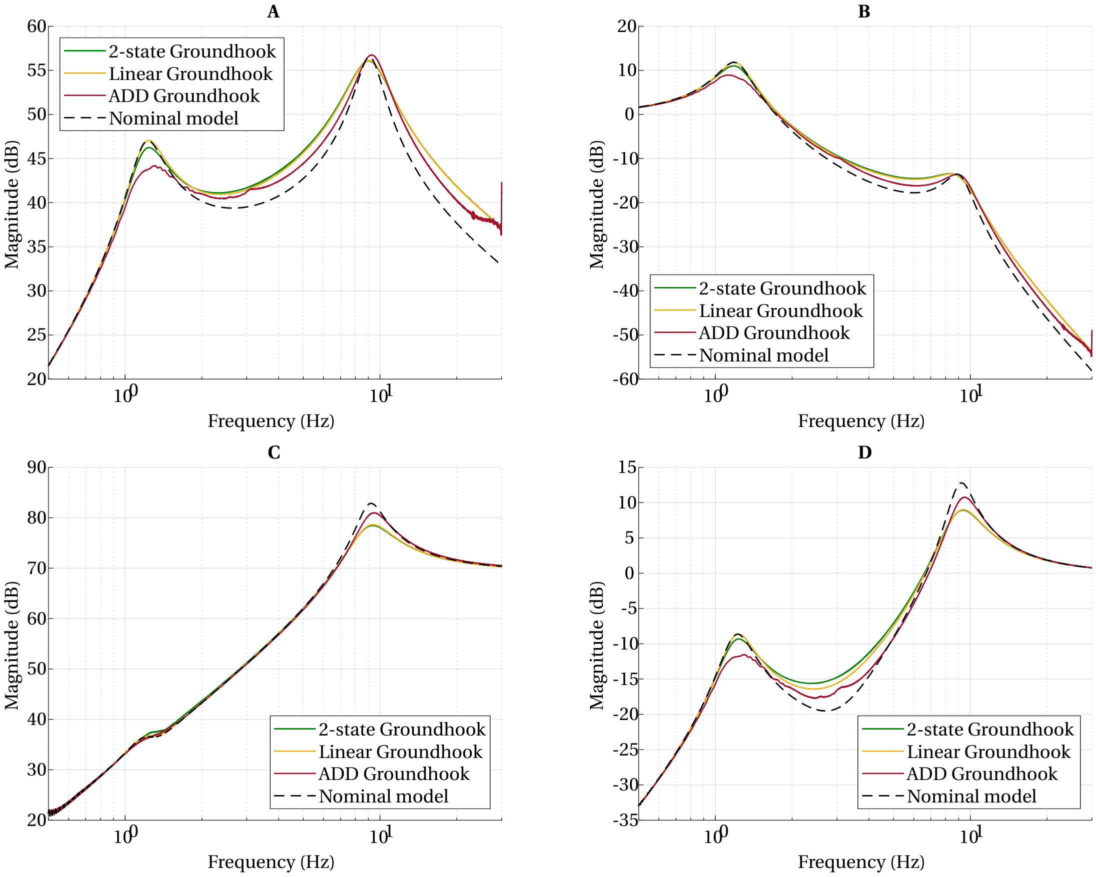

Figure 3.7: *Semi-Active Groundhook suspension control methods. Frequency response of A) Sprung mass acceleration B) Sprung mass displacement C) Unsprung mass acceleration D) Tyre deflection*

GROUNDHOOK CONTROL METHOD COMPARISON

Frequency response The Groundhook control results, shown in Figure 3.7, indicate an overall improvement for the system. It can be seen, however, that the Groundhook control method has less of a negative influence on the system dynamics close to the unsprung mass resonance frequency. An overall performance

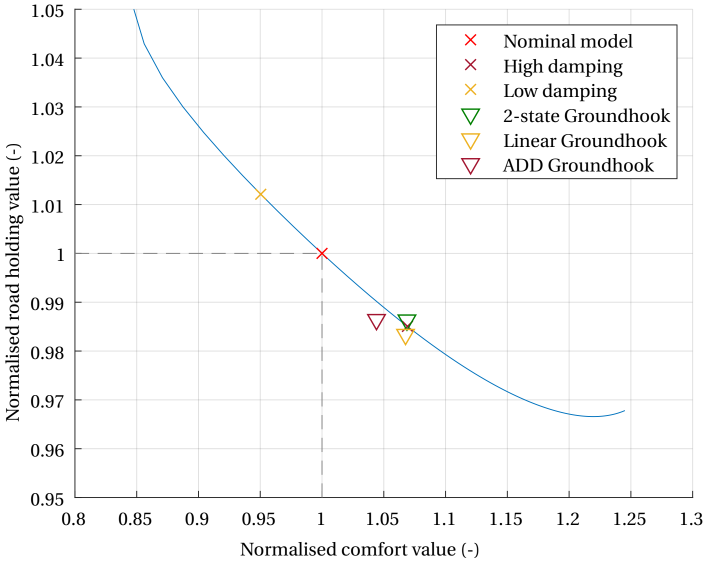

Figure 3.8: *Performance evaluation of semi-active Groundhook control methods versus the reference models: Nominal ($c_s = 1200$) - Low damping ($c_s = 800$) - High damping ($c_s = 2000$)*

value is generally calculated by integrating the measured signal and multiply it by a penalty weight. A lower value therefore indicates better performance. Since the vibrations are in general much higher round the unsprung resonance frequency, a reduction in vibrations at this area will have a larger impact on the overall performance value.

For the Groundhook control method this is especially true for the tyre deflection. Even though the vibrations at the sprung mass resonance seem to be worse than that of the Skyhook, the relative improvement at the sprung mass resonance have a greater impact on the overall performance. This does indicate that the Groundhook control method is more oriented towards Road-Holding capacity than it is comfort oriented.

Performance evaluation The relative performance of the Groundhook control methods are shown in figure 3.8. These results prove that the Groundhook is considered to be a road holding oriented control method as opposed to the comfort oriented Skyhook approach. They also show that the Linear approach once again offers the most improvement, this time in terms of road holding performance. Again, this total performance should be put into perspective as this method requires a more expensive and complex suspension system in order to function.

The simpler approaches, the 2-state and ADD control methods, show a comparable increase in road holding performance. The ADD method, however, offers the best comfort of the three Groundhook approaches. It is therefore easy to see that the ADD method outperforms the 2-state method. As with the Skyhook model, the superior method between the Linear and ADD method should be selected with regard to specific design objectives and the material cost of the suspension system in mind.

3.3.3. HYBRID CONTROL

Finally, there is also a method which tries to combine the best of both the Skyhook and Groundhook methods. This model is known as the Hybrid model and is represented by a linear combination of the two different systems[31]. This linear combination of both the Skyhook and Groundhook model defines the damping ratio slightly differently than seen before. The total damping ratio is divided into a passive and active component.

$$c_d = c_\mathrm{s} + c_\mathrm{hyb} \tag{3.16}$$

This change in definition is made in order to properly describe the Skyhook and Groundhook components. The passive component c_p is a constant value that represents the lowest achievable damping ratio. This

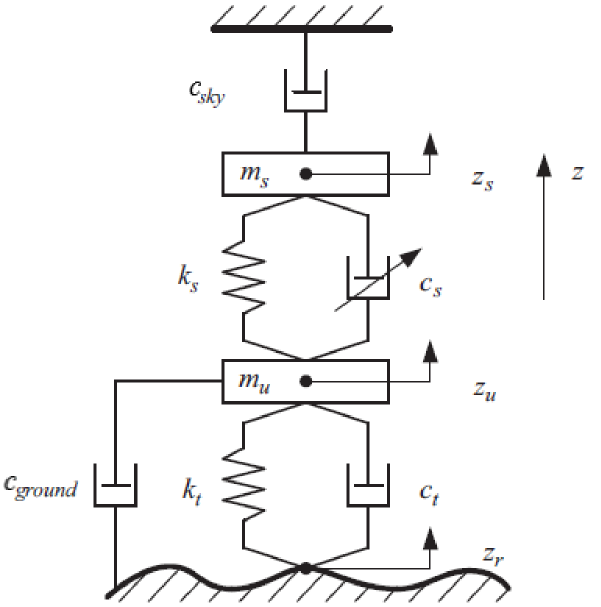

Figure 3.9: *Hybrid control system[1]*

damping ratio is referred to as c_{min} in previous methods. The difference between this minimal and maximal damping ratio is governed by the active component, c_{hyb}. This component is defined as a linear combination of the Skyhook and Groundhook models.

$$c_{\text{hyb}} = G[\alpha_{\text{hyb}}\sigma_{\text{sh}} - (1-\alpha_{\text{hyb}})\sigma_{\text{gh}}] \tag{3.17}$$

Where G is a simple gain used to adjust the linear combination to the appropriate damping value of the variable damper. In this combination α_{hyb} is the tuning parameter for the linear combination. When α_{hyb} is set to 1 the model represents a regular 2-state Skyhook model. Contrarily, when the tuning parameter is set to 0, the model can be made to represent a 2-state Groundhook model. The Skyhook and Groundhook parameters are defined as follows:

$$\sigma_{\text{sh}} = \begin{cases} \dot{z}_s, & \text{if} \dot{z}_{\text{s}}(\dot{z}_{\text{s}} - \dot{z}_{\text{u}}) > 0 \\ 0, & \text{otherwise} \end{cases} \tag{3.18}$$

$$\sigma_{\text{gh}} = \begin{cases} \dot{z}_u, & \text{if} - \dot{z}_{\text{u}}(\dot{z}_{\text{s}} - \dot{z}_{\text{u}}) > 0 \\ 0, & \text{otherwise} \end{cases} \tag{3.19}$$

This representation does offer a little improvement over the previous semi-active systems. In this case the passive damping and active damping are separated in the model. As the damping coefficient of the Hybrid model is determined along a range of coefficients, this method will require the same suspension system as a Linear control method of either the Sky- or Groundhook systems. This means that, even though the Hybrid system can be tuned to personal preferences, this is inherently a more complex and expensive system for manufacturers to incorporate in their design.

HYBRID MODEL TUNING PARAMETER

Obviously the performance of the Hybrid control approach is a compromise between the Skyhook and Groundhook method, depending heavily on the tuning of the model. Figure 3.10 shows the results of differently tuned Hybrid models.

Frequency Response It can easily be seen that the Hybrid model offers a way to tune the vehicle dynamics between the Skyhook and Groundhook methods as desired. A large benefit of this approach is that the tuning

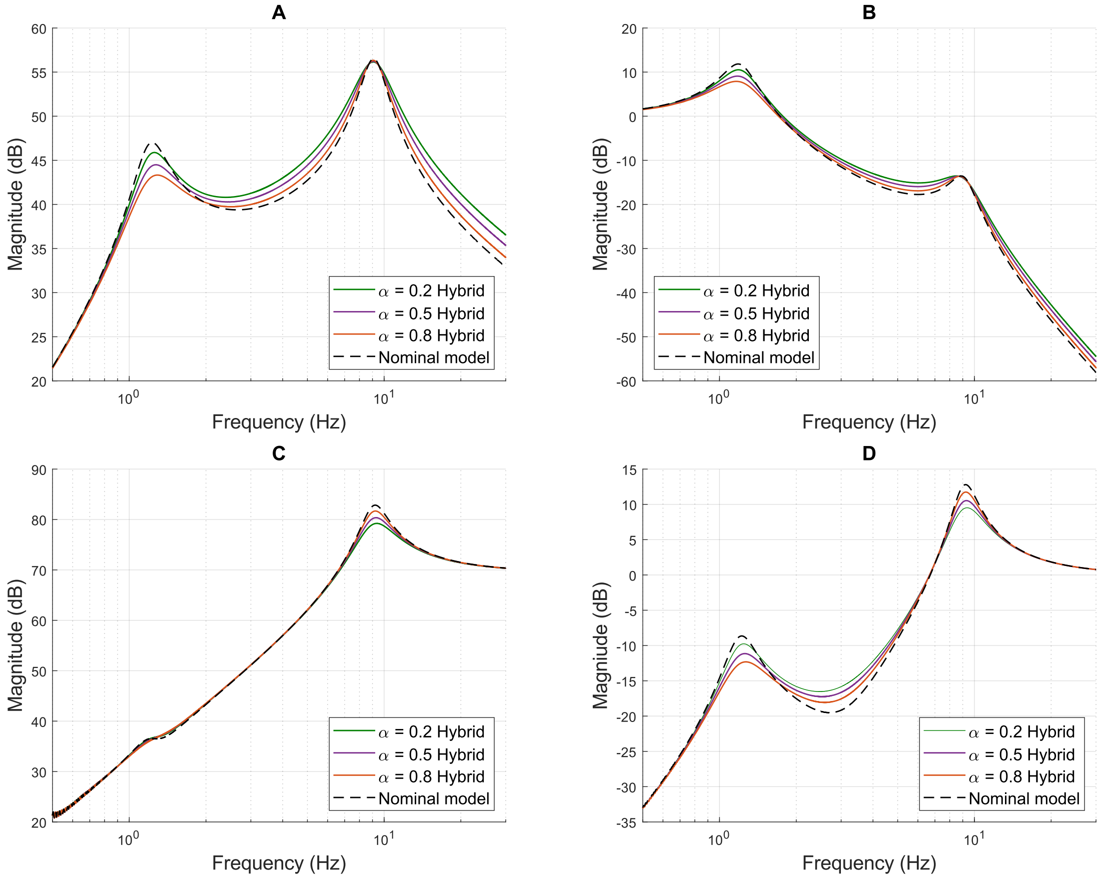

Figure 3.10: *Semi-Active Hybrid suspension control methods. Frequency response o A) Sprung mass acceleration B) Sprung mass displacement C) Unsprung mass acceleration D) Tyre deflection*

parameter α can be easily adjusted after implementation. This offers the driver of the vehicle the opportunity to change the vehicle characteristics. Though this model does not introduce any actual improvements over the separate Skyhook or Groundhook methods, it does introduce additional versatility. Apart from that, the Skyhook and Groundhook models both have different strengths and weaknesses. These weaknesses can be compromised for with the Hybrid model, as the weakness of one model can often be counteracted by the strength of the other model.

Performance Evaluation Just as the results from the frequency responses in figure 3.10, the performance of the Hybrid models in figure 3.11 are a compromise between the existing Skyhook and Groundhook results. It can be seen that the model tends to progress towards the Skyhook results for values of α closer to 1. On the other side of the spectrum, the model approaches the Groundhook performance when α moves towards 0.

3.4. FULLY-ACTIVE SUSPENSION CONTROL

This section will discuss the use of Fully-Active suspensions. In this case the variable damper of the previously introduced models will be replaced by an actuator. Each of the Semi-Active approaches can also be adapted for a Fully-Active suspension. On top of that, a recently proposed control method will also be introduced for Fully-Active systems.

3.4.1. ACTIVE SKYHOOK CONTROL

The Fully-Active adaptation of the Skyhook relies, obviously, on the same principle as the Semi-Active approaches. Therefore the hypothetical model of Figure 3.3 is still valid for this setup. However, as explained previously, the control input now consists of a Force instead of the variation of the damping ratio. Remember equations (3.4), (3.5), and (3.6). These equations describe the situation where the force actuator is connected

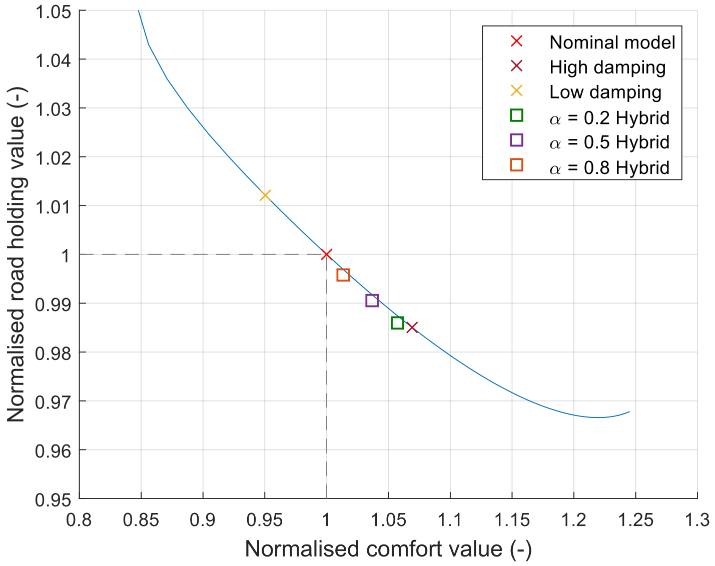

Figure 3.11: *Normalized performance of the semi-active Hybrid model for different values of tuning parameter α versus the reference models Nominal ($c_s = 1200$) - Low damping ($c_s = 800$) - High damping ($c_s = 2000$):*

to a fixed point in space. Applying this desired force to the active situation where the force actuator is actually placed between the sprung and unsprung masses yields:

$$m_s\ddot{z}_s = c_s(\dot{z}_u - \dot{z}_s) + k_s(z_u - z_s) - F_{\text{sky}} \tag{3.20}$$
$$m_u\ddot{z}_u = -c_s(\dot{z}_u - \dot{z}_s) - k_s(z_u - z_s) + k_t(z_r - z_u) + F_{\text{sky}} \tag{3.21}$$
$$F_{\text{sky}} = \dot{z}_s c_{\text{sky}} \tag{3.22}$$

Notice that, when compared to the ideal Skyhook equations, the only difference is that the force F_{sky} also has an influence on the unsprung mass. This force is, of course the reactionary force of the actuator that is connected to both the sprung and unsprung masses, as it is realistically impossible to have this actuator just connected to the sprung mass and a vertically fixed point in space.

3.4.2. ACTIVE GROUNDHOOK CONTROL

As for the Active Groundhook approach, we can use the definition of the Active Skyhook as a starting point. In the Groundhook model, however, the magnitude of the actuator force depends on the velocity of the unsprung mass. Aside from that the force is applied to the unsprung mass as well. We can then determine the E.o.M. for the Groundhook model:

$$m_s\ddot{z}_s = c_s(\dot{z}_u - \dot{z}_s) + k_s(z_u - z_s) + F_{\text{gnd}} \tag{3.23}$$
$$m_u\ddot{z}_u = c_s(\dot{z}_s - \dot{z}_u) + k_s(z_s - z_u) + k_t(z_r - z_u) - F_{\text{gnd}} \tag{3.24}$$
$$F_{\text{gnd}} = \dot{z}_u c_{\text{gnd}} \tag{3.25}$$

Note that the equations for the active Groundhook model are almost identical to that of the active Skyhook model in equations (3.20) and (3.21). The main differences here is that the Force is applied negatively to the unsprung mass, indicating that the focus of this model is to reduce the motion of the unsprung mass.

Also note that, like the semi-active model, the active Groundhook model uses the unsprung mass velocity $\dot{z}_u$ for the determination of the desired force in equation (3.25)

3.4.3. ACTIVE HYBRID CONTROL

As with the Hybrid control for the Semi-Active suspension, the control force of the Hybrid control is a linear combination of the Skyhook and Groundhook forces. The E.o.M. for the Hybrid model can be defined as:

$$\begin{aligned} m_s\ddot{z}_s &= c_s(\dot{z}_u-\dot{z}_s)+k_s(z_u-z_s)-F_{\text{hyb}} && (3.26)\\ m_u\ddot{z}_u &= c_s(\dot{z}_s-\dot{z}_u)+k_s(z_s-z_u)+k_t(z_r-z_u)+F_{\text{hyb}} && (3.27)\\ F_{\text{hyb}} &= \alpha_{\text{hyb}}(\dot{z}_s c_{\text{sky}})-(1-\alpha_{\text{hyb}})(\dot{z}_u c_{\text{gnd}}) && (3.28) \end{aligned}$$

Again the parameter α can be used to tune the Hybrid model towards either the Skyhook behaviour or the Groundhook behaviour. As the Skyhook is a comfort oriented control approach and the Groundhook is performance oriented, the tuning parameter α is to be used to find a desirable compromise between these two methods.

3.4.4. LINEAR QUADRATIC REGULATOR - OPTIMAL CONTROL

One of the currently optimal control approaches is the Linear Quadratic Regulator (LQR). This control method is applicable to active suspensions and uses a cost function J of the different goals in order to determine its effectiveness. This cost function consists of a linear combination of the squares of several system states, the design objectives. These squares are multiplied by a penalty weight in order to address different levels of importance for each state.

$$J=\int_0^T(x^{\mathrm{T}}Qx+u^{\mathrm{T}}Ru)\mathrm{d}t \tag{3.29}$$

In this equation, the vectors x and u represent the system states and control input respectively. The matrices Q and R are matrices that consist of the penalty weights. The definition of equation (3.29) is a standard definition of the cost function used for LQR control. It will therefore be necessary to define the system in such a way that the system can be expressed as in equation (3.29)[32].

We have previously determined that the main indicators for ride comfort and road-holding capacity are sprung mass accelerations $\ddot{z}_s$ and tyre deflections (z_u-z_r). Using these properties we can define a cost function for our design objectives.

$$J=\int_0^T\left(q_{\mathrm{c}}\cdot\ddot{z}_s^2+q_{\mathrm{rh}}\cdot(z_u-z_r)^2+r_{\mathrm{F}}\cdot F_{\mathrm{c}}^2\right)\mathrm{d}t \tag{3.30}$$

In this equation, 1_{c} and q_{rh} are the penalty weights for the comfort objective and Road-Holding capacity objective respectively. The penalty weight r_{F} is the control effort penalty. This penalty emphasizes the need to keep the control input low as well. After all, it is more beneficial to have a low energy requirement of the suspension system.

With these definitions for the cost function, it is possible to determine the required penalty matrices Q and R. Do note that it will be necessary to determine the system states in such a way that it will accommodate for the use of the road deflection z_r[33]. These matrices, along with the system state equation matrices, can be used to determine the LQR control force. The control input, which is the force generated by the actuator, is defined as:

$$u=-K\cdot x=-R^{-1}B^{\mathrm{T}Px} \tag{3.31}$$

Where P can be found by solving the Riccati equation:

$$A^{\mathrm{T}}P+PA-PBR^{-1}B^{\mathrm{T}}P+Q=0 \tag{3.32}$$

This shows that the control force u is less of a simple damper action, as seen before in the Skyhook, Groundhook, and Hybrid methods, but composed of a combination of several states. This makes the control a lot more complex, but also more effective. It should be noted that all of the states should be measurable for this approach to be optimal. As the tyre deflection usually is not readily available, estimators will have to be incorporated in order to acquire useful state signals. For the sake of simplicity, and the fact that the LQR method will only be used for comparison, all states are assumed to be measurable and control is therefore considered optimal for this method.

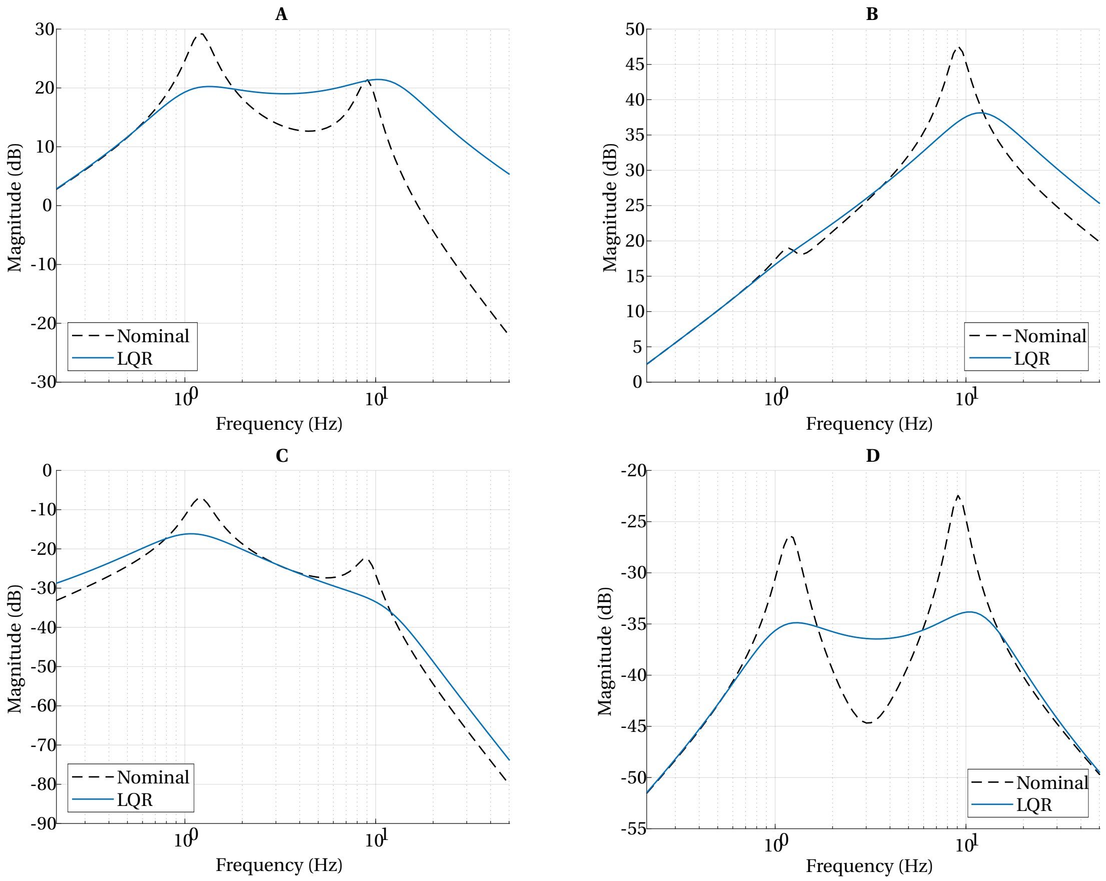

Figure 3.12: *LQR suspension control. Frequency response of A) Sprung mass acceleration B) Unsprung mass acceleration C) Suspension deflection D) Tyre deflection*

Do note that the shape of the passive response curve is different in these graphs. As stated previously, the LQR requires that the road displacement z_r is included in the system states. This displacement has been used as the system disturbance in the previous models. As it is now included in the system states, the system disturbance is defined as the road displacement velocity $\dot{z}_r$. This causes a shift in the shape of the transfer function results. The influence of the controller on the model is still clearly visible.

The graphs in Figure 3.12 show that the LQR control suppresses most motion of the vehicle. It can be seen that this has both positive and negative effects for the sprung mass accelerations. It can be seen that the accelerations at the sprung mass resonance frequency are suppressed. This improves the ride comfort of the system. However, frequencies beyond the sprung resonance frequency are dampened less than the passive system. This may indicate that the ride comfort at higher frequencies can be worse than the passive system, even though the overall ride comfort is improved over the complete frequency range.

Since the LQR also incorporates the Road-Holding capacity, the overall increase of performance can also be derived from the increase in Road-Holding capacity performance. As with the sprung mass vibrations, a lot of motion is suppressed. For the Road-Holding capacity, this is mainly beneficial as the high resonance peaks are heavily reduced.

3.4.5. UNSPRUNG NEGATIVE SKYHOOK DAMPER CONTROL

Recently a new approach to suspension control was proposed. This method proposes a different control force to be exerted on the sprung mass. The magnitude of this force is determined by the velocity component of the unsprung mass. Most notably, the force is to be exerted in the opposite direction of the classical Skyhook approach. This method is therefore called Unsprung Negative Skyhook (UNS) damper control [11].

This force is actually a result from another approach. In fact, the general proposition is to introduce an additional component to the control force that is proportional to the suspension deflection velocity.

$$F_c = -c_{\text{sky}} \cdot \dot{z}_s - c_{\text{def}} \cdot (\dot{z}_u - \dot{z}_s) \tag{3.33}$$

This newly introduced control damping ratio c_{def} is then set to be equal to the already existing control damping c_{sky}. The E.o.M. for the Unsprung Negative Skyhook model can then be completely described by

$$\begin{aligned} m_s \ddot{z}_s &= c_s(\dot{z}_u - \dot{z}_s) + k_s(z_u - z_s) - F_{\text{uns}} && (3.34)\\ m_u \ddot{z}_u &= c_s(\dot{z}_s - \dot{z}_u) + k_s(z_s - z_u) + k_t(z_r - z_u) + F_{\text{uns}} && (3.35)\\ F_{\text{uns}} &= \dot{z}_u k_{\text{uns}} && (3.36) \end{aligned}$$

This method essentially describes an inverted Groundhook model. This approach seems counter-intuitive as it seems that the introduced force accelerates the sprung mass. The study shows, however that this approach actually performs better than most conventional suspension control methods[11]. This method is aimed at improving the comfort of the vehicle for an increased unsprung mass.

3.4.6. ACTIVE MODEL PERFORMANCE EVALUATION

For each of the fully active models, the corresponding frequency responses and performance values have been determined. It will now be possible to examine the performance of the active systems.

FREQUENCY RESPONSE

Figure 3.13 shows an overview of the frequency responses of each of the active systems described in this section[2]. The models that have been described in the semi-active section show the same trends when used in an active application. The active Skyhook method primarily reduces the sprung mass vibrations to increase the comfort of the vehicle, the Groundhook approach mainly reduces the unsprung mass vibrations, and the Hybrid model can be used to tune a model between Sky- and Groundhook model properties as desired.

The newly introduced UNS model, however, shows very interesting results. As expected, the vibrations at the resonance frequencies of the system are greatly increased due to the nature of the added damping force. In the mid- and high-frequency range the UNS outperforms every other active model by achieving smaller sprung mass vibrations and tyre deflections.

PERFORMANCE EVALUATION

Of course, the performance metrics of the active models have also been calculated. The normalised performance of the active models is shown in figure 3.14. This again confirms the performance of the methods that have been applied in a semi-active method. The newly introduced UNS model shows to be somewhat of an extreme model. The comfort of the UNS model is immensely high. The road holding performance shows the exact opposite, enforcing the traditional design trade-off between comfort and road holding. The model does show that there still might be a simple way to improve on the vehicle's performance altogether.

3.5. SUMMARY

In this chapter, several approaches to vehicle suspension control were shown. First a proper vehicle model was selected for this research. Next, a distinction was made between semi-active and active suspension system. Several control methods were discussed for both of these suspension system types. The semi-active methods have shown to increase the performance slightly with relatively small control effort. This increase in

---

[2] The LQR approach is not included as it relies on a different input signal than the other models, namely road displacement velocity as opposed to road displacement. It will therefore not be directly possible to acquire comparable results.

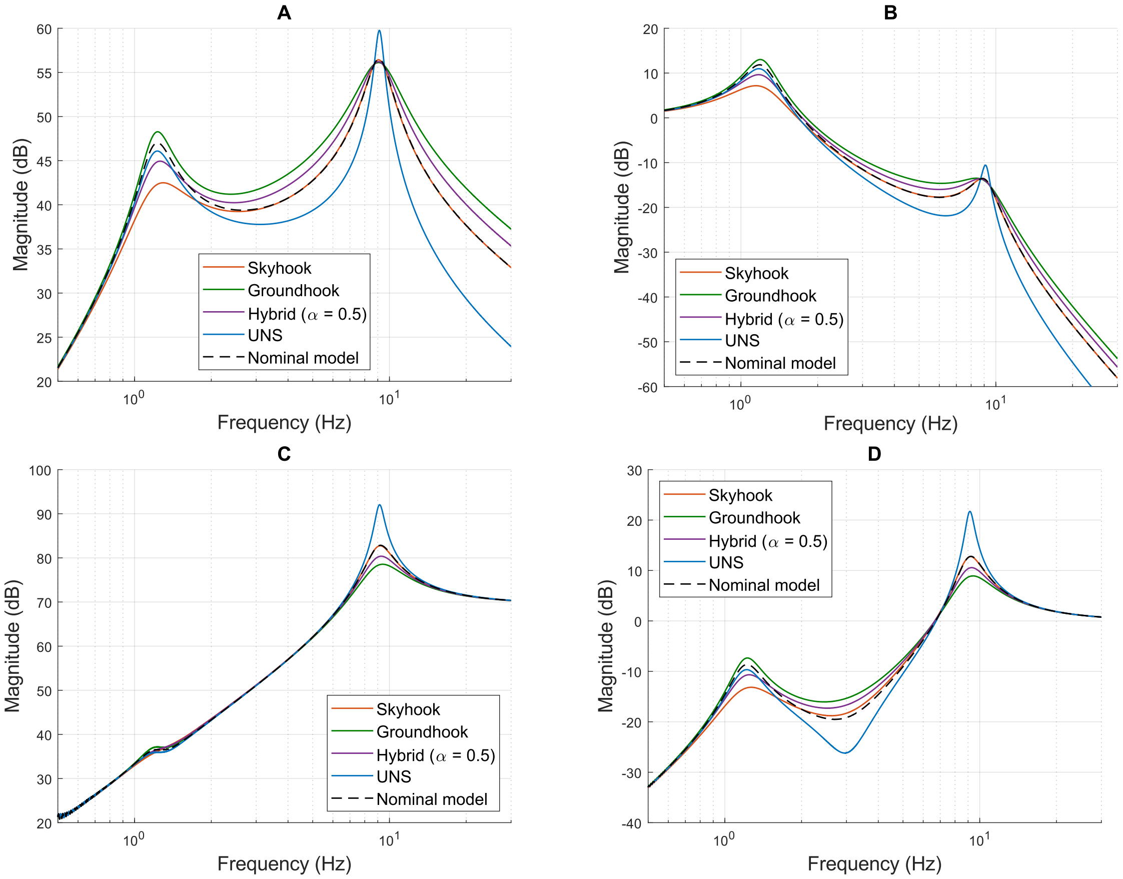

Figure 3.13: *Active system frequency responses of A) Sprung mass acceleration B) Sprung mass displacement C) Unsprung mass acceleration D) Tyre deflection*

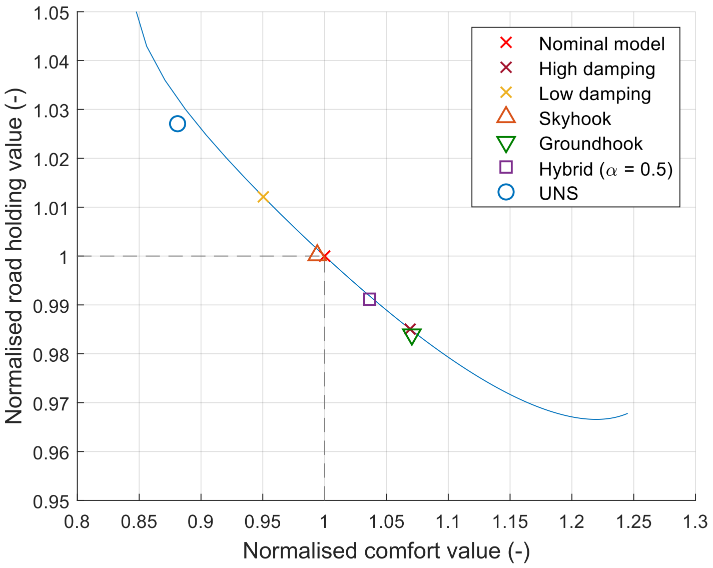

Figure 3.14: *Normalized performance of each of the fully active control methods with reference models: Nominal ($c_s = 1200$) - Low damping ($c_s = 800$) - High damping ($c_s = 2000$)*

performance can either be comfort oriented (Skyhook), or Road-Holding oriented (Groundhook). A Hybrid model has also been shown, compromising the benefits and drawbacks of both systems.

The active models have been shown to achieve better results in improving both ride comfort and road holding. These systems, however, do require a lot more energy to function properly. The LQR control method was shown to achieve the most damping of all the systems. This method does, however, depend on system states that are usually not available for measurement. For this method, the system will need to use an estimator in order to acquire signals for the states that are not available.

Finally, a new method has been introduced. This method uses conventional reference signals but excites the unsprung mass rather than dampens is. It is shown that this method results in extreme vibrations at both resonance frequencies of the system. The vibrations at other parts of the frequency range, however, show significant improvements when compared to conventional methods. When examining the performance evaluation, it can be seen that the comfort of the UNS surpasses all other models. In the frequency response of the active systems it can be seen that this model introduces great vibrations at the resonance frequencies.

Since the other methods do not exhibit increased resonance vibrations, it can be concluded that, for instance, the Skyhook and UNS model complement each other. This observation shapes the foundation of this research. In the next chapter, a new model will be proposed that attempts to combine the strengths of the UNS with that of another model in order to reduce, or eliminate, the drawbacks of this new method.

4

MIXED UNSPRUNG NEGATIVE SKYHOOK CONTROL

In the previously examined models, the distinction between semi-active and active models was made. Due to the operating principles of both systems, differences in control methods are clearly present. This primarily manifests in the manner of influence the controller has on the system dynamics. For semi-active systems, the damping ratio of the controller is adjusted in order to approach the desired force. For active systems, this force is calculated by the controller and exerted by a force actuator. The manner in which this force is calculated, however, is fairly straightforward for all models. All models rely on a simple relationship between an imaginary damping ratio and the velocity of one of the vehicle bodies. Obviously, this is to mimic the behaviour of an actual damper. Even though the LQR control method at first seems more complicated, it still uses a static gain matrix that is to be multiplied by the current state vector.

The drawbacks of using a single system has already been addressed in the design of the Mixed Skyhook-ADD approach for semi-active suspension control[4]. This approach switches behaviour of the suspension between two different types. Unlike the Hybrid model, where the suspension is controlled by a linear combination of different models, this allows us to actually select the best behaviour for given conditions and switch between the different models altogether.

The relatively new Unsprung Negative Skyhook model shows great potential for active suspension applications. The high vibration at resonance frequencies, however, are a cause for concern. It is therefore that a new model will be proposed which combines the active UNS model with another in a mixed model approach. This model will attempt to remove the drawbacks of the UNS while maintaining as much of the performance improvements as possible.

The following chapter will introduce several methods on how to implement the model switching behaviour. It will detail the working principle of these methods. As the simulations of the final model will be carried out by using Simulink, the implementation of the models into the Simulink model will also be addressed.

4.1. GOVERNING MODELS

As previously shown in figure 3.14, the comfort performance of the UNS is superior to the other active control methods. The frequency response graphs of the UNS of figure 3.13 can be seen to have increased performance between the resonance frequencies, but considerably worse performance at those resonance frequencies. The active Skyhook model shows better results around the resonance frequencies. The aim of a mixed model is to combine the strengths of each model in a resulting superior model.

4.1.1. UNSPRUNG NEGATIVE SKYHOOK MODEL

The basis of the Mixed UNS model is defined as a regular active model. Any active model can be described using the following equations of motion:

$$
\begin{aligned}
m_s \ddot{z}_s &= c_s(\dot{z}_u - \dot{z}_s) + k_s(z_u - z_s) + F_c && (4.1)\\
m_u \ddot{z}_u &= -c_s(\dot{z}_u - \dot{z}_s) - k_s(z_u - z_s) + k_t(z_u - z_r) - F_c && (4.2)
\end{aligned}
$$

The difference for each system is the definition of the control force F_c. As with all active system approaches, this force is generally defined as an imaginary damper force.

$$F_c = c_a \dot{z}_i \tag{4.3}$$

Where c_a defines the imaginary damper ratio and $\dot{z}_i$ can be selected from $\dot{z}_s$ or $\dot{z}_u$ to achieve the desired dynamic behaviour. As stated, the active systems employ a constant value for the imaginary damping ratio c_a. The dynamics of the different control approaches is not only defined by the definition of the damping ratio c_a but also by the selection of the body velocity $\dot{z}_i$. The different system forces are defined as follows:

$$
\begin{aligned}
F_{\text{sky}} &= c_a \cdot \dot{z}_s\\
F_{\text{gnd}} &= -c_a \cdot \dot{z}_u\\
F_{\text{uns}} &= c_a \cdot \dot{z}_u
\end{aligned}
$$

In order to obtain better results from the UNS, a mixed model approach will be investigated with both the Skyhook and the Groundhook models. To use these different beneficial characteristics, the mixed models will have to be able to switch between the definitions of the controller force accordingly. An important aspect of the controller is how it determines how to switch the definitions to achieve better performance.

4.1.2. DETERMINING THE OPTIMAL MODEL

As discussed previously, different systems have different strengths at different frequency ranges. The mixed model approach aims to use the best of both models in order to achieve a dynamical behaviour superior to each single model. The model will therefore achieve better performance if the correct model is active corresponding to the instantaneous system frequency. The switching frequency should, obviously, determine the points at which the currently used model is switched for the another. As the mixed model is still primarily intended to be a comfort oriented model, the switching law shall be based on the comfort related frequency response signals. The mixed model will also be a form of active control. The frequency response signals of both active systems should therefore be compared in order to determine the switching crossover frequency, or frequencies.

Figure 4.1 shows that the active Skyhook model and the UNS model intersect a total of 3 times. These intersections indicate the crossover frequency where the mixed model should change the active model type. By finding the intersections of the two different response functions, the crossover frequencies can be determined. The three crossover frequencies are found to be:

$$\omega_1 = 1.752\,\text{Hz} \qquad \omega_2 = 8.707\,\text{Hz} \qquad \omega_3 = 9.593\,\text{Hz} \tag{4.4}$$

Aligning the crossover frequencies with the performance responses of figure 4.1, we can determine four distinct optimal areas of operation.

$$
F_{\text{c}} = \begin{cases}
F_{\text{sky}}, & \text{if } \omega \le \omega_1\\
F_{\text{UNS}}, & \text{if } \omega > \omega_1 \wedge \omega < \omega_2\\
F_{\text{sky}}, & \text{if } \omega \ge \omega_2 \wedge \omega \le \omega_3\\
F_{\text{UNS}}, & \text{if } \omega > \omega_3
\end{cases} \tag{4.5}
$$

Equation (4.5) shows that ideally the model will have four different cases. It may be difficult to properly determine the instantaneous frequency of the system. Because of this difficulty, the model will first be applied to

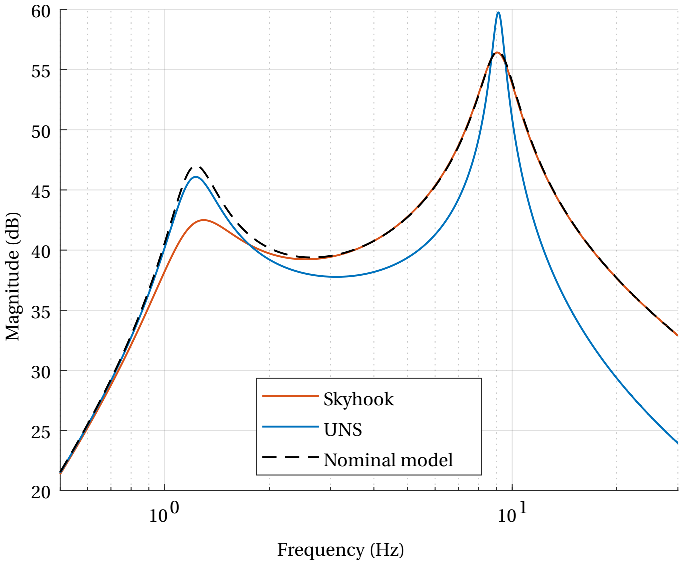

Figure 4.1: *Comparison of the frequency responses of the sprung mass for the active Skyhook and Unsprung Negative Skyhook models*

improve on the most important frequency range, namely the mid-frequencies between the system resonance frequencies.

$$F_c = \begin{cases} F_{\text{UNS}}, & \text{if } \omega > \omega_1 \wedge \omega < \omega_2 \\ F_{\text{sky}}, & \text{otherwise} \end{cases} \tag{4.6}$$

the Skyhook model will be selected for frequencies lower than ω_1 and between the intersection frequencies ω_2 and ω_3. Otherwise, the UNS model is used. This method eliminates the drawback of the UNS model near the system's resonance frequencies and should ensure that the suspension will always at least equal the performance of the passive system.

4.2. FREQUENCY SWITCHING

The governing models perform differently at different frequency ranges. The new model will therefore have to switch the currently active suspension model according to the instantaneous frequency of the current vibration. It is then obvious that the system will need to be able to either measure, or accurately estimate, the frequency of the current system vibration. This section will detail two different approaches to this problem.

4.2.1. FREQUENCY-RANGE SELECTOR

A previous study has shown the effectiveness of combining different models[34]. In this study, the ADD Skyhook model was extended with the regular 2-state Skyhook model in a semi-active application. In this approach a simple Frequency-range selector (FRS) was used to have the model estimate the current frequency of the system and select the proper behaviour of the semi-active damper. Compares the current vibration frequency with a crossover frequency. The active model can then be selected based on whether the current vibration is of a lower or a higher frequency than the crossover frequency. Remember the definitions of the semi-active 2-state Skyhook model and the ADD method, equations (3.7)and (3.9) respectively. The mixed Skyhook-ADD is then defined as:

$$c_s = \begin{cases} c_{max}, & \text{if } \left((\ddot{z}_s^2 - \alpha^2 \dot{z}_s^2) \leq 0 \;\&\; \dot{z}_s(\dot{z}_u - \dot{z}_s) > 0 \right) \text{ or } \left((\ddot{z}_s^2 - \alpha^2 \dot{z}_s^2) > 0 \;\&\; \ddot{z}_s(\dot{z}_u - \dot{z}_s) > 0 \right) \\ c_{min}, & \text{otherwise} \end{cases} \tag{4.7}$$

Keeping in mind that this control law is meant for a semi-active suspension system, it is easy to see the work-

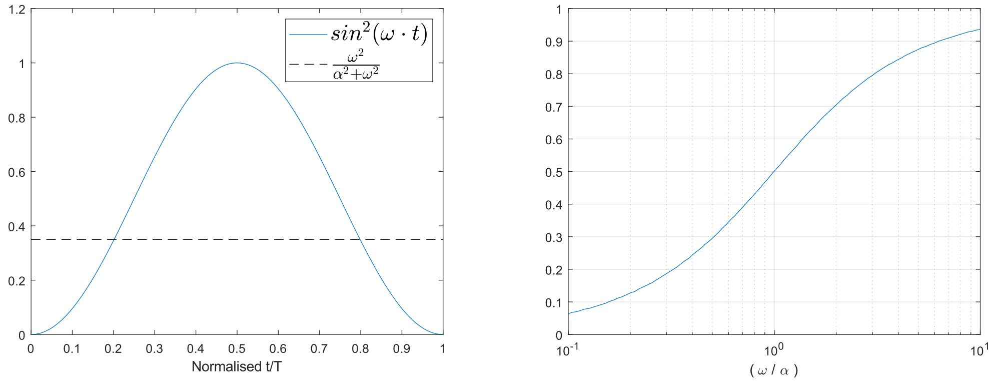

Figure 4.2: *Working principle of the frequency range selector. Left: a visualisation of the inequality equation. Right: the positivity of the inequality function as a function of vibration frequencies.*[4]

ing principle of this approach. Both the 2-state and the ADD Skyhook systems are incorporated in the control law. The method is switched by the so-called Frequency-range selector:

$$\left(\ddot{z}_s^2 - \alpha^2 \dot{z}_s^2\right) > 0 \tag{4.8}$$

The tuning parameter α can be used to select the crossover frequency. Based on the inequality of equation (4.8), the proper governing model for the semi-active suspension can be selected. This effectively turns the governing models into a lower frequency model and a higher frequency model. The principle of the frequency selector can be shown using a single frequency input signal as an example:

$$\dot{z}_s = A \sin(\omega \cdot t) \tag{4.9}$$

Combining the velocity signal of equation (4.9) with the frequency range selector equation (4.8), we get the following inequality equation:

$$A^2\omega^2 - A^2 \sin^2(\omega \cdot t)(\alpha^2 + \omega^2) > 0 \tag{4.10}$$

This equation can be rewritten to obtain the inequality that controls the selection of the model.

$$\sin^2(\omega \cdot t) < \frac{\omega^2}{\alpha^2 + \omega^2} \tag{4.11}$$

It is then by this inequality that the effectiveness of the frequency range selector can be examined. Figure 4.2 visualizes the inequality of equation (4.11) for a normalized period T on the left and shows the relative positivity of the inequality over a range of frequencies ω on the right.

As can be seen in the left plot of figure 4.2, the squared sine function is normalised for a period T. It will remain unchanged for different frequencies ω as it is not dependent on ω. The lower frequency model is then selected when the value of the squared sine function exceeds the inequality threshold. The higher frequency model is selected when the squared sine has a smaller value than the threshold. The inequality threshold $\frac{\omega^2}{\alpha^2+\omega^2}$ will shift upwards towards 1 when ω increases to values much larger than α.

The relative positivity in the right graph denotes the portion of the normalised period T where the squared sine function is smaller than the threshold function in the left graph of figure 4.2. For instance, the positivity graph shows that the positivity equals 0.5 when the signal frequency ω is equal to the crossover frequency α (i.e. $\frac{\omega}{\alpha} = 1$). This means that the inequality equation is true for $0.5T$. As seen in the right graph of figure 4.2, a higher frequency ω results in the inequality function to be true for a larger portion of the normalised period T.

It can be seen that, at any given ratio between the frequency ω and crossover frequency α, the inequality function will yield a positive result only a portion of the normalised period. This means that the selector will never have a single model active for the full duration of a period. Even if it is for a very short amount of time, the incorrect model will be active while the other model should be active at all the times.

This operating range shows the drawback of this method. The method is extremely simple, does not require complex computations and is therefore a very fast method. It will however, not achieve absolute proper model selection for a range of operating frequencies. It will also achieve better results for a model with a single switching frequency. For models with multiple crossover frequencies, the frequency ranges may interfere with each other. For instance, when setting the crossover frequency at the second intersection frequency of the governing model, $\alpha = \omega_2$ as defined in equation (4.4), the full operating range of this switch ranges from approximately 0.87 Hz up to a frequency of approximately 87 Hz according to the range displayed in the positivity function in figure 4.2. It is then obvious that the effect of the frequency selector bleeds into the operating ranges of the frequency selectors for the other switching frequencies, ω_1 and ω_3 of equation (4.4). This shows that this method will probably be less effective when using multiple switching frequencies which are located within each other's operating range.

4.2.2. SHORT-TIME FOURIER TRANSFORM (STFT)

Another method to estimate the instantaneous frequency of the system involves the use of the Fourier transform. In general, the Fourier transform is used to decompose a signal into its frequency components. A special form of the Fourier transform can be used to analyse short sections of a continuous signal, the Short-Time Fourier Transform[35]. This approach uses a short windowed sample of a signal and processes its Fourier transform[36]. If the sample is properly selected and sized, a good spectral analysis of the current vibration dynamics can be calculated. This method consists of three steps. First the signal is windowed using a window function. Next, the frequency spectrum of this window is calculated using the Fourier transform. Finally, the instantaneous frequency can be determined by locating the peak in the acquired spectrum. The following sections will elaborate on the different steps of this method more extensively.

SIGNAL WINDOWING

The first step of this method is to apply a window function on the current signal. This signal can be a signal from any sensor where vibrations can be measured. Since the comfort value was previously determined by the body accelerations, the acceleration signal will also be used in order to determine the instantaneous vibration frequency. The need for windowing rises due to the desired use of the Fourier transform.

The Fourier transform can be used on any signal, but not on a single signal sample. The Fourier transform then decomposes the complete measured signal into its frequency components. It would be possible to continuously apply the Fourier transform to the complete set of measurements. This would however not yield the instantaneous frequency of the input signal. If the Fourier transform would be applied each time step on the complete measured signal, it would generate a frequency response function of all measurements up to that point in time. The history of the measured signal is not important to the STFT. Instead of using the complete and continuously growing signal, the signal is windowed. By applying a window, only a number of the most recent measurement points are included for the Fourier transform. This number is the so-called window size.

A window is generally used to select a portion of a signal rather than a complete signal. This window is non-zero for a given number of measurement samples, the window size. Any samples exceeding that number will be zero. This window function is then multiplied by the signal measurement function. This results in a set of signal measurements where samples beyond the window size are excluded from the new subset.

Hamming window One of the most commonly used windows is the Hamming window, shown in figure 4.3. This window reduces the signal amplification when near the edges of the window. The most important parameters of the window signal are the window size and the overlap fraction. The window size denotes the amount of samples that are included in the resulting windowed signal. For larger window sizes, more data points from the measurements are included in the newly created windowed signal. The overlap denotes the amount of samples that are used in two consecutive windowed signals. The amount of overlap, together with the shape of the window function, determines the amount of information that is maintained in consecutive windowed signals. For a large number of overlap samples, little information is lost. This also increases the

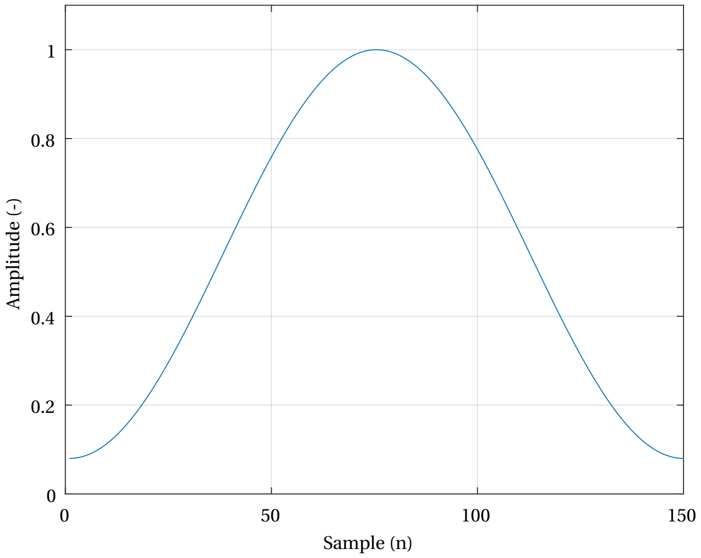

Figure 4.3: *Example of a Hamming window with a window size of* $n = 150$

computational cost of the windowing signal however, as the signal is windowed more often than for small overlap windowing.

It is now necessary to determine the properties of the window, namely the window size and the amount of overlap.

The window length mainly depends on the frequency range that we would like to examine. Since the window is applied to the measured signal of the accelerometer, we will need to know the sampling rate of this sensor in order to properly define the window properties. This sampling rate should be able to cover the dynamics that we are interested in. The Nyquist criterion states that, in order to properly sample a signal, the sampling frequency should at least be twice the highest frequency of the examined signal:

$$f_{\text{sample}} > 2 \cdot f^{\text{max}} \tag{4.12}$$

We have previously determined a frequency range of interest from 1 Hz up to 30 Hz. Combining this with the Nyquist criterion of equation (4.12), we acquire a minimum sampling rate for the acceleration signal (which is also a requirement for the accelerometer):

$$f_{\text{sample}} > 60\,\text{Hz} \tag{4.13}$$

A general rule of thumb however, is to increase this minimum sampling rate by another 25% in order to properly sample the examined signal. It is also generally considered to use the highest possible sampling rate to get the most accurate results. Simple current accelerometers easily achieve sampling rates of 100 Hz or higher. Combining the properties of the state-of-the-art sensors with the required minimum sampling frequency of (4.13), we assume a sampling rate of the accelerometer signal of:

$$f_{\text{sample}} = 100\,\text{Hz} \tag{4.14}$$

Since we now have a set value for the sampling rate of the measured signal, it is possible to define the properties of the window. The length of the window should be equal to the length of the signal that is to transformed by the Fourier transform. The length of the input signal of the Fourier transform influences the characteristics of the output signal, most importantly the frequency resolution, or bin size.

The frequency resolution of a Fourier transform can be calculated as:

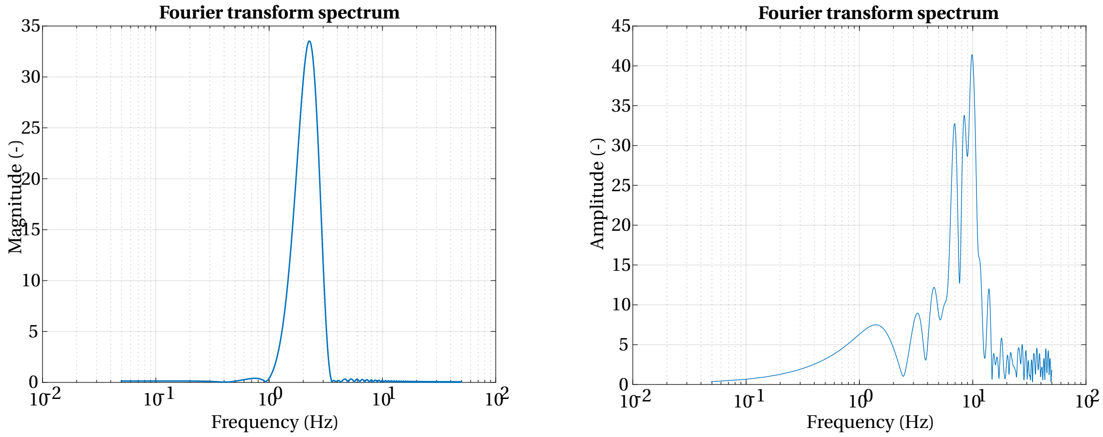

Figure 4.4: *Examples of an STFT spectrum of a windowed signal. Left: Response of a chirp single. Right: Response of a random road signal.*

$$\Delta f = \frac{f_{\text{sample}}}{N_{\text{sample}}} \tag{4.15}$$

Where f_{sample} is the sampling rate which, in this case, has been defined in (4.14). N_{sample} is the number of samples used for the Fourier transform. This amount should be equal to the number of samples that the Hamming window spans.

FOURIER TRANSFORM

After the signal has been properly windowed, it is possible to obtain a frequency component spectrum by calculating the Fourier transform of the windowed signal.

The Fourier transform is used to transfer a time-domain signal into a frequency-domain signal. A Fourier transformed signal then shows contribution of all the different frequency components that are contained in the signal. For instance, imagine a simple sine signal where $y = \sin(2\pi f \cdot t)$. Obviously, this signal only contains a single frequency component. The Fourier transform of this signal would therefore be zero over the complete range except at frequency f, where the Fourier transform will display a peak. Similarly, a signal that contains more than one frequency component, will display peaks at frequencies corresponding to each component.

When using the Fourier transform to investigate more complex, multicomponent signals, it is possible to extract other information, for example which frequency component is the dominant frequency within a vibrating signal. This aspect of the Fourier transform is exploited for the STFT application. Using this aspect, the dominant vibration within the previously determined time window can be identified.

Figure 4.4 shows the frequency component spectra of two different windowed signals. The left graph show the result when the road input signal is a chirp signal. Since the input signal is at any point a single frequency component sine wave, the STFT spectrum clearly shows the identified frequency.

The right graph of figure 4.4 shows the STFT when the road input signal is a random. It is clear to se that the STFT now shows multiple frequency components in the vibration signal, each component being represented by a peak in the spectrum. In this case it is necessary to find the largest peak in order to identify the dominant vibration.

PEAK FINDING

The graphs in figure 4.4 both show clear dominant vibration frequencies, but they still need to be identified by the system. For this, the last step is to find the peaks in the obtained spectrum. A simple peak finding function is used to identify the index of the peak within the array that represents the spectrum. This index number is then cross-referenced with the array of frequency values, which is used for the x-axis of the spectrum graphs. With this, the estimation of the frequency of the dominant vibration can be obtained.

4.3. SUMMARY

The previously discussed frequency estimation methods can then be combined with the governing models to create the complete new control methods. Both the FRS and the STFT frequency estimation can be used for the control approach. This final section provides a summarising overview of the two approaches for the novel control method.

4.3.1. FREQUENCY-RANGE SELECTOR CONTROL

Combining the governing models, their crossover frequencies, and the FRS results in the following law to determine the control force, F_c:

$$F_c = \begin{cases} c_a \cdot \dot{z}_s, & \text{if } (\ddot{z}_s^2 - \omega_1^2 \dot{z}_s^2 > 0) \vee (\ddot{z}_s^2 - \omega_2^2 \dot{z}_s^2 \leq 0) \wedge (\ddot{z}_s^2 - \omega_3^2 \dot{z}_s^2 > 0) \\ c_a \cdot \dot{z}_u, & \text{otherwise} \end{cases} \tag{4.16}$$

Where c_a denotes the imaginary active damping ratio. $\dot{z}_s$ and $\ddot{z}_s$ denote the sprung mass velocity and acceleration respectively while $\dot{z}_u$ is the unsprung mass velocity. Finally, ω_i indicates the crossover frequency as indicated in equation (4.4), for $i = 1, 2, 3$.

This control law summarises the different frequency areas of operation of the new control method as measured by the FRS. The first case denotes the active Skyhook control force as first defined in equation (3.22). This model is selected whenever the frequency of the vibration is estimated to be either below the first crossover frequency ω_1 or between crossover frequencies ω_2 and ω_3. These are the areas which show better performance of the Skyhook model. Consequently, all other frequencies will employ the UNS model.

4.3.2. SHORT-TIME FOURIER TRANSFORM CONTROL

The second approach involves the STFT as a method for estimating the instantaneous frequency. Other than that, the principle of control is identical to the laws for the FRS control. The control force is then governed by the following control scheme:

$$F_c = \begin{cases} c_a \cdot \dot{z}_s, & \text{if } \left(\hat{\omega}_{\text{STFT}} > \omega_1 \wedge \hat{\omega}_{\text{STFT}} \leq \omega_2\right) \vee \hat{\omega}_{\text{STFT}} > \omega_3 \\ c_a \cdot \dot{z}_u, & \text{otherwise} \end{cases} \tag{4.17}$$

Where $\hat{\omega}_{\text{STFT}}$ is the instantaneous frequency estimated by the STFT approach. All other parameters are equal to those in equation (4.16).

5

QUARTER CAR SIMULATION RESULTS

The novel control schemes have been defined and detailed in chapter 4. Their performance will now be analysed be means of simulation. This chapter details the different simulation set-ups and presents the results according performance metrics corresponding to each simulation type.

The chapter can be globally divided into two distinct parts. The first part entails the analysis of the proposed models in the frequency domain. A single-wheel Simulink™ simulation is done using the QC model to obtain the frequency response results of the new models. At first, the performance metrics by which the models will be evaluated are discussed. Next, the road input excitation signal for these simulations are detailed. Lastly for this part, the results of the frequency simulations are displayed and discussed. This will create a first insight of the expected performance of both models.

The second section will detail the analysis for time based measurements rather than the frequency response signals. Since these results are not based on the frequency response, new performance metrics will be introduced for proper evaluation.

5.1. PERFORMANCE METRICS

The analyses for different state-of-the-art semi-active and active systems discussed in chapter **??** are based on frequency response results. In order to accurately compare the performance of the proposed models to that of these state-of-the-art models, the frequency responses will be used to evaluate the proposed models' performance according to the evaluation parameters as defined in chapter 2.3. In summary, this means that the QC models will supply frequency responses for:

- Sprung mass accelerations
- Sprung mass displacements
- Unsprung mass accelerations
- Tyre deflections

Using these frequency responses, the performance of the proposed models, relative to the nominal model, is determined using the normalised performance evaluation methods, which are also defined in chapter 2.

5.2. ROAD INPUT

The aim of the frequency analysis is to obtain meaningful frequency responses. To obtain a clear frequency response of the proposed models, it is necessary to ensure that the system is excited by at least all frequencies of interest. A slowly evolving chirp signal will therefore be used for the road input. The chirp signal can be designed such that all frequencies of interest are incorporated. If the signal evolution is sufficiently slow, it resembles a vibration with a stationary frequency for each excitation frequency. This will minimise transitional behaviour so that the results can be interpreted as steady state responses.

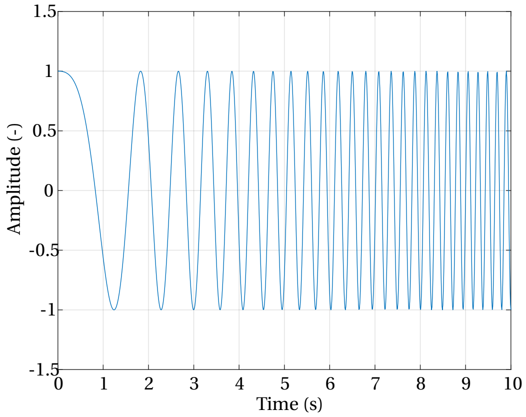

Figure 5.1: *General example of a chirp signal for a low end frequency of* 0.1 Hz *and an upper frequency of* 5 Hz

Figure 5.1 shows an example of a chirp signal. It can be seen that the frequency slowly increases to its maximum over the specified time range. Using this type of signal will make it possible to obtain a clean frequency response. The chirp signal ranges from 0.1 Hz up to a maximum of 30 Hz. In order to have the signal resemble a stationary signal, the chirp signal is designed to evolve over a time of 100 s. This allows the system to be able to approach the steady-state behaviour. This way, the frequency response of the signal will be an accurate representation of the system behaviour.

5.3. SIMULATION RESULTS

The road input signal is now applied to the QC model in a Simulink™ simulation. This section will detail the simulation results and the performance of both the FRS and STFT proposed models.

5.3.1. FREQUENCY-RANGE SELECTOR

This section details the results of the single wheel simulations of the FRS Mixed model. First, the FRS model is excited by the chirp signal to obtain proper frequency responses. These responses are shown in figure 5.4. Using these frequency responses, the normalised performance of the FRS model is displayed in figure 5.3.

At first glance, the FRS Mixed model is an improvement over each of the governing models. In all graphs of figure 5.2 the Mixed model approaches or even equals the performance of the preferred model for frequencies up to the second crossover frequency, ω_2.

However, when examining the responses of the FRS model more closely, the response at the end of the frequency range shows undesired behaviour. The sprung mass accelerations and displacements (graphs (A) and (B) of figure 5.2 respectively) show incorrect and undesirable behaviour at and beyond vibrations of approximately 25 Hz.

The aim of the Mixed model is to improve the performance of the UNS model. The Mixed model attempts to achieve this by reducing the effects of the resonance at the natural frequencies of the dynamic system. The FRS Mixed model better attenuates the sprung mass vibrations at the lower natural frequency. This is achieved by selecting the Skyhook model, as seen in graph (A) of figure 5.2. It does not equal the performance of the Skyhook model at the lower frequencies, however. This is likely caused by the switching behaviour of the FRS as explained in section 4.2.1. As the FRS inherently cannot continuously select the desired model, the performance of the Mixed model will instead be contained within the limit of its governing models. The frequency responses does show that the Mixed model approaches the Skyhook model rather than the UNS model for frequencies lower than the first crossover frequency,ω_1.

For mid-range frequencies, the Mixed model achieves almost ideal performance. Up to the second crossover frequency, ω_2, the model is nearly identical to the preferred UNS model. However, the FRS Mixed model response oscillates around the frequency response of the preferred UNS model. This can be explained as a side-effect of the non-absolute model selection inherent to the FRS model. Below, an explanation for this phenomenon is given by means of an example.

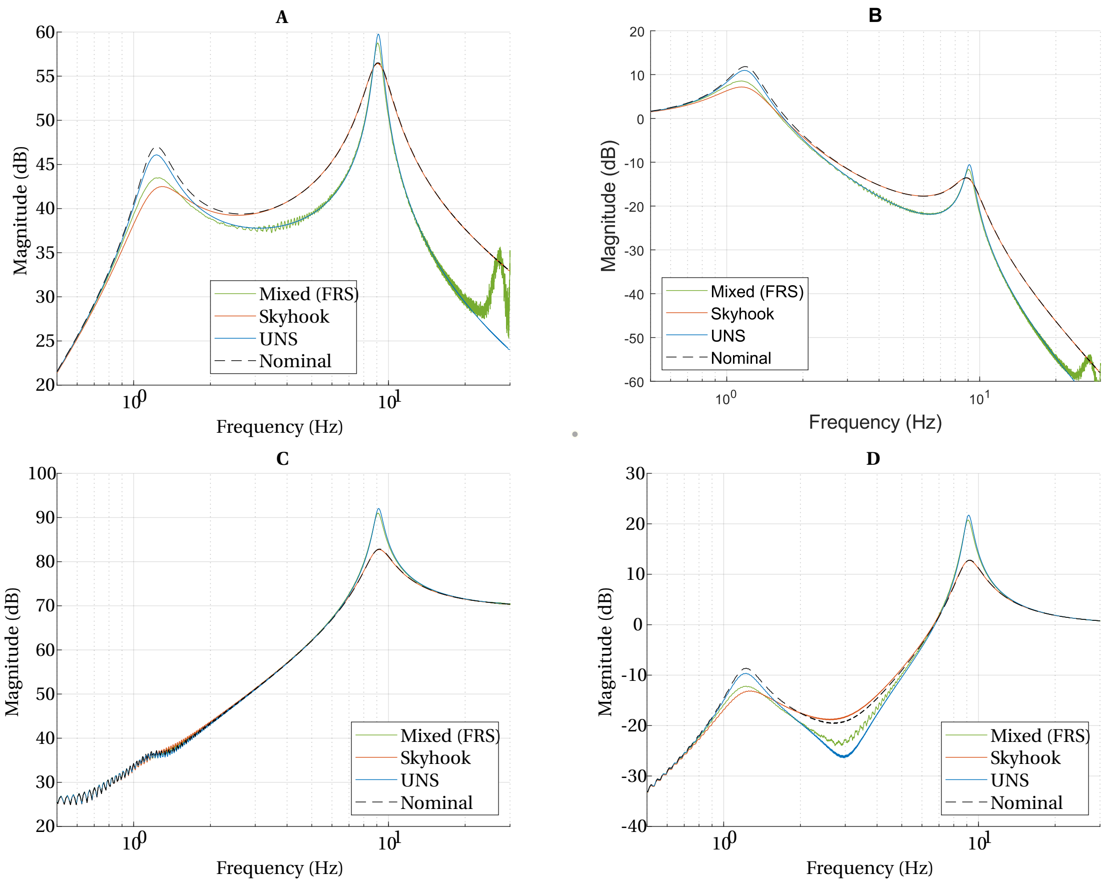

Figure 5.2: *Frequency response results of the FRS model. The figure show the responses of the following signals: (A) Sprung mass acceleration (B) Sprung mass displacement (C) Unsprung mass acceleration (D) Tyre deflection*

Consider the sprung mass acceleration responses of the different systems at a frequency of 5 Hz. At this frequency, the Skyhook model vibrations equal those of the passive model performance. The UNS model better attenuates these vibrations compared to the Skyhook and passive models. The Mixed model is designed to approach the behaviour of the UNS model at this frequency. However, the dynamics of the passive, Skyhook, and UNS models are all continuous, as the definition of the dynamics remain unchanged. This results in a single magnitude at any given frequency.

For the FRS model, however, the non-absolute switching causes switching behaviour between two definitions for the control force. This results in multiple magnitudes of the frequency response for any given input frequency. As the Fourier transform attempts to generate a single response curve from this data, the oscillation of the frequency response should be viewed as an operating range rather than actual singular values.

At the higher natural frequency, where the large vibrations caused by the unsprung mass dynamics, the FRS shows less attenuation of the vibrations. This is likely due to the close proximity of the two crossover frequencies, ω_2 and ω_3. As displayed in figure 4.2, each crossover frequency has a rather large area of operation. Since these two crossover frequencies are very close to each other, their areas of operation largely coincide as well. The switching law decides the active model by using equation (4.8) separately for both crossover frequencies. When the signal is both estimated at a higher frequency than ω_2 and lower than ω_3 simultaneously, the Skyhook model is to be selected. The effect of non-absolute model selection is hereby amplified. Effectively, the non-absolute behaviour estimates the vibration correctly to be higher than ω_2 for a fraction of the normalised period. Simultaneously the inequality equation for ω_3 only estimates the frequency as desired for a fraction of the normalised period as well. Only when these two fractions overlap, the selector actually selects the desired model. This cumulative behaviour then results in a decrease in the effectiveness of the proposed model.

Graph (D) of figure 5.2 shows the tyre deflection of the systems, which is directly linked to the road-holding capacity of the vehicle. It can be seen that the Mixed model outperforms the UNS model around the natural frequencies, but achieves slightly less performance in the mid-range frequencies. This is expected however, as the classic design trade-off predicts worse road-holding capacity for improved comfort and this response corresponds to the behaviour seen in the other graphs as well.

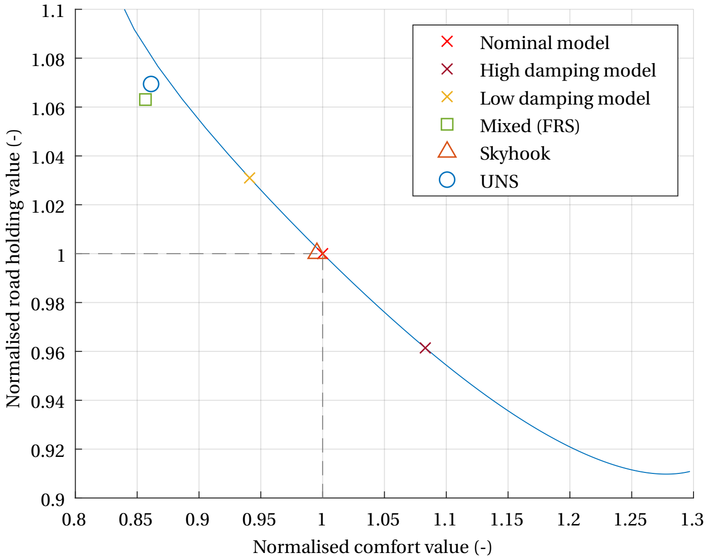

Figure 5.3: *Normalised performance of the FRS Mixed Model compared to its governing models and the passive system. Note that the Passive model of figure 5.2 is displayed here as the nominal model.*

In figure 5.3 the normalised performance of all models are shown. Using this comparison, it shows that the new FRS Mixed model is an improvement over the UNS model in terms of both comfort and road-holding capacity. The aimed goal of achieving better road-holding performance while maintaining the comfort performance is achieved even if only to a small extent. Though it is not as much of a deterioration as the UNS reference model, it is still not an improvement in terms of road holding capacity compared to a passive system.

5.3.2. STFT FREQUENCY ESTIMATOR

The second model to be analysed is the active model using the STFT frequency estimator to switch the active models. The frequency response for different signals, as obtained for the chirp signal, are shown in figure 5.4.

It is clear that the STFT Mixed model both introduces benefits as drawbacks when compared to the results of the FRS Mixed model. Since the STFT does not suffer from the non-absolute model selection, it is better able to achieve the preferred results. The sprung mass vibration attenuation at both natural frequencies is very good, especially for the sprung mass natural frequency.

At the mid-range frequencies, however, the STFT experiences large oscillations in the frequency response. As the STFT model does not switch during the mid-range frequencies, these oscillations might be introduced by the switching behaviour of the model in the overall frequency response calculation and indicate an area of operation as described for the FRS Mixed model previously.

The normalised performance of the STFT Mixed model shows a significant improvement compared to the direct reference, the UNS model. The road-holding performance is clearly improved by the STFT Mixed model. Compared to the FRS Mixed model, the STFT Mixed model seems to achieve approximately equal results in terms of comfort, but even better results in road-holding performance.

The difference in road-holding performance can be explained when examining graph (D) in figures 5.2 and 5.4. Even though the response of the STFT Mixed model displays more oscillations, the overall level of vibration attenuation across the complete frequency range. The main advantage here is the influence of the

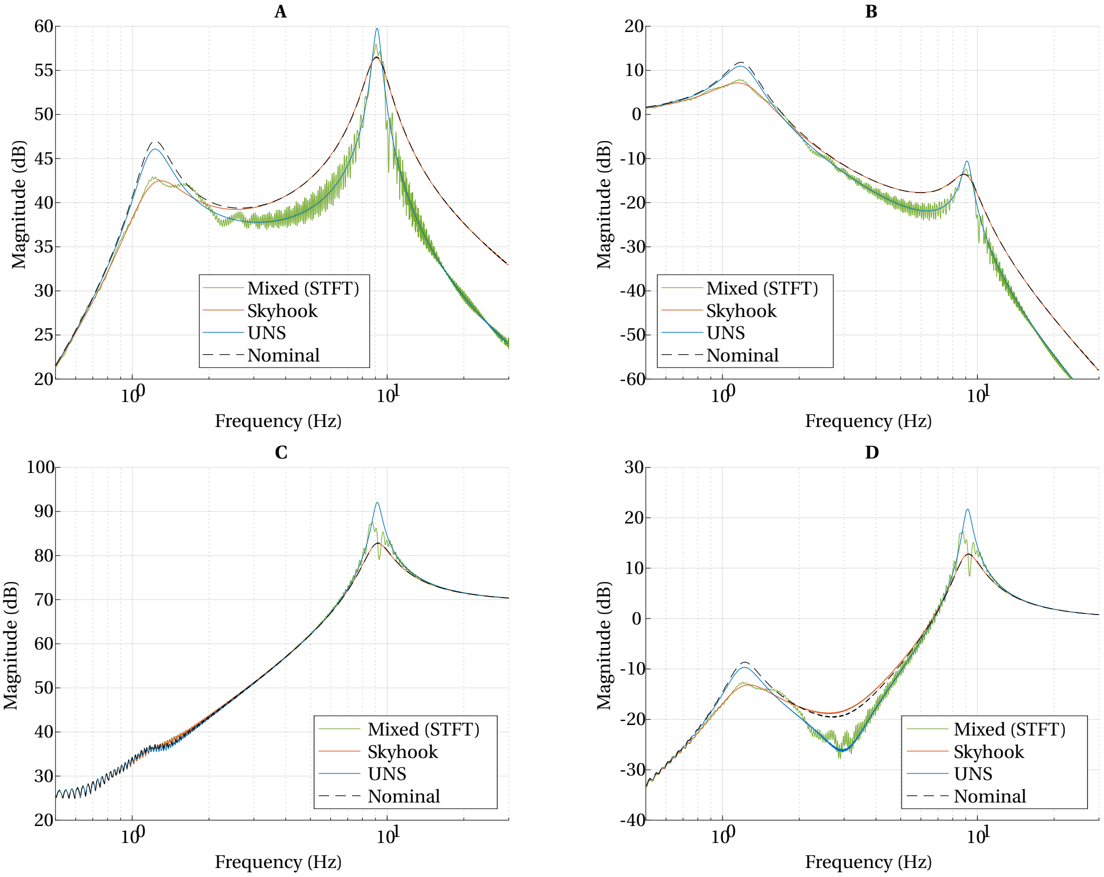

Figure 5.4: *Frequency response results of the STFT model. The figure show the responses of the following signals: (A) Sprung mass acceleration (B) Sprung mass displacement (C) Unsprung mass acceleration (D) Tyre deflection*

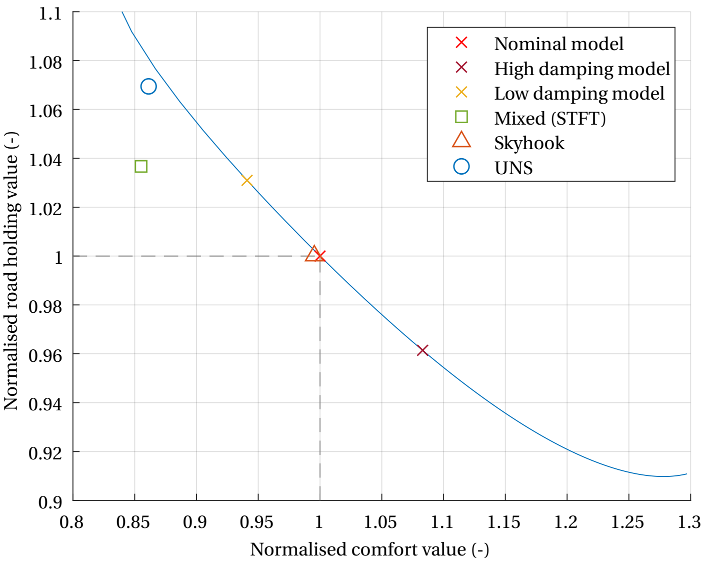

Figure 5.5: *Normalised performance of the STFT Mixed Model compared to its governing models and the passive system.*

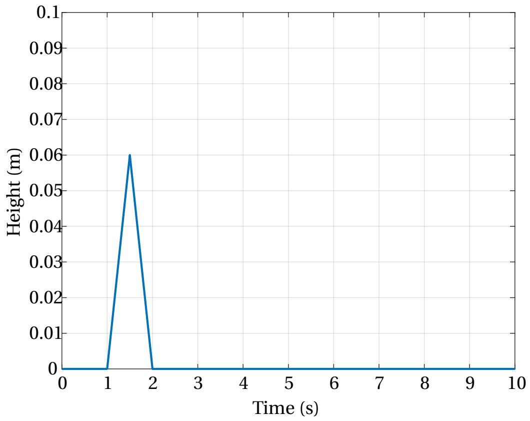

Figure 5.6: *Road input signal for the road bump test*

higher natural frequency response. At this frequency, the FRS Mixed model failed to effectively reduce the vibrations.

The road-holding performance is determined by the integral function of the road-holding response. As the Tyre Deflection is shown on a logarithmic horizontal scale, the seeming small area around the higher natural frequency where the STFT Mixed model achieves better performance, actually contributes to a large extent to the overall performance.

5.4. TIME DOMAIN ANALYSIS

The frequency analysis in the previous section has shed some light on the performance of both proposed models. These simulations were carried out for a chirp signal road input. In reality such a road does not exist. It is therefore not sufficient to draw conclusions solely from the frequency analysis. In these sections, simulations will be carried out for more realistic road input signals. The analysis of these simulations will provide more meaningful insights in the actual behaviour of the proposed models.

Both single-wheel as full vehicle simulations will be carried out for the time domain analysis. Since the simulation method differs between these approaches, road input signals will have to be defined for each simulation method.

The time domain analyses will be based off resulting signals that are defined in the time domain rather than the frequency domain. The performance metrics that have been used for the frequency domain analysis will therefore not be sufficient. These simulations will be evaluated using the methods discussed in chapter 2.8.

5.5. SINGLE-WHEEL ROAD INPUT

For these simulations, a new road input signal is determined as well. These time based road signals will be more representative for real world applications than the chirp signal used in the frequency analysis.

The single-wheel simulation will serve as transition from the frequency response simulation to the full vehicle time simulations. The time based road signals are therefore relatively simple excitations. The first time based road signal will be the single road bump as defined figure 5.6. The time domain responses will then offer a better understanding of the behaviour of the different models.

A second road input signal will be a randomized road signal. A randomized road can be carefully designed to more accurately depict a realistic road profile. This random road is created to specifically contain the frequency range of interest. The random road profile is created using the following algorithm:

1. A random signal of specified time-length is created.[1]
2. The time-domain signal is converted to the frequency-domain using the Fourier transform.

---

[1] The seed of the random signal is kept identical to ensure repeatability.

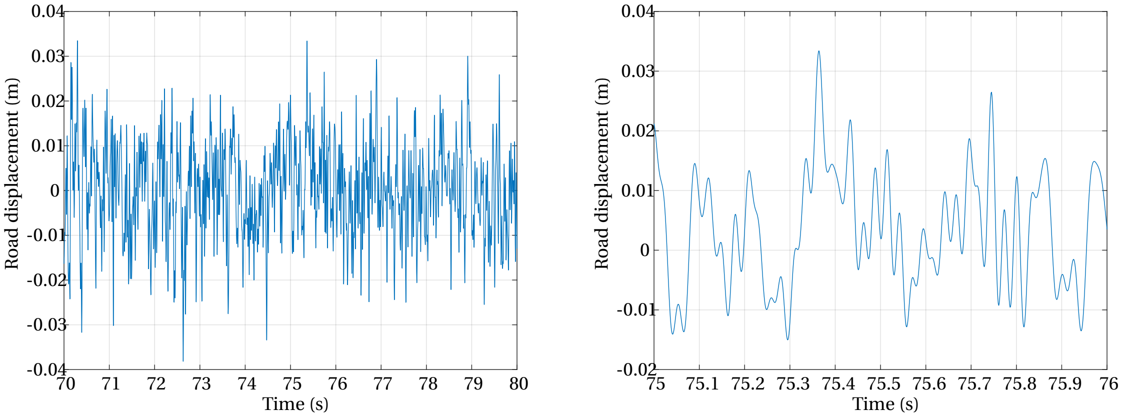

Figure 5.7: *Fragments of the randomly generated road. The left graph shows a 10 second snip of the full signal. The right graph shows a detailed look at the road profile over 1 second*

3. The frequencies not of interest are filtered out of the frequency-domain signal.
4. (Optional) The frequency-domain signal is processed to resemble different types of noise.
5. The frequency-domain signal is converted back into a time-domain signal using the Inverse Fourier transform.
6. The time-domain signal is processed to be a zero-mean signal and have a unity standard deviation.

The optional step 4 of the algorithm can be used to have the signal represent different types of noise. Without any processing, the signal created randomly in step 1 will be a White noise, where the magnitude of all frequencies contained in the signal are equal. In reality, roads tend to be a combination of White and Pink noise. For this application all frequencies up to 5 Hz are considered White noise. Frequencies higher than 5 Hz will experience a decline in Magnitude of 3 dB per octave. This coincides with signals having a power spectral density proportional to $\frac{1}{f}$ for the higher frequencies.

Fragments of the random road signal are shown in figure 5.7. The road input clearly shows a zero-mean behaviour while the unity standard deviation is multiplied with a general road signal amplitude, defined by A in equation (2.6).

5.6. SIMULATION RESULTS

Using the single-wheel road inputs, the system response can be evaluated for the QC model using the time base performance metrics. The results for each road type will be shown numerically and comparatively.

5.6.1. ROAD BUMP

Figures 5.8 and 5.9 show the sprung body displacement for the road bump simulation of the FRS and the STFT Mix models respectively. It is immediately visible that the two models behave very differently. In the response of the FRS model it is clearly visible that the new model properly behaves with a response that is bounded by the governing models.

The response of the STFT Mix model is however not visible in the road bump simulation results. A closer look at the situation gives some insight as to why the model cannot distinguish itself from its governing models.

Figure 5.10 shows the frequency that is estimated by the STFT model. The dotted lines indicate the different crossover frequencies. At $t = 5s$ a small peak is visible. Other than that, the estimated frequency is 0 Hz. As the estimated frequency peak is not high enough to cross any of the crossover frequencies, the control method will not change its active damping model. Therefore the STFT model will be employing the SH model for the complete measurement.

This problem is found in the parametrization of the STFT approach. Regarding the sensor sample time and the measurement window length, the STFT model will estimate the most dominant frequency of the last time

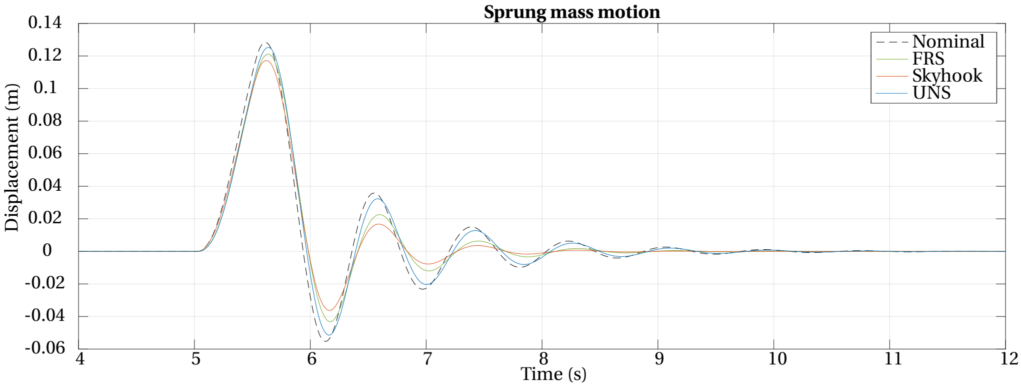

Figure 5.8: *Sprung body displacement for single-wheel road bump using the FRS control method*

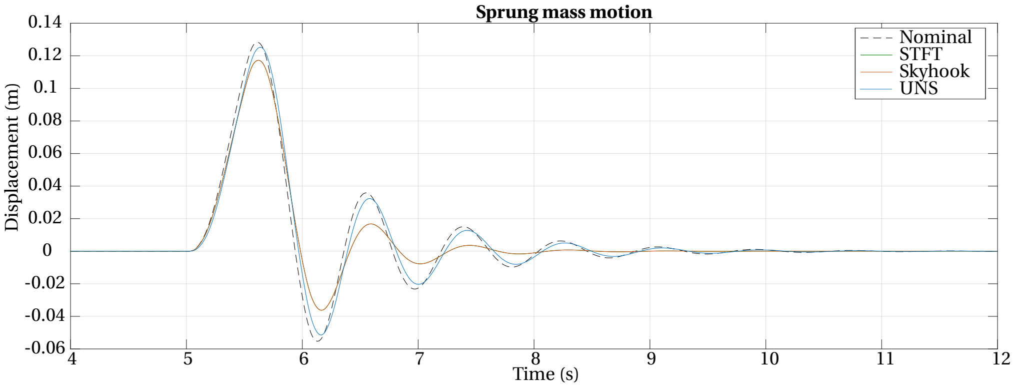

Figure 5.9: *Sprung body displacement for single-wheel road bump using the STFT control method*

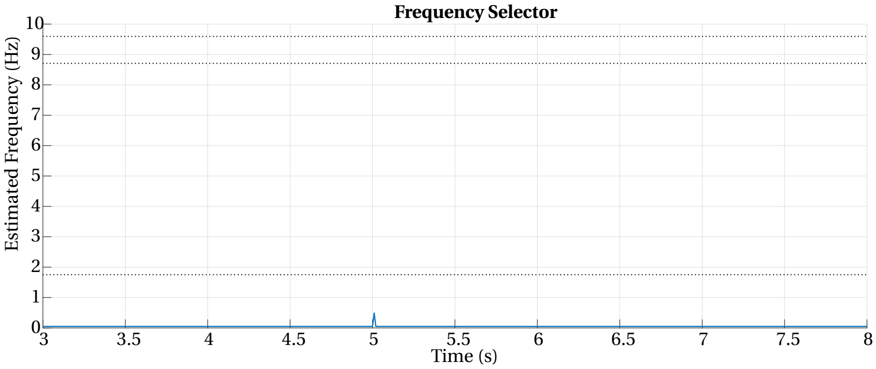

Figure 5.10: *Estimated frequency of the STFT model for the single-wheel road bump*

Table 5.1: *Single-wheel road bump numerical results*

	a_{peak}	VDV_{v}	VDV_{ms}	σ_{Fz}	e_{c}
FRS	3.279	1.096	0.1196	281.672	1004.356
STFT	3.189	1.120	0.1157	236.623	909.037
SH	3.134	1.118	0.1158	236.555	908.528
UNS	3.554	1.242	0.1227	342.081	592.429
Nominal	3.621	1.349	0.1248	309.246	N/A

window of 2 s. Since the road bump introduces only a short excitation, it is difficult for the STFT method to accurately determine the frequency of the vibration. In this case this results in a lack of switching action of the model.

The numerical results of the performance metrics for the Single-wheel road bump simulation are shown in table 5.1. The relative performance of the models, normalised for the nominal model performance, can be seen in figure 5.11 with the exception of the control effort e_{c} which cannot be normalised since the nominal model has no value for the control effort.

Comparing the different models, it can be confirmed that the results of the STFT model are nearly identical to those of the Skyhook model. As expected, all models show an improvement for the comfort metrics when compared to the nominal model. It is however remarkable to see that the plain Skyhook model achieves the best results, along with the STFT model. From earlier simulations, the UNS model is expected to offer the best comfort results while yielding the worst road holding performance. The comparison of figure 5.11 clearly shows that the UNS does indeed yield worse road holding performance than the nominal model where all other control methods do improve on the road holding. It does not, however achieve the best results for ride comfort.

This behaviour may be explained by the nature of the road input signal. Though the simple road bump offers an insight on the behaviour of the suspension control system, it does not offer insights along the complete frequency spectrum.

5.6.2. RANDOM ROAD

This section will discuss the model performance results for the random road input. As this signal is designed to include all frequencies of interest, a more complete assessment of the model performance can be obtained.

Figures 5.12 and 5.13 both show the section between $t = 4$ and $t = 12$ of the random road simulation. It is interesting to see that each model seems to behave quite differently. The STFT model is better able at following the governing models in different situations. Consider, for example, the response between $t = 7$ and $t = 7.5$. In this time frame, the STFT model accurately follows the Skyhook model. The FRS model is incapable of following either governing model at this point. This does however generate beneficial results, as the model displays smaller displacements than either of its governing models.

This is interesting since each model is bounded in the frequency domain by its governing models. In the time

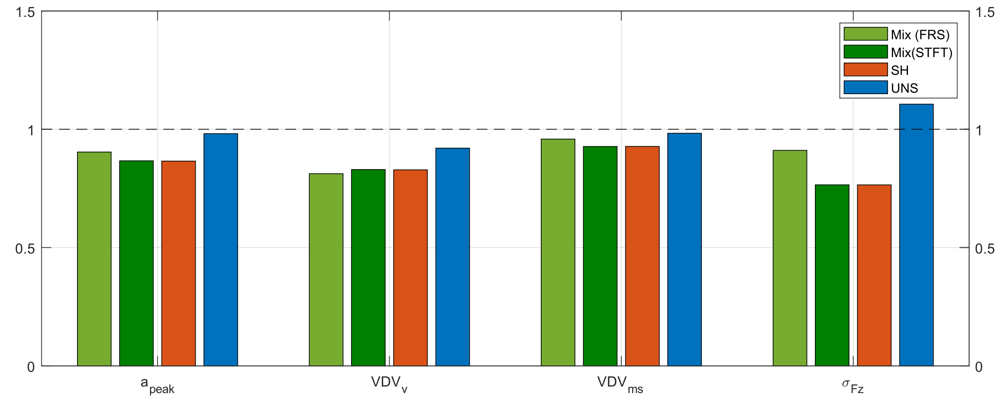

Figure 5.11: *Single-wheel road bump results relative to the nominal results (dashed).*

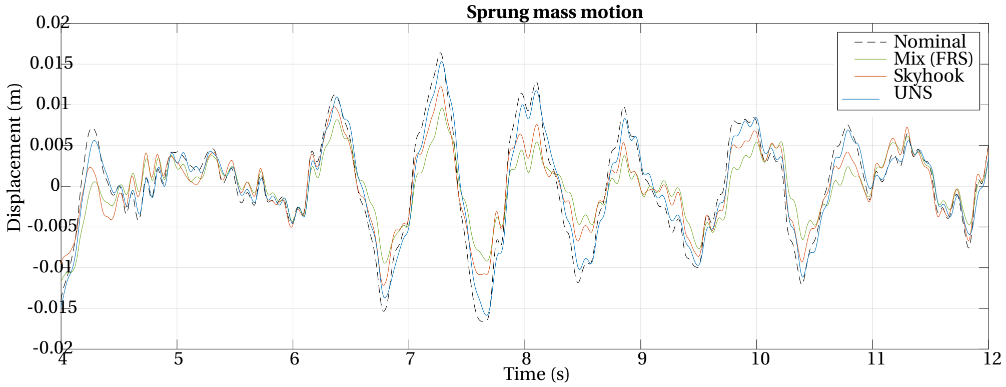

Figure 5.12: *Fragment of the sprung body displacement of the FRS model during the random road simulation*

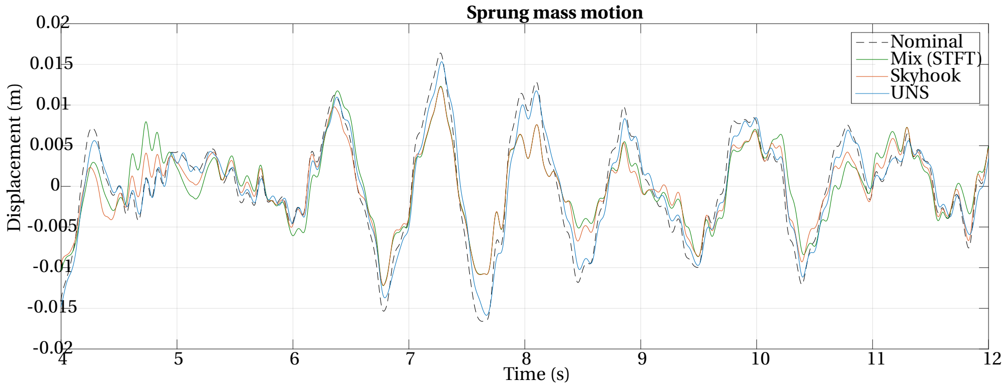

Figure 5.13: *Fragment of the sprung body displacement of the STFT model during the random road simulation*

Table 5.2: *Single-wheel random road numerical results*

	a_{peak}	VDV_{v}	VDV_{ms}	σ_{Fz}	e_{c}
FRS	9.846	7.794	0.0362	7278.115	5987.959
STFT	9.488	9.092	0.0414	6055.839	3970.640
SH	9.648	9.436	0.0391	4814.503	4122.941
UNS	7.520	8.291	0.0393	7745.674	2437.192
Nominal	9.778	9.490	0.0423	4818.313	N/A

domain it seems that the models are capable of achieving even better results, rather than approaching the performance of their governing models.

The numerical results for the random road simulation are displayed in table 5.2. The normalised results are visualised in figure 5.14, again with the exception of the control effort as this cannot be normalised to the passive model performance.

The visualisation of the results figure 5.14 show more promising behaviour. The resulting behaviour of the governing models display behaviour more in line with the frequency analysis. This indicates that the random road simulation captures more of the overall model behaviour than the road bump simulation. This is dominantly present in the Skyhook model showing minor overall improvements for all aspects, even for road holding when compared to the passive model. The UNS model shows greater improvements in terms of comfort, but also a decline in road holding performance.

The mix models are both improvements in some parts as well as declines in others compared to the UNS model. The aim of the proposed models is to maintain the comfort achieved by the UNS while improving its road holding performance. Both the FRS as the STFT model has its own merits in achieving this.

The STFT shows that it improves most on the UNS model road holding performance. In terms of comfort, the STFT seems to be unable to attain the performance of the UNS. Its performance lies between that of both governing models. This model can therefore be viewed as a compromise of improvements versus decline, where the reduction of the decline is its major benefit.

On the other hand there is the FRS Mix model. In terms of road holding capabilities it does not offer as much of an improvement as the STFT model. In terms of comfort, however, the FRS models displays even improvements over the UNS model. Though the largest vibration may not be attenuated as well as by the UNS model, the VDV values for both vertical accelerations and motion sickness show the best results among all models. Though initially it seems unlikely that the VDV values are smaller while the peak acceleration a_{peak} is larger. This can be explained by the frequency weighting filters. The peak acceleration is obtained directly from the unweighted vertical acceleration signal whereas the VDV values use weighted signals. The high peak acceleration may be measured for a frequency which is reduced by the weighting functions. As a result, a higher peak acceleration does no necessarily indicate an overall decline in ride comfort performance.

These results do come at a cost. It is important to keep the numerical information of 5.2 in mind as well as not all data is displayed in figure 5.14. The control effort of the FRS is well above any of the other models'. The control effort of the STFT model is contained within the values of the governing models. This behaviour is a result of the earlier observation that the STFT model is better at following its governing models whereas the FRS model's motion may vary significantly from that of the governing models. In following the governing models, the overall behaviour of the STFT model resembles that of either of the governing models. This model will therefore have a similar resemblance in the performance results. It makes sense that these performance values are then bounded by the values of the governing models as well.

As the FRS model deviates more from both governing models. The overall behaviour of the control input may deviate greatly from the other models, which is also the case for the random road simulation. The FRS shows the largest peak control force during the simulation. This not only affects the amount of energy that is required for this approach, but may also impose additional requirements for the actuator characteristics, as it should be able to supply these higher forces without damaging the system.

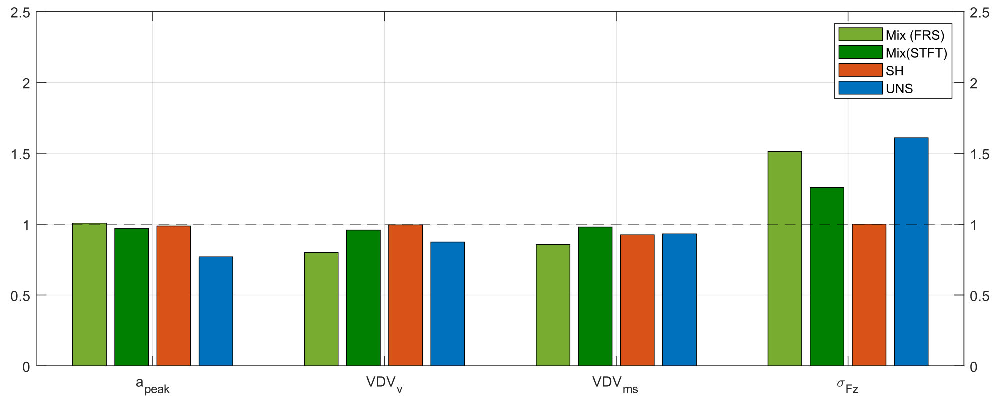

Figure 5.14: *Comparison of model performance for the single-wheel random road simulation. Normalised to the performance of the nominal model (dashed).*

5.7. DISCUSSION

The frequency response QC results show that both models offer improvements compared to the base UNS model for ideal conditions. The FRS model attains only slight improvements while the STFT model seems to offer significant improvements, mainly in terms of road holding.

The FRS control method offers proper model selection for low to mid-range frequencies, as seen in the frequency response results. Around the higher natural frequency of the system this method only offers slight improvements. In this area, the two crossover frequencies ω_2 and ω_3 have greatly overlapping operating ranges. This, combined with the switching method itself, results in poor performance as the control method cannot reliably select the proper model.

At frequencies beyond 25 Hz another anomaly can be seen, shown in figure 5.2. At these higher frequencies the control method is very unreliable. Changing the crossover frequencies did not alter this behaviour. This behaviour can therefore be attributed to the dynamics of the switching mechanics in the simulation model.

The STFT control method shows better overall improvements but also introduces relatively large oscillations. As this control method switches its behaviour based on the current vibration, these oscillations could be a result of curve fitting. Extending the simulation time of the chirp simulation yields smaller oscillations as the Fourier transforms is offered more data points for each vibration frequency. The oscillations can therefore be assumed to be processing noise. Keeping this in mind solidifies the results of the STFT control method. At low to mid-range frequencies the method can accurately select the desired governing model. It is only for the higher natural frequency that the model experiences issues. Since the crossover frequencies ω_2 and ω_3 are located close together in terms of frequency, the model does not have enough time to settle. As the input vibration crosses the second crossover frequency, the active governing model is switched by the controller. It then needs time to properly settle adjust the dynamic behaviour. This behaviour can also be observed around the first crossover frequency, ω_1. Before the system can settle, the input vibration crosses the last crossover frequency and the active governing model is switched once more. This behaviour results in an error around the unsprung natural frequency, which is located between the latter two crossover frequencies.

The road bump simulation yields some unexpected results. While it is interesting to visualize the suspension behaviour for a road bump, shown in figures 5.8 and 5.9, the numerical results show that it is not representative for the overall behaviour. It can be seen that the regular Skyhook achieves better performance than the UNS. Across the entire frequency range this is not the case. The numerical and comparative results can therefore not be assumed to be reliable.

The random road does offer more reliable insights to the overall performance of each control method. The Skyhook and UNS results reflect that of the frequency response results and can therefore be assumed to accurately reflect the performance of the proposed control methods as well.

For these simulations, the FRS control method follows the classic design trade-off. Its ride comfort performance is an improvement on both its governing models, as shown by the VDV for both vertical acceleration and motion sickness while having worse performance in terms of road holding than the STFT control method. It does, however, still improve on the road holding compared to the UNS control. Correspondingly, the STFT control method achieves less improvement in terms of ride comfort performance but also suffers a smaller penalty to its road holding performance.

In conclusion, both proposed control methods offer improvements in terms of ride comfort. In single wheel simulations the FRS control method achieves performances superior to either of its governing control methods while not suffering a greater penalty.

6

FULL VEHICLE SIMULATION RESULTS

After having examined the quarter car simulation results, both proposed control methods have also been implemented in the full vehicle model. All systems have been simulated to drive along each of the four road profiles as established in chapter 2. This chapter will first briefly discuss the results of the simulations corresponding to each of the four road profiles. Finally, the overall results of the full vehicle simulations will be discussed at the end of this chapter.

6.1. FULL VEHICLE SIMULATION RESULTS

This section will detail and discuss the simulation results of the full vehicle simulations. A total of 8 simulation setups will be tested as each of the road profiles will be used in a low and high velocity simulation. For the low velocity simulation, the vehicle model will have a longitudinal velocity of $10\,\mathrm{km\,h^{-1}}$. The high velocity simulations will be carried out at a vehicle velocity of $60\,\mathrm{km\,h^{-1}}$.

In order to calculate the ride comfort performance metrics, the vertical accelerations at the centre of gravity of the vehicle body will be obtained. These acceleration measurements are then used for the ride comfort evaluation. For both road holding capacity and control effort, the corresponding metrics will be calculated individually for each wheel hub and linearly averaged for a single value for evaluation.

6.1.1. SIMULATION RESULTS - PARALLEL CORRUGATIONS

The first set of simulations is carried out for the the Parallel Corrugated road profile. The numeric results of the low and high velocity simulations are displayed in tables 6.1 and 6.2 respectively. The corresponding comparisons to the passive model results are shown in figures 6.1 and 6.2 respectively. Note that these comparisons do not include the control effort. This is due to the fact that the passive control method does not require any external input forces. It is therefore not possible to normalise these values.

Table 6.1: *Full vehicle simulation results for the Parallel Corrugated road,* $v = 10\,\mathrm{km\,h^{-1}}$

	a_{peak}	$\mathrm{VDV_v}$	$\mathrm{VDV_{ms}}$	σ_{Fz}	e_{c}
FRS	3.452	3.079	0.0300	0.190	321.475
STFT	2.656	2.387	0.0270	0.187	470.697
SH	2.970	2.820	0.0272	0.195	152.845
UNS	2.673	2.372	0.0273	0.188	470.127
Nominal	3.018	2.901	0.0283	0.193	N/A

These first simulations show that the FRS control method is not able to improve on the ride comfort performance. Contrary to the expectations, all ride comfort performance metrics indicate a deterioration of the ride comfort when compared directly to the nominal, passive IWM model. When compared to the other control methods, the FRS control method shows a deterioration of more than 10 % for each metric compared to the best scoring method. In line with the classic design trade-off, the FRS control method does offer slight improvements in terms of road holding capacity. It is unexpected however, that the ride comfort show values

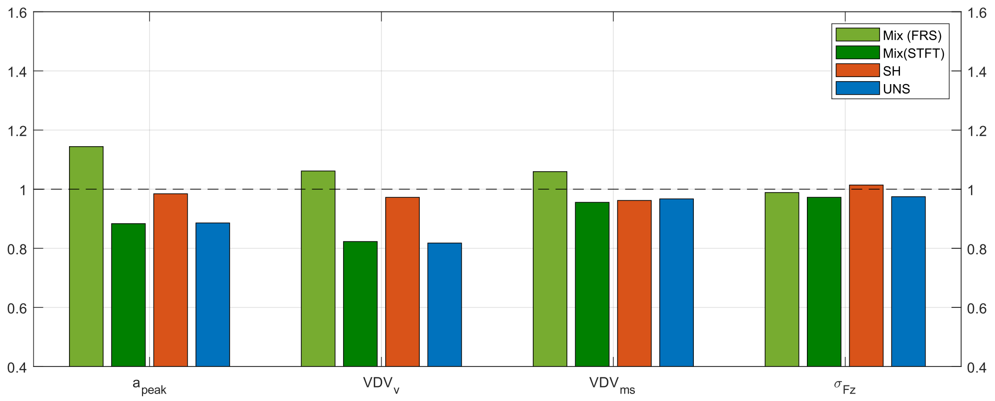

Figure 6.1: *Ride comfort and road holding results compared to the passive nominal model for the Parallel Corrugated road simulation,* $v = 10\,\mathrm{km\,h^{-1}}$

beyond the boundaries that are set by the governing models while the road holding capacity does display a performance between that of the governing models. In terms of control effort, the FRS control method requires more effort than the Skyhook while not achieving the same level of performance.

The STFT control method, on the other hand, shows promising results which are in line with the expectations from the single-wheel simulations. The ride comfort performance achieved by this control method is, first of all, a proper improvement on the nominal model. When compared to the other active control methods, the STFT achievers better results than either governing models in terms of peak acceleration and motion sickness, while also achieving almost equal performance to the desired UNS for the other metrics. Even though the STFT control method achieves increased performance, the required control effort is only slightly higher than that of the UNS model.

Table 6.2: *Full vehicle simulation results for the Parallel Corrugated road, $v = 60\,\mathrm{km\,h^{-1}}$*

	a_{peak}	$\mathrm{VDV_v}$	$\mathrm{VDV_{ms}}$	σ_{Fz}	e_c
FRS	4.906	2.252	0.0395	0.322	484.869
STFT	3.451	2.109	0.0357	0.326	470.102
SH	3.545	2.133	0.0355	0.326	271.064
UNS	2.958	1.926	0.0350	0.341	632.906
Nominal	3.517	2.144	0.0375	0.325	N/A

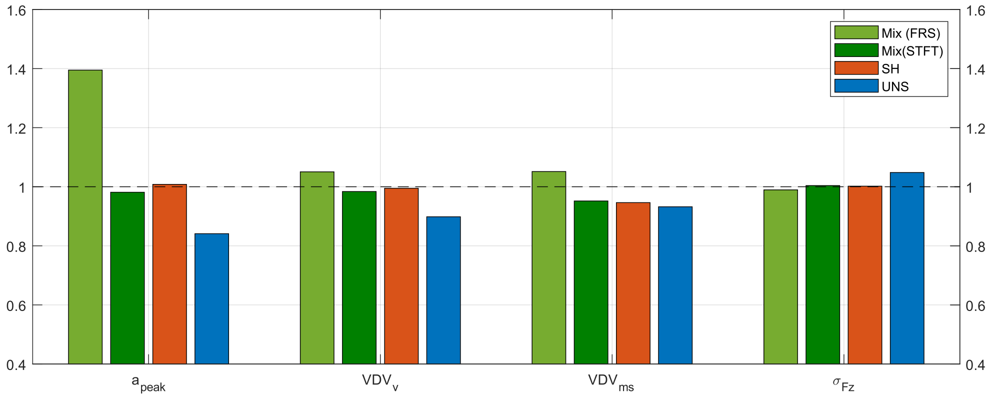

Figure 6.2: *Ride comfort and road holding results compared to the passive nominal model for the Parallel Corrugated road simulation, $v = 60\,\mathrm{km\,h^{-1}}$.*

The high velocity simulation results of the FRS control method follows the same trend as the low velocity simulation. The ride comfort metrics all show a deterioration in performance, not only when compared to the other active models but also compared to the passive nominal model. The peak acceleration in particular stands out. While the other metrics show deteriorations which are not as strong as for the low velocity simulation, the peak acceleration displays a massive deterioration of roughly 40 %. Surprisingly, the FRS control method does achieve a road holding performance which is superior to all active models. A minimal improvement of road holding is achieved compared to the nominal model.

The STFT control method still offers improvements when compared to the nominal model. When compared to the low velocity simulation, less improvement is achieved. For the high velocity simulations, the STFT control method performance is closer to that of the less effective governing model, rather than the desired behaviour. The peak acceleration and VDV for vertical accelerations show that the STFT performance is close to the Skyhook performance. In terms of motion sickness, the STFT even offers the least improvement.

In terms of control effort, table 6.2 shows that both Mixed model control methods require similar effort even though the achieved performance is not comparable.

6.1.2. SIMULATION RESULTS - ANGLED CORRUGATIONS

The second set of simulation is carried out for the road containing the angled corrugations for low and high vehicle velocities. The numerical results of these simulations can be found in tables 6.3 and 6.4 respectively. The normalised ride comfort and road holding performance results are displayed in figures 6.3 and 6.4.

Table 6.3: *Full vehicle simulation results for the Angled Corrugated road,* $v = 10\,\mathrm{km\,h^{-1}}$

	a_{peak}	$\mathrm{VDV_v}$	$\mathrm{VDV_{ms}}$	σ_{Fz}	e_{c}
FRS	3.658	2.318	0.0390	0.200	475.020
STFT	2.719	1.925	0.0352	0.193	578.885
SH	3.145	2.138	0.0346	0.199	190.706
UNS	2.716	1.857	0.0352	0.194	578.157
Nominal	3.282	2.189	0.0366	0.199	N/A

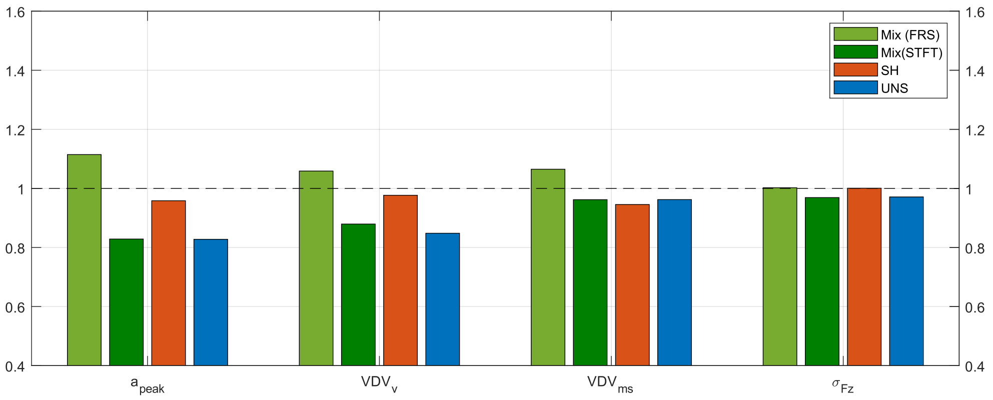

Figure 6.3: *Ride comfort and road holding results compared to the passive nominal model for the Angled Corrugated road simulation,* $v = 10\,\mathrm{km\,h^{-1}}$.

When comparing the results for the low velocity parallel corrugations of table 6.1 with the low velocity angled corrugations results of table 6.3 it shows that this road profile induces more motion sickness, while the vertical acceleration discomfort is generally smaller.

The FRS control method again shows an overall deterioration of the ride comfort. For this road profile, however, the effort is quite higher than for the parallel corrugations. For the parallel corrugations, the FRS required approximately 70 % of the effort that is required for the UNS control method, which has the highest required effort. For the angled corrugations, it requires approximately 80 % of the UNS control method effort. This relative increase in power does not result in better performance, as the ride comfort performance values still range to deteriorations up to approximately 11.46 % when compared to the passive nominal model.

The STFT control method shows similar improvements for the angled corrugations as it does for parallel corrugations. Its performance nears that of the UNS control method for each of the parameters. All ride comfort performance values are within the range that is set by the governing models. The road holding capacity shows an insignificant improvement of less than 0.5 % while the control effort is again higher than any of its governing models.

Table 6.4: *Full vehicle simulation results for the Angled Corrugated Road,* $v = 60\,\mathrm{km\,h^{-1}}$

	a_{peak}	$\mathrm{VDV_v}$	$\mathrm{VDV_{ms}}$	σ_{Fz}	e_c
FRS	5.916	2.550	0.0375	0.398	605.409
STFT	4.551	2.340	0.0326	0.405	594.700
SH	4.540	2.408	0.0326	0.404	338.988
UNS	4.019	2.171	0.0326	0.421	777.982
Nominal	4.636	2.444	0.0345	0.403	N/A

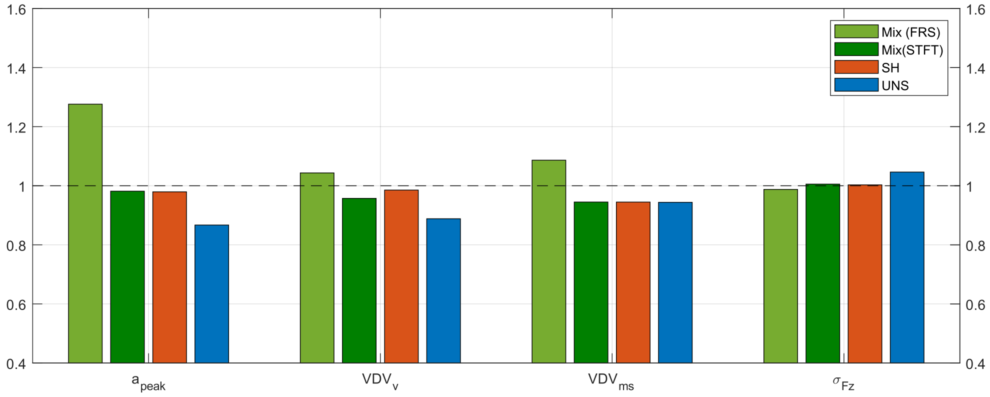

Figure 6.4: *Ride comfort and road holding results compared to the passive nominal model for the Angled Corrugated road simulation,* $v = 60\,\mathrm{km\,h^{-1}}$.

The high velocity results for the Angled Corrugations show that the high velocity simulations are more representative of the overall performance, indicated by the superior comfort performance of the UNS model while it has worse road holding performance.

Comparing the two mixed models, it is shown that the STFT outperforms the FRS model in terms of ride comfort while requiring slightly less effort. It is however interesting to see that the FRS model outperforms all other models in terms of road holding comfort.

6.1.3. SIMULATION RESULTS - POTHOLES

The simulation results of the pothole road are displayed numerically in tables 6.5 and 6.6, and comparatively in figures 6.5 and 6.6.

Table 6.5: *Full vehicle simulation results for the Pothole road,* $v = 10\,\mathrm{km\,h^{-1}}$

	a_{peak}	$\mathrm{VDV_v}$	$\mathrm{VDV_{ms}}$	σ_{Fz}	e_{c}
FRS	14.529	8.267	0.0884	0.364	1471.859
STFT	11.098	6.662	0.0633	0.316	1990.913
SH	12.973	7.512	0.0612	0.340	820.657
UNS	11.093	6.577	0.0623	0.312	1982.171
Nominal	13.896	7.867	0.0703	0.346	N/A

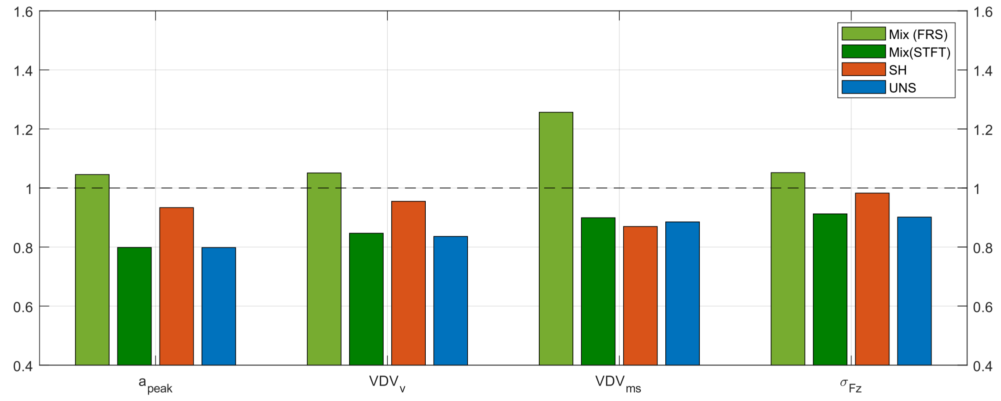

Figure 6.5: *Ride comfort and road holding results compared to the passive nominal model for the Pothole road simulation,* $v = 10\,\mathrm{km\,h^{-1}}$.

For the slow velocity simulation, the effect of the large road displacement is noticed most severely. It shows that the FRS model has worse performance for all aspects when compared to the passive nominal model. All other models show improvements, however. This discrepancy may be explained by the non-absolute switching of the FRS model. This mixed model will inherently select the less effective model during the simulation. It may occur that the dynamics of the road result in a sequence where the FRS selects the wrong model for most of the time, rather than least. This discrepancy with the desired behaviour may result in an amplification of vibrations.

Table 6.6: *Full vehicle simulation results for the Pothole road, $v = 60\,\mathrm{km\,h^{-1}}$*

	a_{peak}	VDV_{v}	VDV_{ms}	σ_{Fz}	e_{c}
FRS	12.658	5.720	0.0457	0.397	1479.453
STFT	12.499	5.183	0.0431	0.428	1994.991
SH	10.725	5.642	0.0428	0.421	545.449
UNS	8.178	4.878	0.0402	0.444	2250.439
Nominal	10.660	5.577	0.0443	0.413	N/A

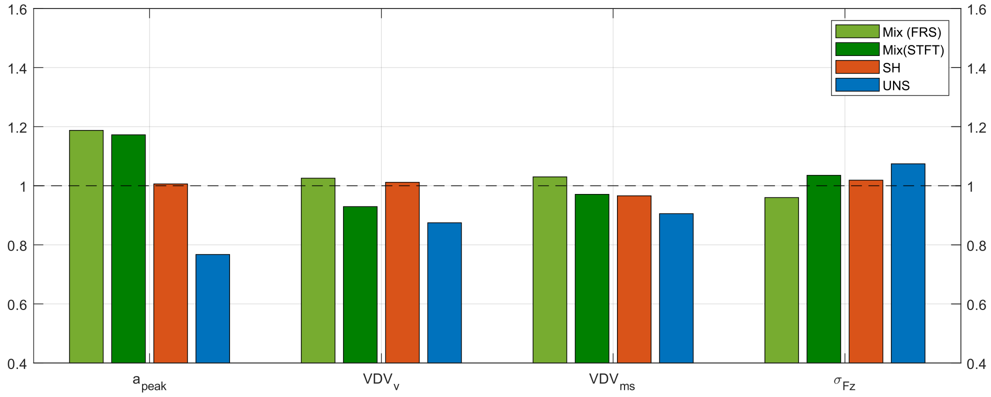

Figure 6.6: *Ride comfort and road holding results compared to the passive nominal model for the Pothole road simulation, $v = 60\,\mathrm{km\,h^{-1}}$.*

The results for the Pothole road at high velocities show other remarkable behaviour, this time of the STFT model. While it accurately selects the UNS model during the low velocity simulation, it displays uncharacteristically high peak accelerations during the high velocity simulation. Even while the UNS model achieves far superior results in terms of peak acceleration when compared to all other models.

As the VDV values still show performance between the governing models, it can be concluded that the high peak acceleration is exerted for a frequency that is attenuated by the frequency weighting filters, effectively reducing its effect on the total ride comfort performance.

6.1.4. SIMULATION RESULTS - FATIGUE

The final and most exhausting test for the vehicle is the Fatigue road simulation. The low velocity numerical and comparative results are shown in table 6.7 and figure 6.7 respectively while the high velocity results are displayed in table 6.8 and figure 6.8.

Table 6.7: *Full vehicle simulation results for the Fatigue road,* $v = 10\,\mathrm{km\,h^{-1}}$

	a_{peak}	VDV_{v}	VDV_{ms}	σ_{Fz}	e_{c}
FRS	4.381	2.258	0.0604	0.203	658.154
STFT	2.730	1.682	0.0483	0.164	569.033
SH	3.273	1.785	0.0464	0.168	396.313
UNS	2.626	1.642	0.0497	0.162	686.658
Nominal	3.153	1.916	0.0528	0.181	N/A

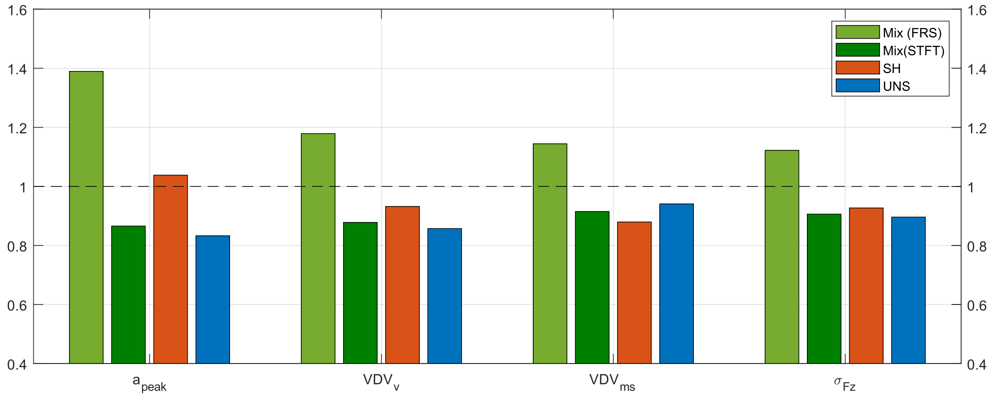

Figure 6.7: *Ride comfort and road holding results compared to the passive nominal model for the Fatigue road simulation,* $v = 10\,\mathrm{km\,h^{-1}}$.

Once again the results of the FRS model show the highest numbers for each metric, portraying the worst results of the set of control methods. The STFT model on the other hand achieves improvements across all metrics, again bounded by the performance of the governing models as expected. Interestingly the STFT model achieves this performance with less effort than the FRS model.

Table 6.8: *Full vehicle simulation results for the Fatigue road,* $v = 60\,\mathrm{km\,h^{-1}}$

	a_{peak}	$\mathrm{VDV_v}$	$\mathrm{VDV_{ms}}$	σ_{Fz}	e_{c}
FRS	16.356	6.658	0.0514	0.580	1679.103
STFT	9.592	5.777	0.0486	0.608	2150.382
SH	10.842	6.313	0.0475	0.597	573.942
UNS	9.755	5.674	0.0500	0.609	2206.877
Nominal	11.019	6.306	0.0497	0.588	N/A

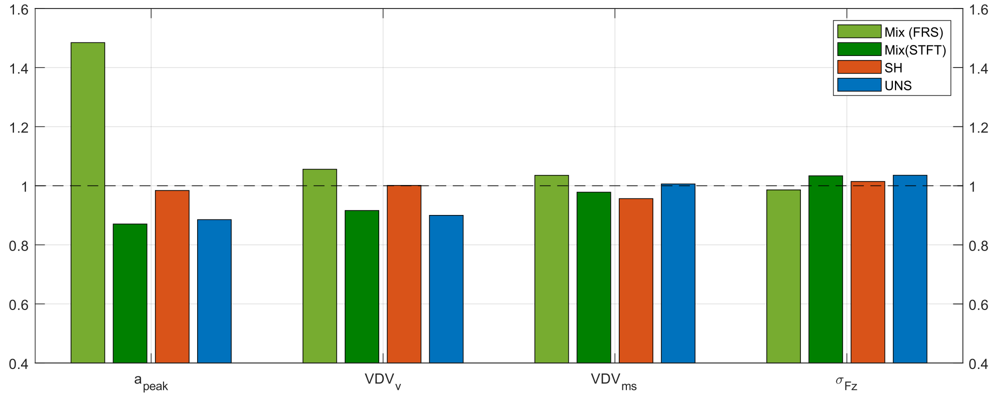

Figure 6.8: *Ride comfort and road holding results compared to the passive nominal model for the Fatigue road simulation,* $v = 60\,\mathrm{km\,h^{-1}}$.

The high velocity results show why this road profile is most taxing for the vehicles. The FRS mixed model displays the largest deterioration for the peak acceleration across all control methods and all simulations.

It is however unexpected that the STFT model achieves the best peak acceleration attenuation as its performance has been a compromise between the performance of its governing models in all other simulations. This shows that the overall performance may improve beyond the performance of the governing models if used effectively.

6.2. DISCUSSION

When comparing all simulations, the high velocity simulations seem to be more representative of the complete vehicle behaviour than the low velocity simulations. This is displayed by the decrease in performance in terms of road holding capacity. For the low velocity simulations, most models do no only improve on the ride comfort but also on the road holding capacity. According to the classic design trade-off, control methods focussed on ride comfort inherently decrease their road holding performance. This is reflected only in the high velocity simulations. This may be caused by the disturbances of the road profile. It seems that the low velocity simulations do not represent vibrations of the complete frequency spectrum. The high velocity simulations do resemble the classic design trade-off and therefore seem to be able to represent road profile disturbances for a greater frequency spectrum, giving a more complete overview of the control method performance.

Across all simulations, the FRS mixed model is shown to be inadequate to improve on the performance of its governing models. Even though the performance did slightly increase for the single-wheel simulations, the full vehicle simulations have shown that the non-absolute switching behaviour causes deteriorations in terms of comfort rather than improvements. The road holding capacity is shown to increase for the full vehicle simulations. This is undesired behaviour however, since the control method is designed to improve on the ride comfort of the vehicle. Since the improved road holding behaviour is completely opposite to the goal of the control method, its results are unpredictable. The FRS method could therefore also not be used as a road holding oriented control method.

The STFT was shown to be effective in achieving its goals. In nearly every situation the performance of the UNS control method is improved by employing the SH model when preferred. This behaviour was however not predicted by the single-wheel random road simulation. This method might therefore be inefficient for specific situations rather than a sure overall improvement. It should also be noted that the improved comfort performance does not cost additional control effort, as the control effort of the STFT control method only rarely exceeds that of the most effort expensive UNS control method.

7

CONCLUSION

The goal of this research is the improvement of ride comfort for In-Wheel Motor vehicles using a mixed suspension control model based on the Skyhook and Unsprung Negative Skyhook (UNS) models. Two mixed control methods have been designed.

The first control method is based on a semi-active approach, used in mixed Skyhook-ADD suspension control. This approach uses a simple comparative equation that uses the velocity and acceleration measurements of the sprung vehicle body to estimate whether the vibration frequency is higher or lower than a set crossover frequency. Using several of these Frequency-range selector (FRS) switches, it is possible to switch between optimal suspension control models for different frequency ranges.

The second control method uses a Short-Time Fourier Transform (STFT) estimator to estimate the instantaneous frequency of the vehicle vibration. The frequency spectrum of a windowed signal is obtained. In this spectrum, the strongest frequency component of the complete vibration is identified. Corresponding to this frequency component, the optimal suspension control model is selected.

Both proposed control methods, as well as existing state-of-the-art control methods have been implemented in both a single-wheel as well as a full vehicle configuration. Performance metrics are established to evaluate the ride comfort and road holding performance of the vehicle models. Simulations are carried out for each configuration to evaluate the performance according to the performance metrics.

7.1. CONCLUSIONS

The following conclusions are made from this research.

- For single-wheel simulations, both Mixed model control methods show an improvement over the UNS control method.
- The single-wheel simulations of the FRS control method show less vibration attenuation at the unsprung natural frequency and seems incapable of selecting the proper model for frequencies beyond 25 Hz because of the dynamics of the switching behaviour.
- The single-wheel simulations of the STFT control method show proper model selection across the complete frequency range but oscillates around the governing model's response curves, indicating it requires a relatively long time to settle to the correct model after switching.
- Full vehicle simulations of the FRS control method indicate that, in more realistic situations, the model does not improve on the ride comfort of the vehicle. For the high velocity simulations, this control method even improves on the road holding capacity rather than ride comfort, which offers performances opposite to its goal.
- It is concluded that the FRS control method is not able to improve on the overall ride comfort of the vehicle.
- Full vehicle simulations of the STFT control method show that the performance of this method lies between that of its governing models, both in terms of ride comfort and road holding capacity. It therefore does achieve improvements over the UNS control method but does not offer superior overall performance.
- Overall, the mixed Skyhook-UNS show that it is possible to improve on vehicle ride comfort by switching between suspension control strategies rather than using a single strategy. These improvements are limited in this research by the frequency dependent switching laws.

7.2. RECOMMENDATIONS

The STFT has shown potential to even further increase the ride comfort to become a superior control method over the SH and STFT control methods. Further research is required to more completely assess the Mixed models' behaviour and to improve on their performance. The following subjects should be researched to advance on the models proposed in this research:

- The model can be expanded to include more governing models. Including a Groundhook control law for vibration frequencies near the unsprung mass natural frequency may further improve overall performance.
- The frequency estimator should be investigated for improvements. In this research, the STFT estimator is incapable of accurately estimating the instantaneous vibration for rapidly changing dynamic vibrations. Further improvements on the estimation of the instantaneous frequency can be beneficial for the Mixed model application. This may be achieved by improving the STFT method or the implementation of another instantaneous frequency estimator.
- The introduction of high level control should be investigated to the goal of increasing overall performance. In this research, each suspension is controlled independently. In single-wheel simulations, the proposed control methods show improvements. Studies have shown that roll and pitch vibrations are only small contributors to vehicle ride comfort. Still, a high level controller that accounts for these motions may influence the overall behaviour of the control methods.
- Subjective assessments should be carried out to more diligently evaluate the ride comfort of the proposed models. Studies have shown that ride comfort cannot completely be described by objective performance values[25]. The main part of ride comfort of a vehicle is still the subjective comfort perception by the passengers. Therefore, subjective assessments, such as questionnaires after test rides, should be incorporated in order to obtain a more complete picture of the performance of the proposed models.

A

APPENDIX: SUSPENSION TYPE PROPERTIES

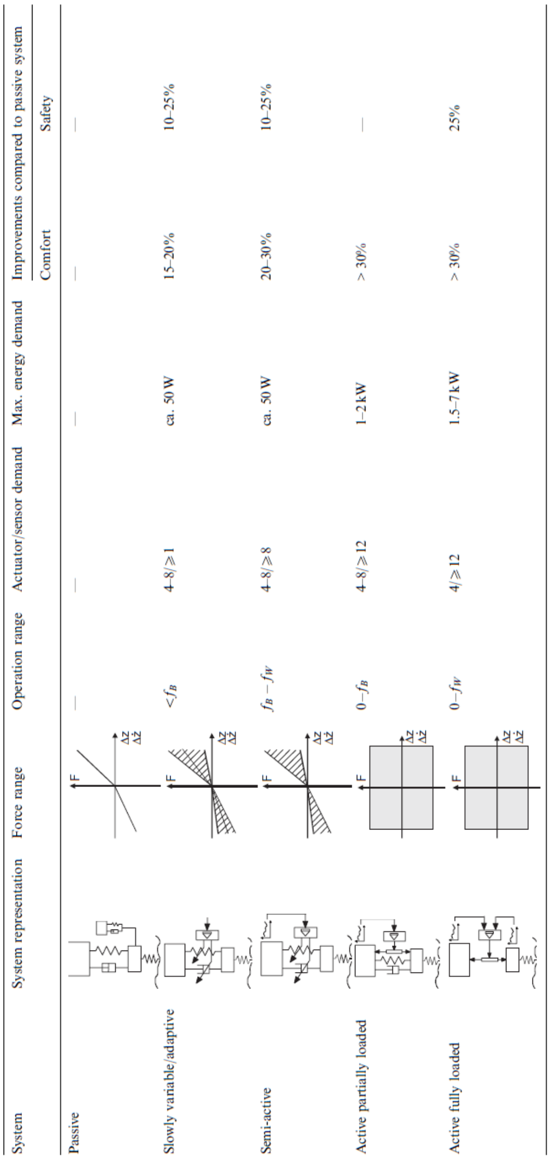

System	System representation	Force range	Operation range	Actuator/sensor demand	Max. energy demand	Improvements compared to passive system	
						Comfort	Safety
Passive			—	—	—	—	—
Slowly variable/adaptive			$<f_B$	4–8/≥1	ca. 50 W	15–20%	10–25%
Semi-active			$f_B - f_W$	4–8/≥8	ca. 50 W	20–30%	10–25%
Active partially loaded			$0–f_B$	4–8/≥12	1–2 kW	> 30%	—
Active fully loaded			$0–f_W$	4/≥12	1.5–7 kW	> 30%	25%

Figure A.1: *Full detailed overview of different suspension system types and their properties[4]*

BIBLIOGRAPHY

[1] A. Ferrara, *Sliding mode control of vehicle dynamics* (IET, 2017).

[2] C. M. Becker and P. S. Els, *Profiling of rough terrain,* (2014).

[3] D. Fischer and R. Isermann, *Mechatronic semi-active and active vehicle suspensions,* Control engineering practice **12**, 1353 (2004).

[4] S. M. Savaresi, C. Poussot-Vassal, C. Spelta, O. Sename, and L. Dugard, *Semi-active suspension control design for vehicles* (Elsevier, 2010).

[5] T. Dahlberg, *Ride comfort and road holding of a 2-dof vehicle travelling on a randomly profiled road,* Journal of Sound and vibration **58**, 179 (1978).

[6] M. Crosby and D. C. Karnopp, *The active damper—a new concept for shock and vibration control,* Shock and Vibration Bulletin **43**, 119 (1973).

[7] L. Chang, *Recent developments of electric vehicles and their propulsion systems,* IEEE Aerospace and Electronic Systems Magazine **8**, 3 (1993).

[8] S. Murata, *Innovation by in-wheel-motor drive unit,* Vehicle System Dynamics **50**, 807 (2012).

[9] K. Sawase and Y. Ushiroda, *Improvement of vehicle dynamics by right-and-left torque vectoring system in various drivetrains,* Mitsubishi Motors Technical Review **20**, 14 (2008).

[10] D. Hrovat, *Influence of unsprung weight on vehicle ride quality,* Journal of Sound and Vibration **124**, 497 (1988).

[11] E. Katsuyama and A. Omae, *Improvement of ride comfort by unsprung negative skyhook damper control using in-wheel motors,* SAE International Journal of Alternative Powertrains **5**, 214 (2016).

[12] M. Ahmadian and F. D. Goncalves, *A frequency analysis of semiactive control methods for vehicle application,* SAE transactions , 1141 (2004).

[13] *CarMaker|IPG Automotive,* (2019), retrieved from https://ipg-automotive.com/products-services/simulation-software/carmaker/.

[14] *Gerotek - ARMSCOR,* (2016), retrieved from http://www.armscor.co.za/?page_id=3967.

[15] R. Lundström, P. Holmlund, and L. Lindberg, *Absorption of energy during vertical whole-body vibration exposure,* Journal of biomechanics **31**, 317 (1998).

[16] K. Parsons and M. Griffin, *Whole-body vibration perception thresholds,* Journal of sound and Vibration **121**, 237 (1988).

[17] R. Hassan and K. McManus, *Perception of low frequency vibrations by heavy vehicle drivers,* Journal of low frequency noise, vibration and active control **21**, 65 (2002).

[18] W. F. Faris, Z. BenLahcene, and F. Hasbullah, *Ride quality of passenger cars: an overview on the research trends,* International Journal of Vehicle Noise and Vibration **8**, 185 (2012).

[19] T. D. Gillespie, *Fundamentals of vehicle dynamics*, Vol. 400 (Society of automotive engineers Warrendale, PA, 1992).

[20] H. B. Pacejka and E. Bakker, *The magic formula tyre model,* Vehicle system dynamics **21**, 1 (1992).

[21] M. Griffin, *Discomfort from feeling vehicle vibration,* Vehicle System Dynamics **45**, 679 (2007).

[22] L. Zuo and S. Nayfeh, *Low order continuous-time filters for approximation of the iso 2631-1 human vibration sensitivity weightings,* Journal of sound and vibration **265**, 459 (2003).

[23] F. Du, *Frequency weighting filter design for automotive ride comfort evaluation,* Chinese Journal of Mechanical Engineering **29**, 727 (2016).

[24] S. Nishiyama, N. Uesugi, T. Takeshima, Y. Kano, and H. Togii, *Research on vibration characteristics between human body and seat, steering wheel, and pedals (effects of seat position on ride comfort),* Journal of Sound and Vibration **236**, 1 (2000).

[25] P. Els, *The applicability of ride comfort standards to off-road vehicles,* Journal of Terramechanics **42**, 47 (2005).

[26] L. Z. Ben, F. Hasbullah, and F. W. Faris, *A comparative ride performance of passive, semi-active and active suspension systems for off-road vehicles using half car model,* International Journal of Heavy Vehicle Systems **21**, 26 (2014).

[27] A. A. A. Omar and B. Özkan, *Evaluation of effect of in-wheel electric motors mass on the active suspension system performance using linear quadratic regulator control method,* Evaluation **4** (2015).

[28] P. J. T. Venhovens, *Optimal control of vehicle suspensions.* (1995).

[29] X. C. Akutain, J. Vinolas, J. Savall, and M. Castro, *Comparing the performance and limitations of semi-active suspensions,* Int. J. Vehicle Systems Modelling and Testing **2**, 296 (2007).

[30] S. M. Savaresi, E. Silani, and S. Bittanti, *Acceleration-driven-damper (add): An optimal control algorithm for comfort-oriented semiactive suspensions,* Journal of dynamic systems, measurement, and control **127**, 218 (2005).

[31] F. D. Goncalves and M. Ahmadian, *A hybrid control policy for semi-active vehicle suspensions,* Shock and Vibration **10**, 59 (2003).

[32] Y. M. Sam, M. R. H. A. Ghani, and N. Ahmad, *LQR controller for active car suspension,* in *TENCON 2000. Proceedings,* Vol. 1 (IEEE, 2000) pp. 441–444.

[33] H. G. Ohadi, *Load-based active suspension control,* (2011), delft University of Technology.

[34] S. M. Savaresi and C. Spelta, *Mixed sky-hook and add: Approaching the filtering limits of a semi-active suspension,* Journal of dynamic systems, measurement, and control **129**, 382 (2007).

[35] J. Allen, *Short term spectral analysis, synthesis, and modification by discrete fourier transform,* IEEE Transactions on Acoustics, Speech, and Signal Processing **25**, 235 (1977).

[36] F. J. Harris, *On the use of windows for harmonic analysis with the discrete fourier transform,* Proceedings of the IEEE **66**, 51 (1978).